Application of High Performance Concrete in the Pavement System

Structural Response of High Performance Concrete Pavements

Final Report
March 2002

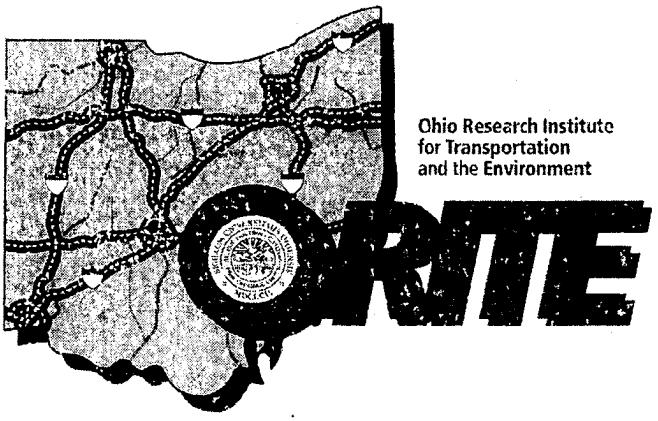

Stocker Center
Ohio University
Athens, OH
45701-2979

APPLICATION OF HIGH PERFORMANCE CONCRETE IN THE PAVEMENT SYSTEM

STRUCTURAL RESPONSE OF HIGH PERFORMANCE CONCRETE PAVEMENT

FINAL REPORT

Prepared in Cooperation with the

OHIO DEPARTMENT OF TRANSPORTATION and
U.S. DEPARTMENT OF TRANSPORTATION
FEDERAL HIGHWAY ADMINISTRATION

Principal Investigators:	Shad M. Sargand William Edwards Issam Khoury
Graduate Research Assistants:	Daniel Wasniak Demond James Ricky Selle

Ohio University
Ohio Research Institute for Transportation and the Environment
Department of Civil Engineering
Athens, Ohio

March 2002

1. Report No.	2. Government Accession No.	3. Recipient's Catalog No.
FHWA/OH-2001/15 FHWA/OH-2001/16		

4. Title and Subtitle	5. Report Date
Application of High Performance Concrete in the Pavement System Strucutral Response of High Performance Concrete	March 2002
	6. Performing Organization Code
7. Author(s)	8. Performing Organization Report No.
Dr. Shad Sargand	10. Work Unit No. (TRAIS)
9. Performing Organization Name and Address Ohio University Department of Civil Engineering College of Engineering & Technology Stocker Center Athens, Ohio 45701	11. Contract or Grant No. State Job No. 14666(0) State Job No. 14696(0)
	13. Type of Report and Period Covered Final Report
12. Sponsoring Agency Name and Address Ohio Department of Transportation 1980 West Broad Street Columbus, OH 43223	14. Sponsoring Agency Code

15. Supplementary Notes

Prepared in cooperation with the U.S. Department of Transportation, Federal Highway Administration

16. Abstract

A concrete pavement was constructed on US 50 east of Athens Ohio to determine the influence of ground granulated blast furnace slag on the curing of a high performance concrete pavement, and on the performance of that pavement as it was subjected to environmental cycling and nondestructive testing with a Falling Weight Deflectometer (FWD). Three test sections of high performance concrete and one control section constructed with ODOT Class C concrete were instrumented and monitored closely to determine any differences in response and performance. The high performance sections contained 25% ground granulated blast furnace slag. Several joints were not sealed to evaluate their performance when compared to joints sealed in accordance with ODOT specifications.

Based upon laboratory tests and field data obtained during this study, the following conclusions were derived from this pavement. Temperature gradients generated between the surface and bottom of concrete slabs during the curing process can have a significant impact on the formation of early cracks. Large values of strain recorded in the field during the curing period indicated that the two sections of high performance pavement constructed in October 1997 would likely experience early cracking, as was observed. Field data indicated that a third high performance section and a control section containing standard ODOT Class C concrete, both constructed in October 1998, had a lower probability of exhibiting early cracking, and no cracks were observed. The uncracked section of high performance concrete had less initial warping than did the control section constructed at the same time with standard ODOT Class C concrete. Early cracking in the other two cracked high performance sections precluded any comparison with the uncracked sections. FWD data indicated that the uncracked high performance section experienced slightly less deflection at the joints than did the section containing standard concrete, suggesting less curvature and less loss of support under these slabs than under slabs constructed with standard concrete. FWD joint deflections were higher in the cracked high performance sections after one year of service than before the sections were opened to traffic, probably due to the presence of the cracks. Limited data suggested that moisture in the subgrade at sealed and unsealed joints was similar and, in some cases, more under the sealed joints than under the unsealed joints. FWD deflections at sealed joints were generally higher than at the unsealed joints.

17. Key Words		18. Distribution Statement
High Performance Conrete Deflection Strain Granulated Blast Furnace Slag	Temperature gradient US 50	No Restrictions. This document is available to the public through the National Technical Information Service, Springfield, Virginia 22161

19. Security Classif. (of this report)	20. Security Classif. (of this page)	21. No. of Pages	22. Price
Unclassified	Unclassified		

Form DOT F 1700.7 (8-72) Reproduction of completed page authorized

Table of Contents

List of Tables

List of Figures

List of Figures

List of Figures

List of Figures

Chapter1 Introduction

1.1 General Statement

Rigid pavements make up a significant percentage of highway systems in the United States and abroad. Concrete pavements provide an economical and durable solution for highway systems, because the pavements last longer and require less maintenance. Recently, there has been great interest in the construction of a higher quality concrete pavement, referred to as High Performance Concrete Pavements (HPCP), which could be in service longer and have lower maintenance and life cycle costs. General criteria were established by federal and state highway agencies to help in the design of these more durable and economical concrete pavements. This higher quality concrete pavement should incorporate recycled waste products, and utilize innovative construction equipment and procedures. These pavements should also have a shorter construction time and an ultra-smooth ride quality surface. With these criteria in mind, investigations have been launched to discover methods for improving the quality of concrete pavements. One area of interest involves the use of ground granulated blast furnace slag (GGBFS) as a cementitious material in concrete pavement.

High Performance Concrete containing GGBFS has been used in the construction of structures for many years. Its use in pavement systems is a recent development in the United States, and the practice is not very widespread. Information regarding the actual field performance and benefits of using HPC containing GGBFS in pavements systems is not readily available. Therefore, highway engineers need more information about the performance of these pavements in order to design more efficient pavement systems. The performance of concrete pavements is dependent on many factors, including

environmental effects, the rate of traffic loading, and subbase conditions. The determination of how these factors affect the performance of the pavement is very difficult. However, the collective efforts of agencies and universities around the world can provide a better understanding of HPCP and the effects of selected factors on pavement performance.

This report investigates the effect of GGBFS on the behavior and properties of a HPCP as determined from field and laboratory tests. It presents results of an estimation of early concrete strength using the maturity method, as well as a HIPERPAVE™ analysis. The data was collected from four rigid pavement sections. Three of these sections were constructed with high performance concrete containing GGBF slag, and one was constructed with normal concrete. The sections were constructed in close proximity to each other and possessed similar subbase and drainage systems. All concrete used in the highway construction complied with Ohio Department of Transportation's (ODOT) specifications. Each of these sections was instrumented identically to monitor the strain and temperature present at different locations in the pavement. Profiles of the slabs in all the sections were also collected during the early stages of curing.

1.2 GGBFS as a Cementitious Constituent in Concrete

Blast furnace slag is a byproduct of iron production. The blast furnace produces molten slag from iron oxide, fluxing stone (limestone), and fuel (coke). The iron slag floats on top of the molten iron, and both are periodically removed from the furnace at temperatures of about 1500°C (2732°F). The main constituents of the slag are silica and

alumina from the iron ores; these combine with calcium and magnesium oxide from the fluxing stone.

The composition of the slag and rate of cooling determines the cementitious properties of the slag. To maximize these properties, the slag must be cooled rapidly after removal from the furnace. This rapid cooling or quenching minimizes crystallization and converts the molten slag into grain-sized particles that are then dried and ground into GGBF slag. The slag is typically ground to finer-than-Portland cement in an effort to increase reactivity at early ages. Factors that affect the cementitious properties of the slag are the alkali concentration of the reacting system, the glass content of the slag, and the temperature during the early phase of the hydration process.

The hydration of slag in the presence of Portland cement depends on the breakdown and dissolution of the glassy structure by hydroxyl ions that are released during the hydration of PCC. Calcium silicate is formed in the hydration of Portland cement, as well as mixtures of Portland cement and GGBF slag. However, GGBF slag hydrates are generally found to have a more gelatinous nature than Portland cement hydrates; this characteristic adds density to the cement paste.

The addition of GGBF slag to concrete has numerous effects on the properties of the concrete. Research has shown that concrete containing GGBF slag is easier to work and place. This can be attributed to the smooth dense surface of the GGBF slag particles. In this situation, the GGBF slag particles absorb less water and there is a higher paste content, which increases the viscosity of the mixture. Concrete containing GGBF slag also requires a longer curing period, the extent of which is dependent on factors such as the initial curing temperature, the water to cementitious material ratio, the proportion of

blend used, the addition of fly ash, and the characteristics of the Portland cement. Temperatures above 29°C (85°F) generally show little, if any, change in setting time. However, lower temperatures involve a significant reduction in the setting time. This can be remedied by the use of accelerating admixtures such as calcium chloride.

Proper curing conditions are needed for concrete to obtain its desired strength regardless of the cement or cementitious material used in the mixture. Concrete containing higher than 30% GGBF slag is more susceptible to poor curing conditions (Fulton, 1976). A relatively lower strength at early ages (1 to 3 days) is typical in concrete containing GGBF slag. Strength development is dependent on factors such as the proportion of GGBF slag used, the type or grade of GGBF slag, and the curing temperature. At an early age, higher strength has been observed in PCC-GGBFS concrete that had higher curing temperatures. Blends of 40 to 50% of highly reactive GGBF slag have been found to develop the highest 28 day strength. Above 50%, there is generally a reduction in the 28 day strength.

The use of GGBF slag in the PCC mixture reduces the temperatures during the curing process. GGBF slag also reduces the permeability and increases the sulfate resistance of mature concrete. There is essentially no difference in the resistance to freeze-thaw cycles and to de-icing chemicals. The effect of GGBF slag on creep modulus and shrinkage is inconclusive; some studies indicate an increase, while others have found no change.

1.3 Literature Review

There has been some research on the use of GGBF slag as a partial replacement to Portland cement in concrete mixtures for building and bridge construction. Currently,

more research is being conducted on pavement systems that contain PCC with GGBF slag. The following provides a review of articles and papers that are relevant to this research.

Miura and Iwaki (2000) investigated the effect of mixture proportions and curing methods on the strength development of concrete incorporating high levels of GGBF slag at low temperatures. Test parameters included the percentage of cement replaced by GGBFS (50, 60, 70, and 80% by mass); the curing method (water curing, sealed curing, and air curing) and temperature (20 and 5°C) (68°F and 41°F); and the specific surface area measured by the Blaine method (400, 600, and 800 m^2/kg) (1953, 2930 and 3906 ft^2/lb.). The test results demonstrated that the strength development at early ages of GGBFS mortar cured at 5°C (41°F) is lower than that of plain mortar. The periods of heat curing suitable for each mixture proportion and the strength development after heat curing were also examined. The test results indicated that GGBFS concrete with a specific surface area of 400 m^2/kg (1953 ft^2/lb) had serious problems with strength development at early ages and low curing temperatures. Conversely, GGBFS concrete with a specific surface area of 800 m^2/kg (3906 ft^2/lb) had no strength development problems at early ages, even when cured at 5°C (41°F). Overall, heat curing seemed to have an adverse effect on strength development, particularly at later ages.

Zhang et al. (1999) investigated the effects of curing methods on the compressive strength of concrete incorporating supplementary cementing materials, such as GGBFS, fly ash, and silica fume, as well as the resistance of the concrete to chloride-ion penetration by curing the concrete under wet burlap, exposing it to the laboratory air, and using one of three different of curing compounds. They also investigated the effect of the

water-cement ratio and the type of supplementary cementing materials and found that the compressive strength at 7 and 28 days of PCC incorporating silica fume and GGBFS with a w/c ratio of 0.32 was not affected by the curing method. Their results also indicated that the penetration of chloride ions was also not affected. However, concrete cured under wet burlap demonstrated higher compressive strengths at 91 days than concrete cured with curing compound. In general, the type of curing compound used did not significantly affect either the compressive strength of the resistance or the concrete to chloride-ion penetration.

1.4 Objectives

The objectives of this investigation were to determine the influence of GGBF slag on the curing process of a HPCP and on the performance of the pavement when subjected to environmental and dynamic loading. This has been accomplished through the collection of field data on the strain, temperature, and displacement that develops in HPCP incorporating GGBF slag. Laboratory tests have been used to determine the effect of GGBF slag on PCC material properties.

1.5 Outline

This report is organized as follows:

Chapter 2 provides a description of the site location and a brief description of the project background. The instrumentation and a detailed layout are given, as well as a description of the equipment test procedures, and data collection methods.

Chapter 3 provides an analysis of the results of the maturity method used to assess the strength development of the concrete. The results of the HIPERPAV analysis are also given.

Chapter 4 provides an analysis of field data.

Chapter 5 provides summary and conclusions for this research and also gives implementations and recommendations for future research.

Chapter 2 Site Description and Layout; Pavement Base and Instrumentation

2.1 Project Background and Site Layout

In March 1996, sections of U.S. Route 50 between the City of Athens and U.S. Route 7 in southeastern Ohio were reconstructed. This reconstruction consisted of the replacement of the deteriorated two-lane roadway with a divided four-lane rigid pavement highway. The Ohio Research Institute for Transportation and the Environment (ORITE) along with the Ohio Department of Transportation (ODOT) and the Federal Highway Administration (FHWA), made arrangements to have four sections of the new pavement instrumented and monitored in an effort to obtain field performance data for this experimental rigid pavement technology. High Performance Concrete that incorporated Ground Granulated Blast Furnace Slag (GGBFS) as a partial replacement of Portland cement was used in the construction of three sections of the new pavement. For comparison, one section was constructed of PCC without GGBFS, and is referred to as "standard concrete pavement" (SP). This data can be used to help highway engineers understand the effects of using GGBF slag in pavement systems.

The four instrumented sections were identified during Phase I of the project, which consisted of the reconstruction of 10.5 km (6.5 miles) of roadway starting just outside the City of Athens and ending near Guysville. The highway is located in the flat alluvial bed of the Hocking River, which flows about 61 meters (200 feet) south of the roadway at the instrumented sections. Approximately 91 to 183 meters (300 to 600 feet) north of the roadway, the terrain consists of small low-lying hills.

The four sections on the project were identified as HP1, HP2, and HP3 for the high performance sections and SP for the standard concrete section. The HP1 and HP2 sections were located on the eastbound lanes of the highway and were constructed in October 1997. These two sections were constructed adjacent to each other. The HP3 and SP sections were constructed on the westbound lanes of the highway 1.4 km (0.85 miles) west of the HP1 and HP2 sections, and were placed in October of 1998. Sections HP3 and SP were approximately 91 meters (300 feet) apart. All instrumented slabs were located in the right driving lane of the highway. Figure 2.1 shows a schematic of the site with the test sections identified by start and end station numbers.

Figure 2.2 shows a typical cross-sectional drawing of the pavement and drainage system used in the new pavement. This layout was typical throughout the entire construction project except in areas where special sections were needed, such as super elevated sections in the curves. The new pavement utilized standard 254 mm (10 in.) thick JRCP with 3.7 meter (12 foot) wide lanes that sloped 15.6 mm/m (3/16 in/foot) away from the center of the highway. The highway consisted of two lanes in each direction with 3.1 meter (10 foot) and 1.2 meter (4 foot) wide shoulders on the outer and inner edges of the lanes, respectively. The slope of these shoulders was 42 mm/m (½ in/foot) away from the driving lanes. Transverse joints ran perpendicular to the direction of traffic flow and were evenly spaced at 6.4 meters (21 feet) apart.

Figure 2.2 also shows the locations of the pipe underdrains that collected runoff from the bases. A four-inch-diameter pipe underdrain was placed approximately 457 mm (18 in.) below the New Jersey/Iowa Base. Two 102 mm (4-in.) diameter pipe

underdrains were placed at either end of the section, approximately 762 mm (30 in.) below the dense graded aggregate base (DGAB), ODOT 304.

Figure 2.1 Schematic Plan of the US50 Project Site

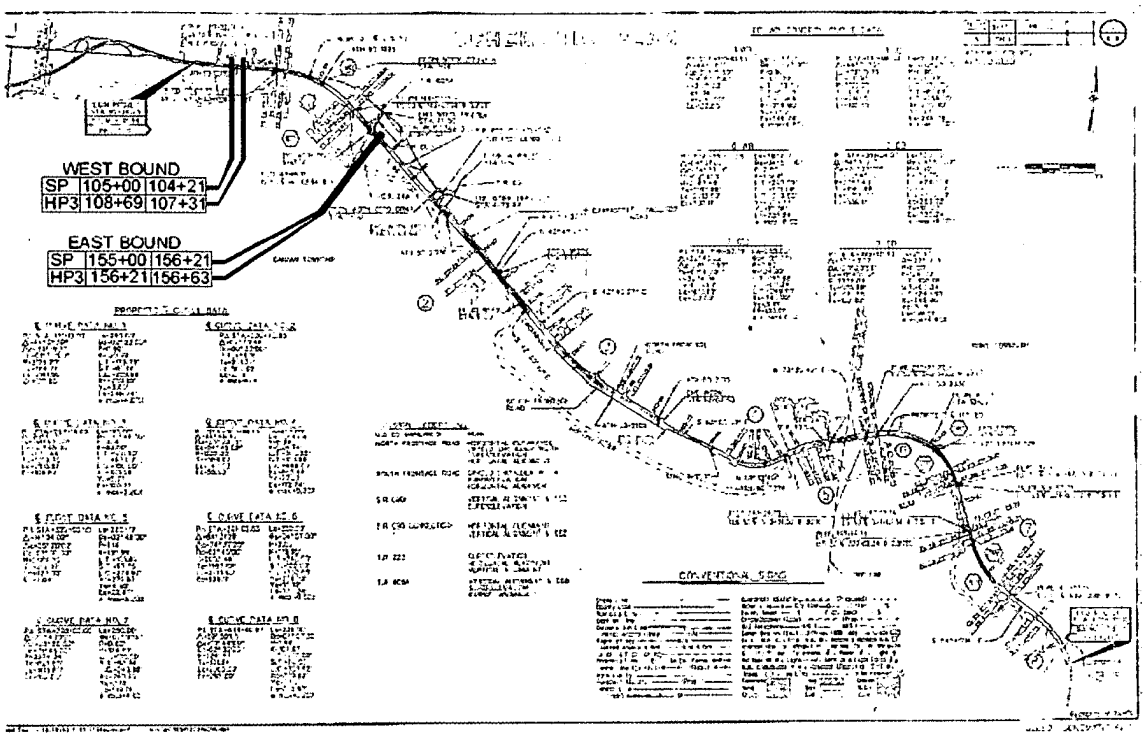

Figure 2.2 Pavement and Drainage System Cross Section

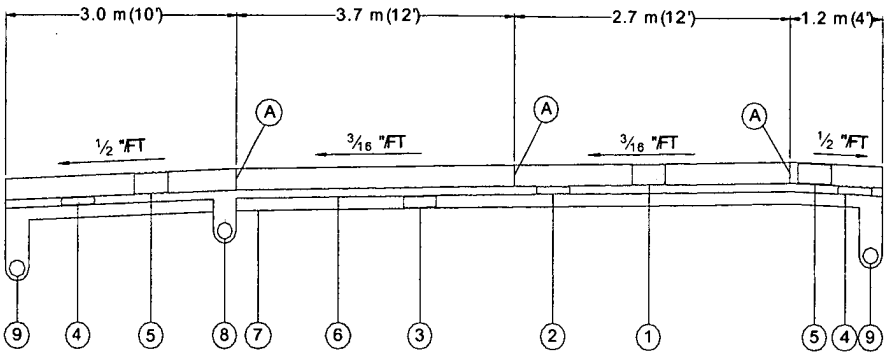

(1)	10" Reinforced Pavement	(6)	Bituminous Prime Coat
(2)	4" Non-stabilized Drainage Base, Type NJ	(7)	Subgrade Compaction
(3)	6" Aggregate Base (Odot Item 304)	(8)	4" Shallow Pipe Underdrain
(4)	4" Aggregate Base (Odot 304)	(9)	4" Pipe Underdrain
(5)	10" Plain Concrete Pavement	(A)	Longitudinal Joint

2.2 Materials

Concrete reinforced with wire mesh was used for the driving lanes, while plain concrete was used for the shoulders. Concrete classified as high performance concrete was used for the construction of three sections of the project, and one section was constructed with standard concrete. Table 2.1 shows the mix design for both types of concrete used in the construction of the highway. Concrete placed between stations 94+34.25 and 104+40 was proportioned in accordance to Item 499 in the ODOT Construction and Materials Specifications for Class C concrete. The remainder of the pavement was constructed with concrete proportioned as specified in Item 499 of the ODOT Construction and Materials Specifications with the following modifications:

Use of proportioning options 1 and 2 in Item 499 was not permitted. Portland cement content was allowed to be reduced by as much as 30-kg/m^3 with the substitution of an equivalent volume of aggregate and the addition of an appropriate water-reducing admixture. Cementitious materials content consisted of a combination, by weight, of a minimum of 75 percent Type I Portland cement (701.04 or 701.01), and a maximum of 25 percent ground granulated blast furnace slag, ASTM C 989, grade 100 or 120.

Admixtures used in the High Performance Concrete mix included Master Builders Master Pave N-Type, a water reducer; and Master Builders Pave Air 90, an air entrainer. Thermal expansion tests were conducted at the Turner Fairbanks FHWA Concrete Lab on core samples taken from the test sections. Results are summarized in table 2.2.

Table 2.1 Concrete Mix Designs

High Performance Concrete Mix Design		Normal Pavement Concrete Mix Design	
Components	Weight per cubic meter (per cubic yard)	Components	Weight per cubic meter (per cubic yard)
Fine Aggregate	847 kg (1428 lb.)	Fine Aggregate	762 kg (1285 lb.)
Coarse Aggregate	810 kg (1365 lb.)	Coarse Aggregate	967 kg (1630 lb.)
Cement	244 kg (412 lb.)	Cement	356 (600 lb.)
Water	187 kg (316 lb.)	Water	178 kg (300 lb.)
GGBF slag	82 kg (138 lb.)	GGBF Slag	N/A
Total Weight	2172 kg (3661 lb.)	Total Weight	2263 kg (3815 lb.)
Water Reducer	2 oz/cwt	Water Reducer	-
Air Entraining	4.2 oz/cwt	Air Entraining	-

A free drainage base was used for the new pavement system. In the eastbound lanes, the base consisted of 4 inches of a non-stabilized New Jersey Base (NJ) on top of 6 inches of DGAB. In the westbound lanes between stations 110+50 and 374+00 in the driving lane and between stations 98+00 and 397+00 in the passing lane, 4 inches of non-stabilized Iowa Base (IA) were placed on top of 6 inches of DGAB. NJ was used in all other locations in the westbound lanes. ODOT Item 304 was used for the DGAB. Table

2.3 lists the sieve analysis specifications for the DGAB, New Jersey Base, and Iowa Base. A thin bituminous prime coat was placed between the base and subbase, applied at a rate of 1.8L /m^2 (0.4 Gal / Yd^2).

Table 2.2 Thermal Expansion Coefficients

Test Section	Station	Thermal Expansion (μ Strain/°K)
HP1/2	156+92	11.9
HP3	106+48	12.1
SP	104+48	11.8

Figure 2.3 shows a plot of the grain size distribution of samples taken from the New Jersey Base used on U.S. Route 50, along with the ODOT grain size distribution specifications to help determine if the sample falls with the given specifications. The result of the sieve analysis on the New Jersey Base sample is listed in Table 2.4.

Table 2.3 ODOT Specification for Aggregate Base

ODOT 304 DGAB		Iowa Base		New Jersey Base	
Sieve Size	Total % Passing	Sieve Size	Total % Passing	Sieve Size	Total % Passing
50 mm	100	25 mm	100	38 mm	100
25 mm	70 ~ 100	12.5 mm	50 ~ 80	25 mm	95 ~ 100
19 mm	50 ~ 90	2.36 mm	10 ~ 35	12.5 mm	60 ~ 80
4.75 mm	30 ~ 60	300 μm	0 ~ 15	4.75 mm	40 ~ 55
600 μm	9 ~ 33	75 μm	0 ~ 16	2.36 mm	5 ~ 25
75 μm	0 ~ 13			1.18 mm	0 ~ 8
				300 μm	0 ~ 5

Figure 2.3 Grain-Size Distribution Curve for New Jersey Base

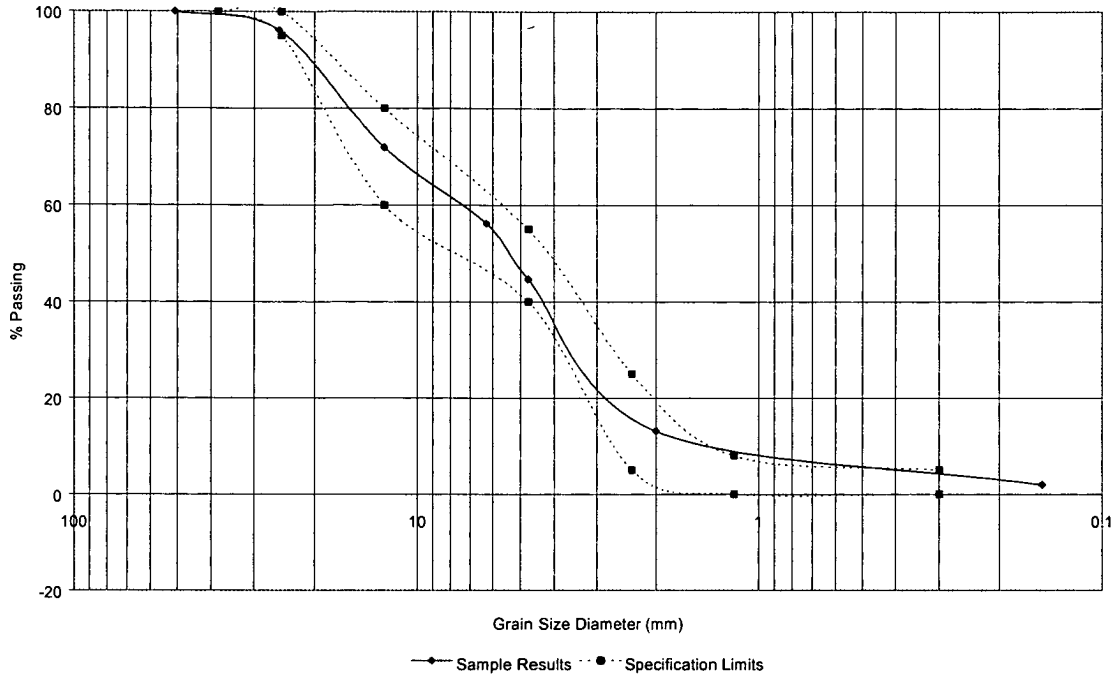

Table 2.4 Sieve Analysis Results for New Jersey Base

Sieve Number	Sieve Opening (mm)	Weight Retained (gm)	Percentage Retained	Cumulative Percentage Retained	Percentage Passing
2 in	50.80	0.00	0.00	0.00	100
1 in	25.40	40.60	3.87	3.87	96.13
½ in	12.5	254.60	24.25	28.12	71.88
¼ in	6.25	164.90	15.70	43.82	56.18
No. 4	4.75	120.70	11.50	55.32	44.68
No. 10	2.00	331.10	31.53	86.85	13.15
No. 100	0.15	117.60	11.20	98.05	1.95
Pan	-	20.50	1.95	100	-

Table 2.5 lists results provided by ODOT for sieve analysis tests conducted on IA base samples.

Table 2.5 ODOT Sieve Results for IA Base

Sieve Size	Total % Passing
38 mm (1.5 inches)	100
25 mm (1 inch)	98
19 mm (0.75 inches)	87
12.5 mm (0.5 inches)	63
9.5 mm (0.375 inches)	58
4.75 mm (No. 4)	42
2.36 mm (No. 8)	12
1.18 mm (No. 16)	6
300 μm (No.50)	4

The concrete joints were either unsealed or sealed using a variety of sealant materials, as shown in Table 2.6.

Table 2.6 Sealant Types

Manufacturer	Sealant Type
Crafco	221 ASTM 3405 Hot Pour
	903-SL Self Leveling Silicone
	444 ASTM 3406 Hot Pour
	902 SL Silicone
Dow	888 Silicone
	888-SL Self Leveling Silicone
	890-SL Self Leveling Silicone
Watson Bowman	WB-812 Compression Seal
	WB-867 Compression Seal
Delastic	V-687 Compression Seal
Tech Star	W-050

2.3 Instrumentation and Layout

An acclaimed instrumentation and layout procedure for obtaining accurate pavement response data has been developed by ORITE, and was used for the U.S. Route 50 test project. This procedure allows for the instruments to be installed within the

pavement itself, while maintaining the integrity of the delicate gages during the harsh construction process.

The instrumentation in a typical section layout consisted of 3 different types of gages strain gages to monitor strain within the slab, thermocouples to monitor temperature within the slab, and Time Domain Reflectometry (TDR) probes to monitor subsurface moisture. Other equipment was used to record temperature, changes in the shape of the slabs, and the response of the pavement to dynamic loads. The sections that follow provide a more detailed description of the various instruments and equipment used in this project.

2.3.1 Strain Gages

Pavement strain was collected using three different types of strain gages: the VCE-4200 vibrating wire strain gage, the EGP-5-120 embedment strain gage, and the TML KM-100B strain transducers. The arrangement and orientation of the strain gages is shown in Figures 2.4 and 2.5. The strain gages were placed in the wheel path and center of the lane, oriented in the longitudinal and transverse direction. The wheel path was assumed to be approximately 0.9 m (3 feet) in from the edge of the pavement. Two gages were placed at each location, one 38 mm (1.5 in.) below the surface of the slab, and the other 38 mm (1.5 in.) above the base of the slab. Metal stands were used to hold the gages in position within the concrete and a metal box was placed around the gages to protect them during construction. After the concrete was placed and the paver had passed, the metal boxes were removed from around the gages.

Figure 2.4 VCE 4200 Vibrating Wire Strain Gage and KM 100B Strain Gage Layout

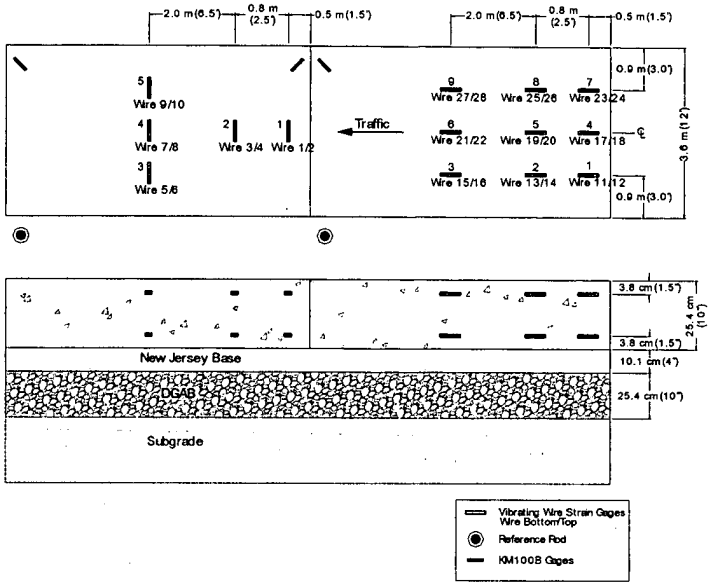

Figure 2.5 EGP-5-120 Embedment Strain Gage Layout

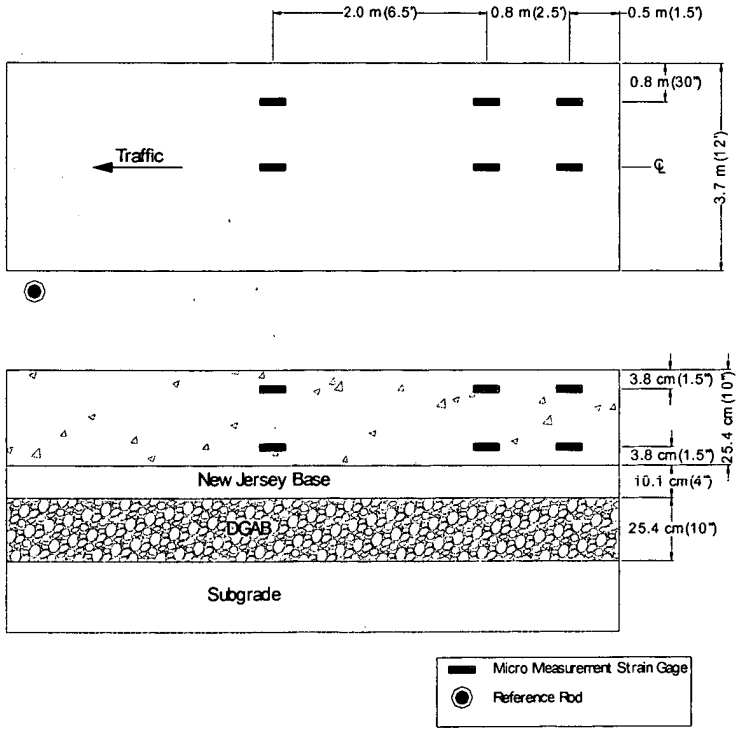

The VCE-4200 vibrating wire strain gages, manufactured by Geokon Inc., of Lebanon, NH, are made for direct embedment into concrete and are typically used in foundations, piles under bridges, dams, tunnels and containment vessels. The gage consists of two parts: a rubber-coated steel tube that houses the steel wire and a plastic cylinder that houses and protects the electronics. These gages have an active gage length of 152 mm (6 in.) and can measure a maximum of 3000 microstrains with a sensitivity of 1 microstrain. Strain measurements are performed by a length of steel wire tensioned between the two end blocks that are embedded in the concrete. When the concrete mass deforms, causing a change in strain, the two end blocks will move relative to each other; this in turn will cause the tension in the wire to change. The wire tension is measured by the electromagnetic coil that "plucks" the wire and measures the resonant frequency of the vibration. Vibrating wire gages are only capable of measuring static strains.

The use of the resonant frequency as an output signal is what gives the vibrating wire strain gages an advantage over conventional electrical resistance types. Since cable resistance, contact resistance or leakage does not affect the signals send by the strain gages longer cable lengths can be used.

A thermistor, placed in the plastic cylinder along with the plucking coil and provided with each gage, enables temperature to be measured. Measuring temperature when the gage is installed allows for the compensation of change in the length of the steel wire due changing temperatures.

Twenty-eight vibrating wire strain gages were placed in each section of the highway, 18 oriented longitudinally and 10 oriented transversely. These gages were

placed in the center of the slab. Gages were located 0.5 m, 1.2 m, 3.8 m (1.5, 4, and 12.5 feet) (in the direction of traffic) from the transverse joint.

Measurements Group Inc. of Raleigh, North Carolina manufactures the model EGP-5-120 strain gage designed for direct embedment in concrete. This gage consists of a K-alloy strain gage that is mounted on a carrier. The sensing grid is constructed of a nickel-chromium alloy similar to Karma foil, and is enclosed in a proprietary polymer concrete that protects it from physical damage and moisture. The sensing grid is also self-temperature-compensated to minimize errors in strain readings caused by temperature changes. The normal operating temperature for the EGP-5-120 is –5°C to +50°C (23°F to 122°F); however, the gage is stable in the extended temperature range of –30°C to +60°C (-22°F to 140°F). The EGP-5-120 strain gage is 127 mm (5 in.) long, 17.8 mm (0.7 in.) wide, and 10.2 mm (0.4 in.) thick. It has a four inch average active gage length, and a gage factor of 2.05 +- 1.0%. Strain is measured by changes in the electrical resistance that is caused by strain changes in the concrete mass. This gage is used for pavement response measurement due to dynamic loading.

Twelve Micro-Measurements EGP-5-120 strain gages were placed in each section. These were located in similar locations as the vibrating wire gages, but on a different slab. The EGP-5-120 gages were installed in the outside, or right wheel, path.

Tokyo Sokki Kenkyojo manufactures the model KM-100B strain gage for direct embedment in concrete. These gages are designed to measure strain in materials such as concrete that undergoes a transition from a compliant to a hardened state. The TML KM-100B strain transducer contains four separate strain gages arranged in a 350 ohm full Wheatstone bridge configuration with a gage factor of 2.00. The protective casing of this

gage is constructed of a rubber-coated sleeve with two metal flanges at either end. The TML KM-100B operates in a temperature range of –20°C to +80°C (-6°F to 176°F). The gage length is approximately 101.6 mm (4 in.) and a 19 mm (¾ in.) diameter. Strain is measured by electrical resistance using four active electrical strain gages, while temperature is measured using one active strain gage and three external resistors. TML KM-100B strain transducers are capable of measuring both dynamic and static strain.

Six TML KM-100B strain transducers were placed in each highway section. These gages were placed in the corners of the slab and oriented at a 45-degree angle to the edges.

2.3.2 Thermocouples

Thermocouples are constructed of two different types of metal that are joined at one end, and open at the other. The thermocouples used in this project consisted of copper and constantan wires, and are referred to as "T" type thermocouples. The temperature at the ends where the wires connect is measured by inducing a small voltage through the wires, each of which has a different number of free electrons at a specific temperature. The electromotive force (EMF) at the output end is a function of the temperature at the closed end. As the temperature rises, the EMF goes up.

Thermocouples were installed at various locations and depths throughout the slab. Each location had five single thermocouples that were tied to a steel rod that held them at depths of 51, 127, 203 and 229 mm (2, 5, 8 and 9 in.) below the surface of the pavement. Several thermocouples were placed on the stand that held the strain gages. This setup was used to verify the temperature at that gage location.

2.3.3 Time Domain Reflectometry Probes

Campbell Scientific, Inc. has developed a system that measures in-situ soil moisture using time domain reflectometry (TDR). TDR probes use an electric pulse that is sent though coaxial cables to the probes located in the soil. The moisture content of the soil around the probe influences the velocity of the wave that is reflected. The velocity of the wave is inversely proportional to the dielectric constant of the soil, a property of the soil that is influenced by the moisture content.

Three TDR probes were placed in five different locations in the subbase layer beneath the DGAB, Figure 2.6. The center of the driving lane of slab 5 was located and marked using stringlines. The first TDR location was 3.2 m (10.5 feet) along the center stringline. The second was in the middle of slab 5 at the wheel path. The third was under the transverse joint between slabs 5 and 6. The fourth location was under the center of the last transverse joint of slab 6. The fifth location was 3.4 m (11 feet) from the stringline under a sealed transverse joint. Specific locations are listed in Table 2.7.

Table 2.7 TDR Probe Locations

TDR Location #	Station	Distance from Shoulder Edge
1	156+51.5	183 m (6 ft.)
2	156+51.5	152.4 m (6 ft.)
3	156+62	152.4 m (6 ft.)
4	156+83	1.33 m (6 ft.)
5	160+19	1.83 m (6 ft.)

The TDR probes were installed before the 102 mm (4 in.) layer of New Jersey Base was placed. TDR holes were excavated to the correct depth with a 305 mm (12 in.) auger using the ODOT boring rig. A 356 mm (14 in.) diameter hole was cut out of a sheet of cardboard and the bit was placed inside. The cardboard caught the displaced soil and prevented it from falling back into the hole. This soil was placed in containers and set aside for later use. A straight edge was placed across the top of the hole to measure the correct depths for the TDR probes after the hole was completed. The TDR probes

were placed parallel to each other at 610, 305, and 152.44 mm (24, 12, and 6 in.) below the DGAB layer. The soil from the containers was replaced and compacted in between the probes in 38 mm (1.5 in.) lifts. The TDR probes cables were routed in a shallow trench in the 152.4 mm (6 in.) layer of DGAB to the 10 foot shoulder. A diagram of TDR positions is given in Figure 2.6. Table 2.8 contains a list of TDR wire numbers and corresponding locations.

Table 2.8 TDR Probe Wire Numbers and Locations

TDR Location	Station	Depth	Wire Number
1	156+51.5	152.4 mm (6 in.)	7
1	156+51.5	304.8 mm (12 in.)	8
1	156+51.5	609.6 mm (24 in.)	9
2	156+51.5	152.4 mm (6 in.)	10
2	156+51.5	304.8 mm (12 in.)	14
2	156+51.5	609.6 mm (24 in.)	15
3	156+62	152.4 mm (6 in.)	16
3	156+62	304.8 mm (12 in.)	17
3	156+62	609.6 mm (24 in.)	18
4	156+83	152.4 mm (6 in.)	19
4	156+83	304.8 mm (12 in.)	20
4	156+83	609.6 mm (24 in.)	21
5	160+19	152.4 mm (6 in.)	4
5	160+19	304.8 mm (12 in.)	5
5	160+19	609.6 mm (24 in.)	6

Figure 2.6 Locations of TDR Probes

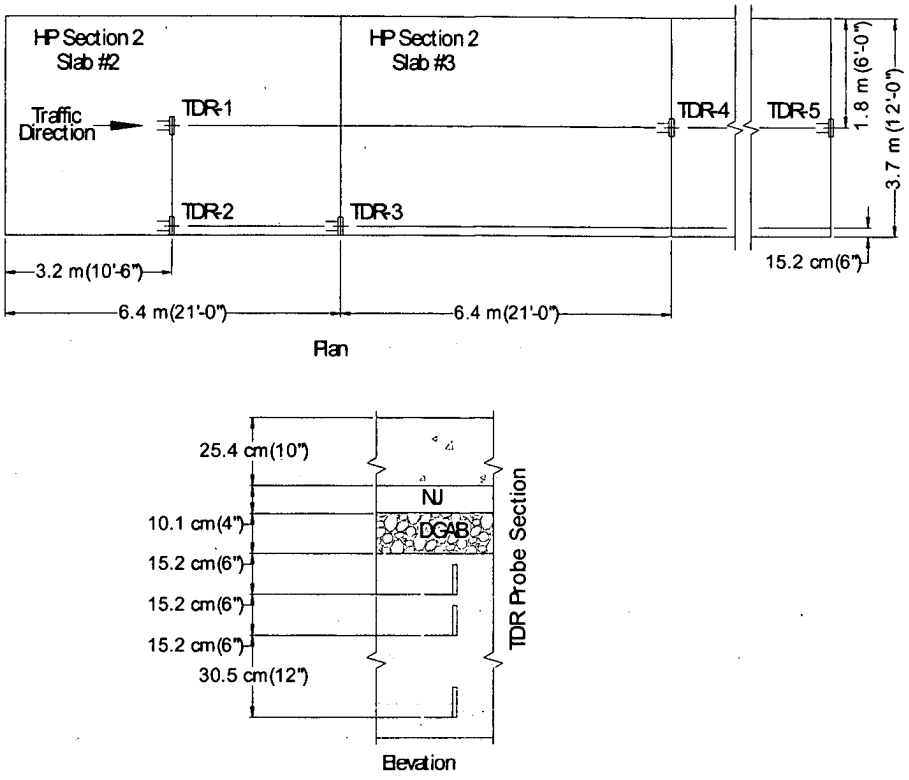

2.4 Dynamic and Environmental Testing

To determine the response of the pavement, dynamic and environmental tests were conducted. Changes in slab profile due to the environment were also monitored. Equipment used in these tests included a Falling Weight Deflectometer, and a Dipstick® 2000 road profiler. A Humboldt maturity meter was used to monitor the curing process. The pavement response was monitored from the time the concrete was placed, through the early stages of curing, and after the pavement was in service. Attributes of the pavement that were monitored included the strain and temperature within the slabs, and the shape of the slab.

2.4.1 Falling Weight Deflectometer (FWD)

The Falling Weight Deflectometer (FWD) used for dynamic testing, is a nondestructive testing device widely used for pavement testing, research, and construction monitoring. It delivers a transient force impulse to the pavement layers by raising a weight to the desired height on a guide system and dropping it onto the 300-mm diameter circular footplate.

The Model 8000 Dynatest Falling Weight Deflectometer (FWD) used for this research weighs about 1134 kg (2500 lbs) and is a trailer-mounted NDT device capable of being towed by a SUV type vehicle or truck at regular highway speed. The transient pulse-generating device consists of a trailer-mounted frame capable of directing different sets of mass configurations to fall from a predetermined height at right angles to the surface.

For this study, the FWD simulated heavy tire loads on the pavement by imposing a load ranging from 40 kN to 80 kN (9000 lbs to 18,000 lbs) through a 300 mm (11.82-in.) diameter plate. Applied pressures to the pavement ranged from 623 kPa to 1.168 MPa (90.4 psi to 169.4 psi). Geophones connected to the FWD measured the deflection of the pavement -304.8, 0, 304.8, 457.2, 609.6, 914.4 and 1524 mm (–12, 0, 12, 18, 24, 36, and 60 in.) from the applied load. The data was collected and stored on a PC.

For FWD testing, TML KM-100B and EGP-5-120 strain gages were connected to a Megadac data acquisition system by means of screw terminal blocks (STB's). Locations of these gages in the pavement were marked so that loads could be applied directly above them. FWD testing was performed over Micro Measurement EGP-5-120 gages at locations 4, 5, 6, and 7. The gages were then checked and balanced on the Megadac using the appropriate software.

FWD testing was performed on November 6th, 1997 and on December 3rd, 1997. On November 6th, only four locations on HP1 were tested; however, all locations were tested in the HP1 and HP2 sections on December 3rd. FWD testing of the HP3 and SP sections and some locations in the HP1 and HP2 sections was performed in November 1999. FWD testing was also done around transverse joints, both sealed and unsealed.

2.4.2 Humboldt Maturity Meter

The Humboldt concrete maturity meter (System 4101) was used during the curing process, to collect and store temperature and time history data of the slab. The temperature is obtained from thermocouples connected to the meter and embedded in the concrete at the corners, top and bottom of the slab.

2.4.3 Dipstick

The Dipstick® 2000 was used to obtain the slab profile; it has a greater accuracy than traditional rod and level surveys, capable of measurements within one thousandth of an inch. The Dipstick® 2000 consists of an LCD display, two footpads, and a main body that houses a pendulum (inclinometer). The sensor in the profiler is positioned so that its axis and a line passing through the footpads are co-planar. This sensor measures the difference in the elevation of points on which the footpads rest.

Slab profiles were monitored twice a day for the first 14 days of curing using the Dipstick® 2000 road profiler. An eleven by twenty foot box was drawn one foot in from the edge of the slab, as well as diagonals between the corners (Figure 2.7). The profile of this inner perimeter and its diagonal were traversed with the Dipstick® once in the morning, and then again in the afternoon in an effort to determine the effect of the varying

environmental conditions. All data collection and processing was done by a mini notebook computer that was attached to the handle of the Dipstick® 2000.

Figure 2.7 Perimeter Traversed with the Dipstick

2.5 Data Acquisition

Three data acquisition systems were used on this project to execute the programs and to collect, store, and process the data. The particular system was determined using factors such as the gage type and the type of testing, dynamic or environmental. All systems used were wired in the appropriate configuration in accordance with the manufacturer's and ORITE's specifications and tested for accuracy. The systems selected for use on this project have been proven accurate and reliable in previous research projects similar to this one.

2.5.1 Dynamic Testing

Dynamic testing was performed with a Megadac 5108AC acquisition system, from Optim Electronics Corporation, because of its ability to collect data at a rate of 1200 data points per second. The Megadac was connected to personal computer, with software installed to interface with the Megadac. The Megadac consisted of input/output modules that were connected to the gages and a PC via an IEEE-488 communication bus card. The gages were connected to a screw terminal block (STB) that was used to complete the Wheatstone bridge, and then connected to the Megadac. Depending on the gage to be connected to the Megadac, 120 or 350 ohms STB's were used. The KM-100B strain transducers required a 350 ohm full bridge while the EGP-5-120 strain gages required a 120 ohms quarter bridge arrangement. An AD808 FB-1 input module was used to interface between the strain gage STB and the Megadac.

2.5.2 Environmental Testing

The instrumentation and data acquisition systems for the environmental testing were placed and operational before the concrete was poured over the gages. Data was collected throughout the curing process of the concrete in 30 minute intervals. Vibrating wire gages, KM-100B strain transducers, and thermocouple data were collected using the CR7 and CR10 systems from Campbell Scientific, Inc. These systems were connected to an external power source and left in the field, and data was downloaded to a computer every two weeks.

These acquisition systems have the ability to store a greater amount of data than the Megadac system and were installed in weatherproof containers that allowed them to be left on site for extended periods. These systems also have a battery power supply that

may be used if no external power source is available. An IBM compatible PC that contained the PC208 software was used to interface with the data acquisition systems. This software was also used to write the programs that were executed by both the CR7 and CR10 acquisition systems.

The CR7 system was used to collect and store data from the thermocouples and static strain data from the KM-100B strain transducers. The CR7 data acquisition system consisted of a control module, an input/output module, a battery supply, and sensor ports, all housed in an environmentally sealed fiberglass box. The I/O module contained an I/O cards that was used to connect to strain gages, and another specially designed for thermocouples. The I/O module also contained an I/O processor card and a 16-bit analog interface card. Bridge completion for the strain gages was done using external resistors, and an AM416 multiplexer was used to accommodate the larger number of strain gages.

The CR10 data acquisition system was used to collect and store data from the vibrating wire strain gages. This system was comprised of a watertight canister that contained the bulk of the electronics. This watertight canister was placed in an environmentally sealed box along with a battery power supply and an AVW1 vibrating wire interface. Because of the number of vibrating wire gages per section, an AM416 multiplexer was also used on this system.

2.6 Field Observations

The placement of all concrete sections proceeded normally with no unusual circumstances. However, the combination of three factors created a critical condition for the curing of the concrete in the eastbound section. First, as evening approached, the air temperature decreased and reached lows of 3°C during the night. Second, the presence of

GGBF slag cement in the mix slowed down the curing process. Third, the contractor was not able to cut the joints with a regular saw without spalling because the surface of the concrete had not developed sufficient strength. Eighteen hours after placement, cracks had formed randomly in the pavement. Figure 2.8 shows an example of the cracking that occurred in the slab. The contractor changed from a regular saw to a lightweight saw. Use of the lightweight saw enabled joints to be cut, but some spalling was still experienced.

Throughout the 610 mm (2000 ft.) length of pavement, a dozen of the slabs were rehabilitated. Figure 2.9 shows the extent of pavement on either side of a crack that was removed and replaced with a 6 foot wide full depth concrete repair. It should be noted that these temperature conditions and the resulting cracking were not observed in the westbound lanes in 1998. The westbound sections were constructed at temperatures between 8°C and 27°C (46.4°F and 80.6°F).

Figure 2.8 Cracking 18 Hours after Concrete Placement

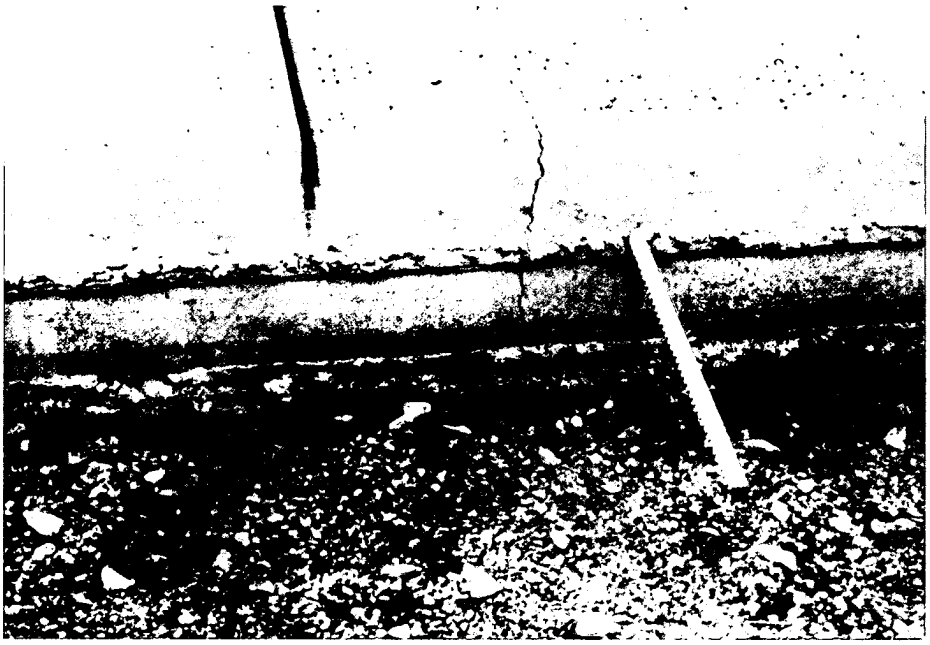

Figure 2.9 Typical Extent of Concrete Removal for Rehabilitation

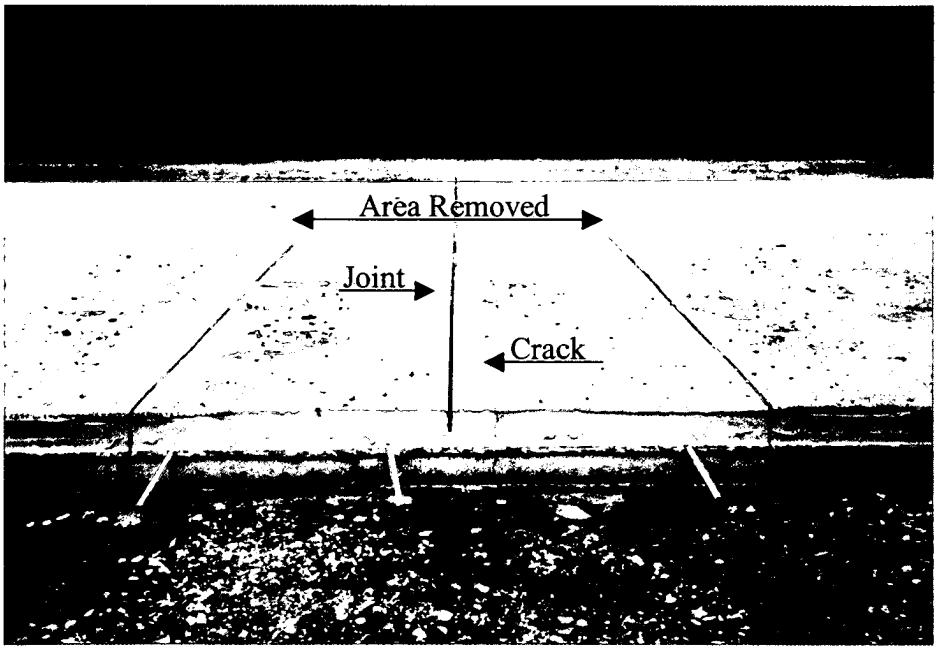

Chapter 3 Analysis of Laboratory Data

3.1 Introduction

Various analytical procedures were used in this investigation for the evaluation of the HP and SP concrete data. This chapter presents the analysis of the laboratory data by the maturity method to determine the strength development of the HP and SP concrete.

3.2 Maturity Method

In accordance with ASTM Standards, a maturity function was determined for estimating the strength development of high performance concrete with GGBF Slag. The maturity function was applied to the temperature history and field strength data of the HP Concrete pavement used in the Route 50 project.

The maturity method is a technique for estimating the strength development of in-place concrete during its curing period by measuring the temperature history of the concrete. The early stage of concrete is defined as an age at which the concrete has gained strength no greater than 50 percent of its 28-day strength while curing at normal temperatures (Guo, 1989; Malhotra, 1991). Estimating concrete strength at early stages using the maturity method can provide results that are as accurate as those from compression tests in the lab. However, no theoretical correlation between the ultimate strength and maturity of concrete can be expected since curing temperatures at early stages impact the ultimate strength (Carino, 1997; Guo, 1989).

Researchers primarily use two equations to calculate the maturity of concrete. Both are described in the ASTM Standard C1074 relative to the maturity method (ASTM, 1987). The first is the famous Nurse-Saul maturity function which is defined as follows:

$$M = \Sigma (T - T_0) \Delta t \qquad \text{Eq. 3.1}$$

where,

M = maturity index (temperature-time factor (degree-hours)

T = average concrete temperature (Δt °C)

T_0 = datum temperature (°C)

Δt = time interval (hours)

This equation is founded on the so-called maturity rule: concrete of the same mix at the same equivalent age has approximately the same strength regardless of the combination of temperature and time (Saul, 1951). Although this equation provides acceptable results under conditions where temperatures do not vary greatly, it has been found inaccurate in situations where the curing temperature varies over a wide range. This subject was addressed by Freiesleben and Pedersen (1977) in a proposed new function (Eq. 3.2), based on the Arrhenius equation and the reaction rate of cement, which computes a maturity index from the recorded temperature history of the concrete.

$$t_e = \Sigma e^{\frac{-E}{R}\left(\frac{1}{T} - \frac{1}{Tr}\right)} \Delta t \qquad \text{Eq. 3.2}$$

where,

t_e = equivalent age at the reference temperature (days)

E = apparent activation energy (kJ / mol)

R = universal gas constant (kJ / (mol · K))

T = average absolute temperature of concrete (K)

T_r = absolute reference temperature (K)

Δt = time increment (days)

Using this equation, the maturity of concrete expressed by the reaction rate of cement was found to be superior to the Nurse-Saul maturity function (Carino, 1997; Guo, 1989). A maturity function from Equation 3.2 was used to calculate the equivalent age of the HP concrete with GGBF slag used in our investigation.

3.2.1 Laboratory Data

Compression tests were performed in the laboratory on the HP concrete mixes with GGBF slag in accordance with ASTM C 192 (1987). The concrete was cured at three different temperatures: 5, 12, and approximately 23° C (room temperature). Both the concrete temperature while curing and the compressive strength at different ages were recorded for room temperature cure.

Six, 6 x 12-inch cylindrical specimens were made, and cured at 23° C. Eleven, 2-inch cubic specimens were used for the 5 and 12° C curing. These specimens were cured in a water bath with assumed isothermal conditions. The compressive strength of the cube specimens was tested at different real ages. Six compressive strength tests for the HP concrete were performed at the room temperature cure, five at the 5° C cure, and 6 at the 12° C cure, for fourteen age groups as detailed in table 3.1.

Table 3.1 Compressive Strength Data of HP Specimens

Age (days)	Compressive Strength in MPa (psi)		
	Room Temp.	5 °C	12 °C
1	6.8 (993)	-	1.8 (255)
1.5	-	1.7 (248)	-
2	-	-	6.1 (879)
3	13.0 (1879)	5.4 (778)	-
4	-	-	8.6 (1248)
6	-	8.7 (1261)	-
7	17.6 (2558)	-	-
8	-	-	14.9 (2166)
14	22.5 (3258)	-	-
16	-	-	16.8 (2437)
18	-	14.9 (2154)	-
28	25.3 (3671)	-	-
32	-	-	22.3 (3239)
48	-	19.9 (2885)	-

In an effort to use all of the available compressive strength data for the maturity function, a ratio was used to convert the compressive strength of the cube specimens to the compressive strength of the cylindrical specimens. This involved dividing the compressive strength of the cube by 1.08 for the effect of size differences, and by 1.15 for the effect of height/diameter ratio differences (Neville, 1997).

From this table, a temperature curve (Figure 3.1) for room temperature compressive strengths was created. This curve is very similar, within the first 24 hours, to a temperature curve created from data collected in 1997 at the bottom of the HP1 section of the Route 50 project (Boltz, 1998).

Figure 3.1 Concrete Temperatures versus Time of the Room Temperature Curing

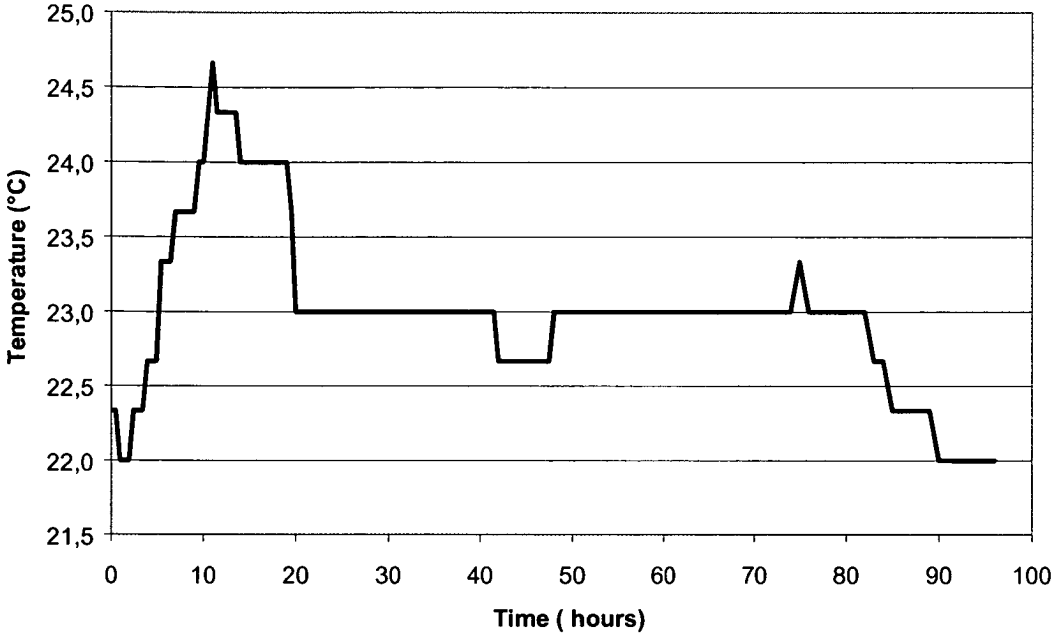

3.2.2 Strength versus Equivalent Age

The equivalent age of the HP concrete was calculated from equation (3.2) and the following assumptions were made. First, the apparent activation energy was estimated from different sources (Carino and Tank, 1992; Gauthier and Regourd, 1982) by using the following relationship:

$$E = 43.0 + 1.47\ (20 - T)\ kJ / mol$$

when $T < 20°C$

$$E = 43.0\ kJ / mol, \text{ when } T \geq 20°C$$

However, the impact of the apparent activation energy on the calculated equivalent age is very limited. Second, the reference temperature was assumed to be 23°C. The relationship between the HP concrete strengths from the compressive strength tests and the equivalent age calculated from Equation 3.2 are shown in Figure 3.2.

Figure 3.2 HP Concrete Compressive Strength vs. Equivalent Age

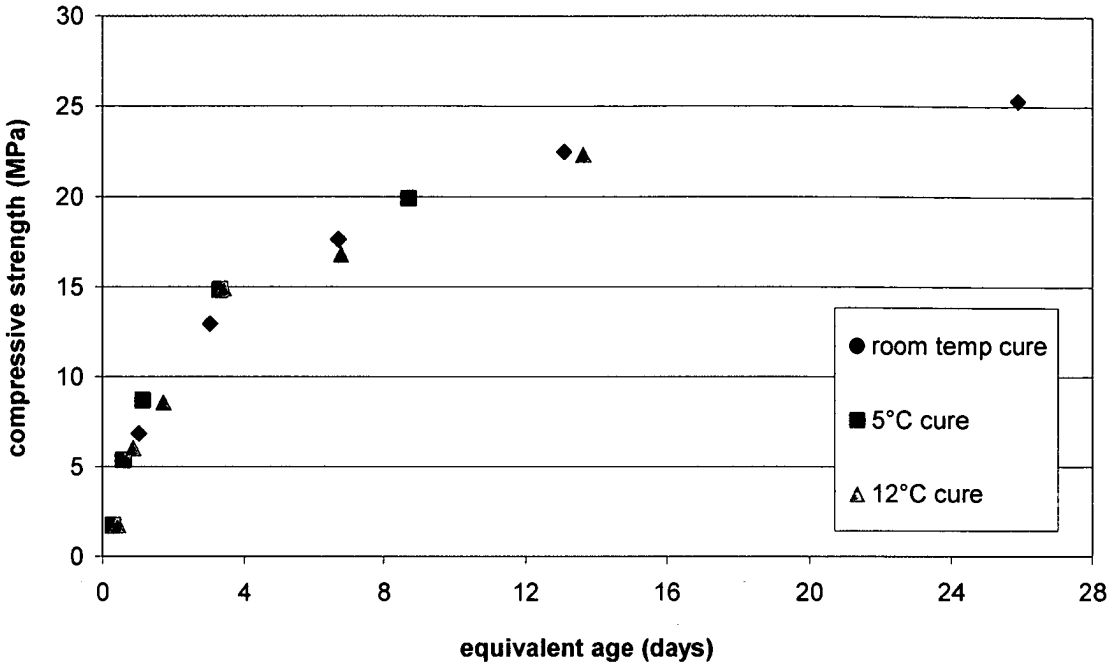

3.3 Estimating Strength of the HP Concrete

Various equations have been used to examine the maturity-to-strength development relationship. A hyperbolic equation has been successfully used for strength gain up to equivalent ages of about 28 days at 23°C (Carino, 1997). Equation 3.3, considered to be the standard, was used in this investigation:

$$S = S_u \frac{k(t - t_0)}{1 + k(t - t_0)} \qquad \text{Eq. 3.3}$$

where,

S = strength at age t in MPa (psi)

S_u = limiting strength in MPa (psi)

k = rate constant

t_0 = age at start of strength development in days

Since the ultimate strength of concrete is not independent of the curing temperature, Equation 3.3 can be further improved. We propose that the correct application of the maturity method is in the estimation of the relative strength rather than the ultimate strength. With regard to the problems predicting the ultimate strength, the relative strength is expressed as a fraction of the strength at an equivalent age of 28 days (Eq. 3.4) (Carino, 1997).

$$\frac{S}{S_{28}} = \beta \frac{k(t - t_0)}{1 + k(t - t_0)} \qquad \text{Eq. 3.4}$$

where,

S = strength at age t in MPa (psi)

S_{28} = strength at age of 28 days in MPa (psi)

k = rate constant

t_0 = age at start of strength development (days)

β = factor describing relative strength gain

The following assumptions were made when using Equation 3.4 for the HP concrete mix designs. First, the strength at an equivalent age of 28 days was estimated to be 25.9 MPa (3,750 psi) relative to the strength development of the room temperature cure. Second, the age at the start of strength development is the age at the time of final setting as determined by the penetration resistance using Method C 403 of the ASTM Standards (ASTM, 1987). For curing at room temperature, the age at the start of strength development was determined to be 6 hours (t_0 = 0.25 days). Third, the rate constant represents the rate at which a chemical reaction occurs at a given temperature, and the determination of the rate constant is the key to developing an accurate maturity function

for a particular concrete mixture. The parameter k in Equation 3.4 has been obtained by least-squares curve fitting to strength versus equivalent age data by several researchers (Carino and Tank, 1992; Guo, 1989). The parameter k was obtained in this investigation from the apparent best-fit curve for the strength versus equivalent age data. The HP Concrete mix design with GGBF slag was equal to 0.26. The value for β (1.14) was determined in the same manner. Substituting these parameters into Equation 3.4 yields Equation 3.5:

$$\frac{S}{S_{28}} = 1.14\,\frac{0.26(t-0.25)}{1+0.26(t-0.25)} \qquad \text{Eq. 3.5}$$

The relative strength versus the equivalent age relationship estimated from Equation 3.3 and the compression test data is illustrated in Figure 3.3.

Figure 3.3 Estimation of the Strength vs. Equivalent Age Relationship

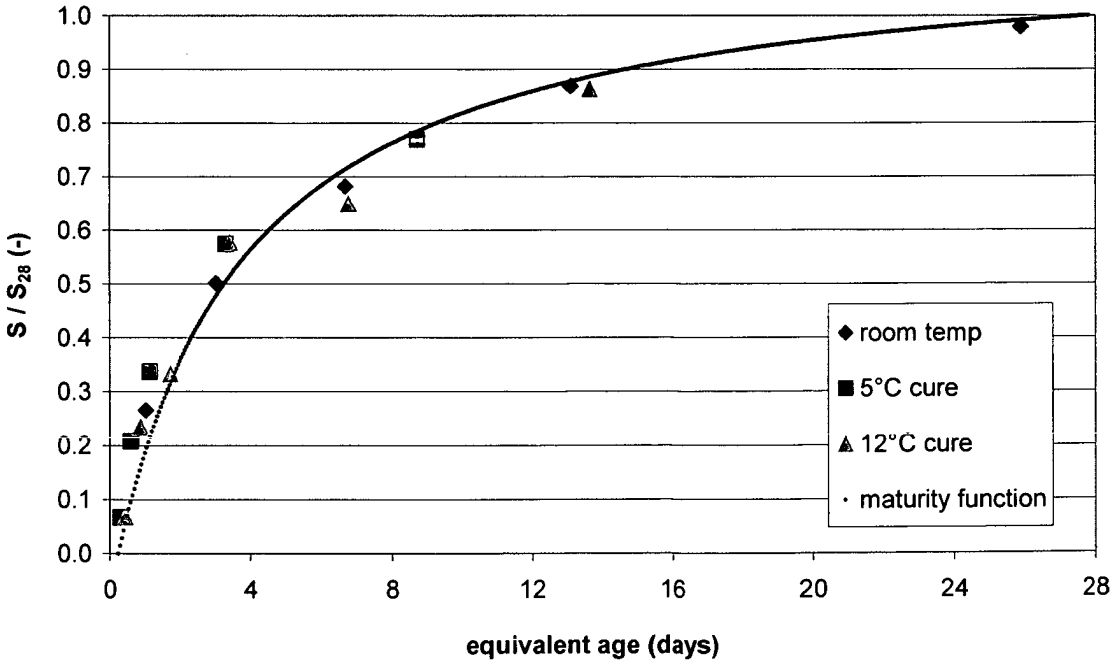

3.4 Application of the Maturity-Strength Development Relationship

Two HP concrete sections were placed in 1997 within the U.S. Route 50 project. Thermocouples were set 1.5 inches and 8.5 inches below the pavement surface of the concrete to measure the temperature of the slabs during curing. Six cylindrical specimens, 6 inches in diameter by 12 inches in height, were made and compression tests were conducted in the field after 7, 22, 28, and 365 days. The specimens remained in the field near the slab until the day of testing. Thus, they cured under similar circumstances as the slab did relative to the surrounding air temperature. The compressive strength data at the varying ages is shown in Table 3.2. Figure 3.4 shows the concrete temperature at one point on the center slab up to the age of 28 days. One line represents the temperature at the top of pavement, and the other represents the bottom temperature (1.5 inches and 8.5 inches below the pavement surface, respectively).

Table 3.2 Compressive Strength Data for HPConcrete Specimens

Age (Days)	Strength in MPa (psi)
7	20.0 (2900)
22	26.2 (3799)
28	27.6 (4002)
365	48.1 (6973)

Figure 3.4 Temperature History of the HP Concrete Slab

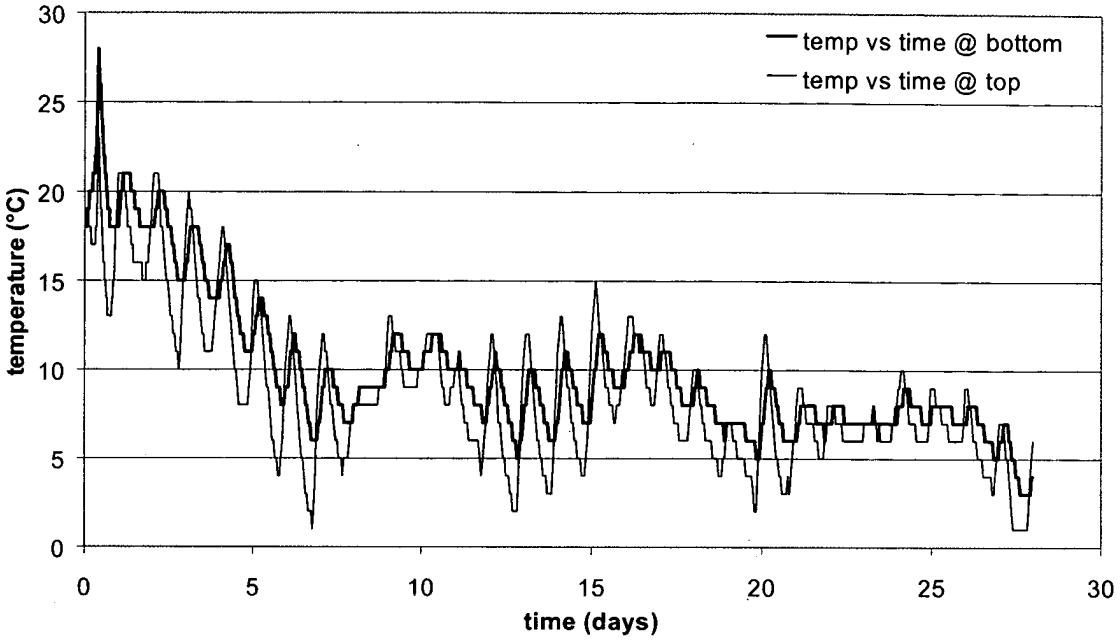

Since the temperatures between the bottom and top of the slab were different, the concrete had different maturities. This raises a question as to what temperature history, i.e. equivalent age, to which the strength data should be set in a relationship. The most reasonable approach was to take the temperature history of the concrete from the bottom of the slab given the 6-inch diameter of the cylinders and the insulating impacts of the molds. The curing conditions of the specimen appeared to vary significantly from the curing conditions 1.5 inches below the pavement surface.

It should be noted that the temperature at the bottom of the slab was measured at two different points, the center and the corner. Thus, each compressive strength coincides with two slightly varying equivalent ages. Figure 3.5 shows the strength versus equivalent age relationship of the specimens, as well as the same relationship estimated from Equation 3.5.

Figure 3.5 Strength vs. Equivalent Age Relationship of Test Specimen and Estimated with Equation 3.5

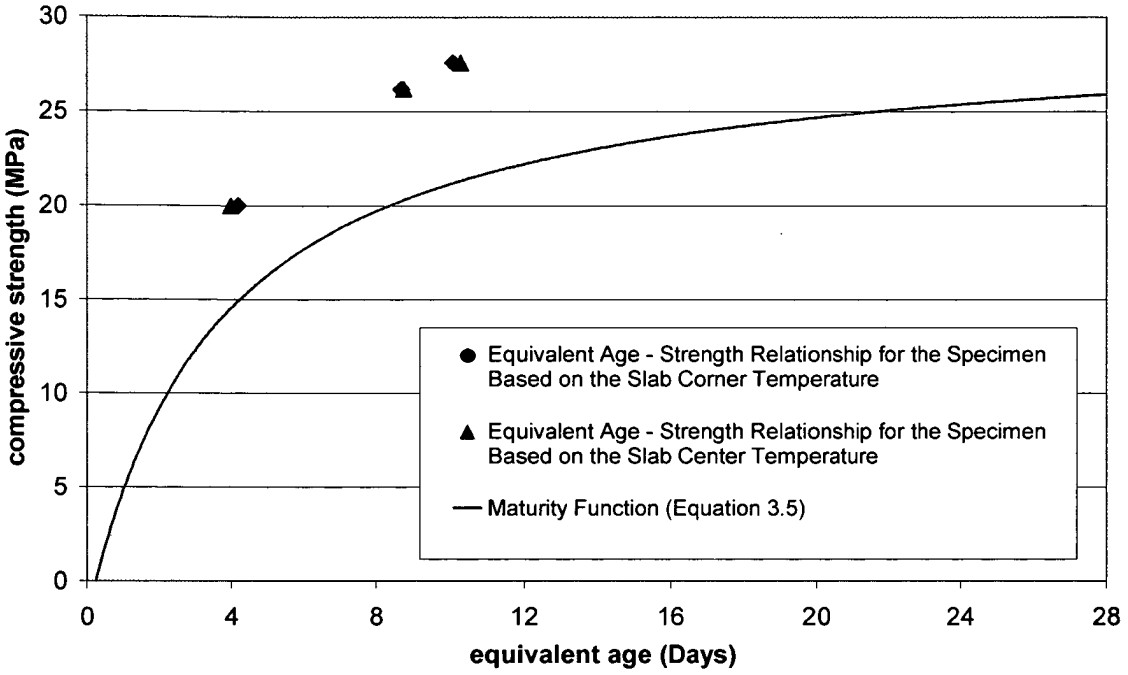

As can be seen in the figure 3.5, the fit between the strength data of the specimen to the estimated strength from Equation 3.5 is poor. The strength values of the specimen are between 30 and 40 percent higher than the values estimated with Equation 3.5. All test results exceed 50 percent of the compressive strength at an equivalent age of 28 days. Although every effort was made in the laboratory to duplicate the mix that was used in the field, discrepancies between the field and laboratory test results indicate that the mixes were slightly different.

Furthermore, it should be stressed that determining the exact equivalent age of the specimens cured in the field is somewhat complicated, since no thermocouples were set in the cylinders and the temperature history can only be assumed.

3.5 Strength Gain at Different Points in the Concrete Slab

When the HP1 and HP2 sections were placed in 1997, the concrete at the top of the pavement hardened slowly because of low air temperatures. A different strength gain at the bottom and top of the slab was assumed since cracks developed at the not-yet-hardened surface of the slab. Conversely, both the very slow hardening at the top of the pavement and the accompanying cracks were absent when the third HP concrete section was placed in 1998. Figure 3.6 shows the air temperature in both 1997 and 1998 within the first 36 hours after the concrete was placed.

Figure 3.6 Air Temperatures for the First 36 Hours after Placement of Concrete in 1997 and 1998

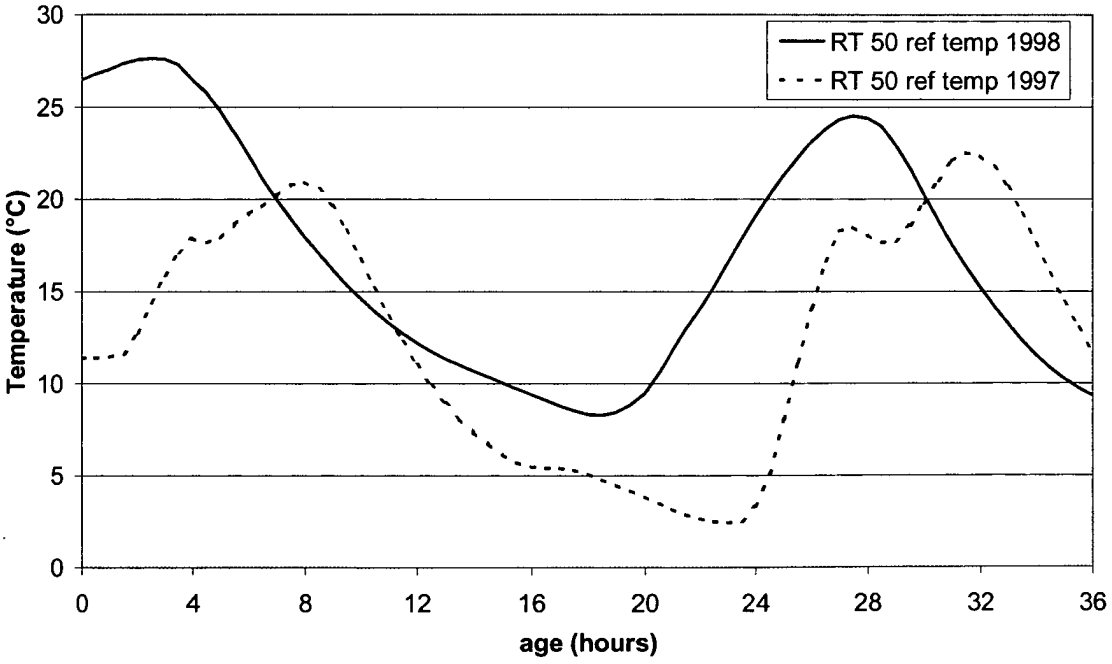

Figure 3.6 dramatically illustrates the difference between the air temperatures in 1997 and 1998 at the very early stage after final setting was reached after approximately 8 hours. This difference has a significant effect on the strength gain.

The maturity function developed from Equation 3.5 was used to determine the different strength gains at the bottom and the top of the slab. As noted previously, the concrete mix design that was used to determine the maturity function was probably not the same as the concrete mix design used for the HP concrete in the field. However, the use of Equation 3.5 is reasonable, since at the very early stage of curing, the discrepancies were found to be very limited and the rate constant was nearly the same for both mix designs. Thus, Equation 3.5 presents realistic variations in the magnitude of hardening for the bottom and top layers of the slab.

In 1997, the concrete temperature of a concrete slab at station 103+00 was measured at both the center and the corner of the slab. This evaluation involved the temperature history data from the bottom and top of both points. Figure 3.7 shows the strength versus age relationship at different points and depths of the slab up to 36 hours after the concrete was placed. For the maturity function developed from Equation 3.5, it can be assumed that hardening begins instantly after final setting, which is reached at an equivalent age of 0.25 days for this mix design.

Figure 3.7 Strength Gain at Various Locations of the Concrete Slab

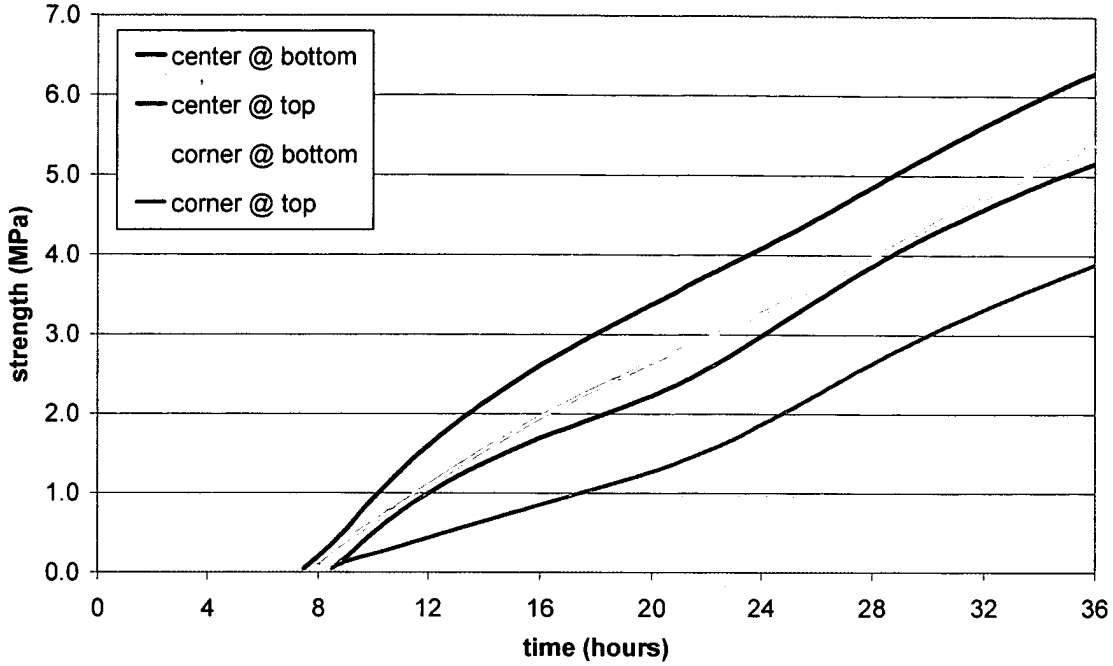

The above graph represents the varying strength gain at different points and depths of the HP concrete slab. The different concrete temperatures during curing and the resulting varying equivalent ages caused the gap between the strength observed at the bottom and top layer of the slab. The cold air highly influences the concrete temperature at the top layer of the slab, which incidentally has an insulating effect on the bottom layer. Figure 3.8 shows the varying concrete temperatures at different points and depths of the concrete slab up to 36 hours after placing the concrete.

Figure 3.8 Concrete Temperatures at Various Locations in the Concrete Slab

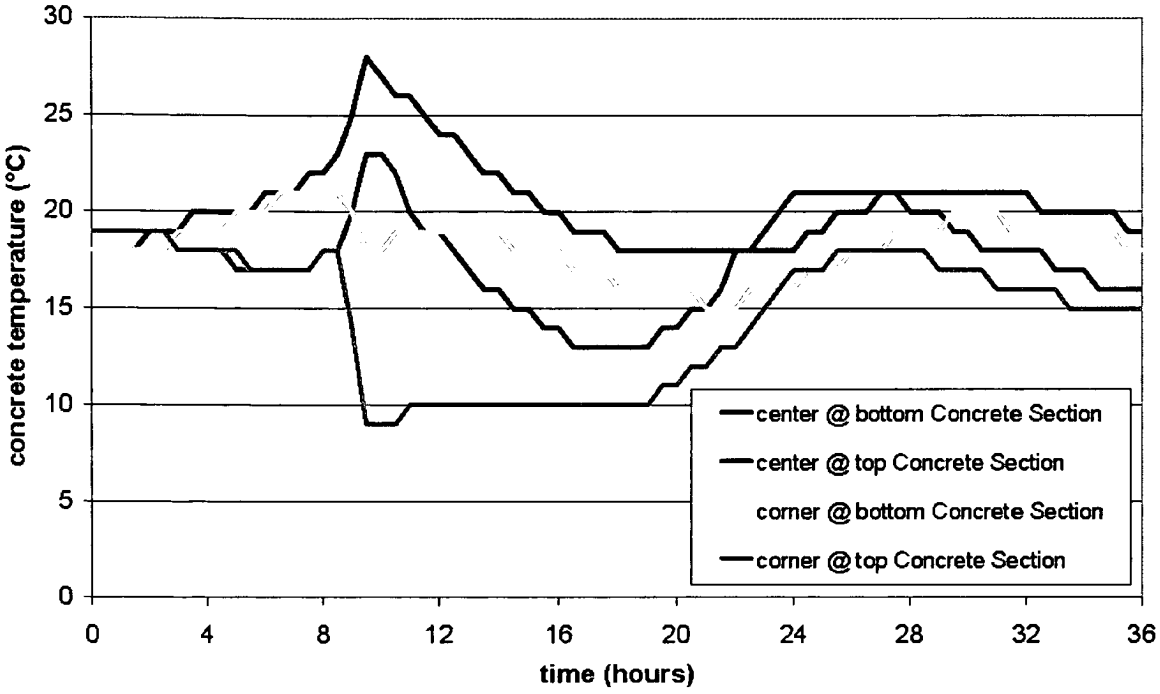

In 1998, the concrete temperature of the HP3 concrete section was measured during curing. In this case, thermocouples were set at the center, top, and bottom of the slab. Figure 3.9 shows the strength versus age relationship at the different layers of the slab up to 36 hours after the concrete was placed.

Figure 3.9 Strength Gain at Different Slab Depths for Section HP3

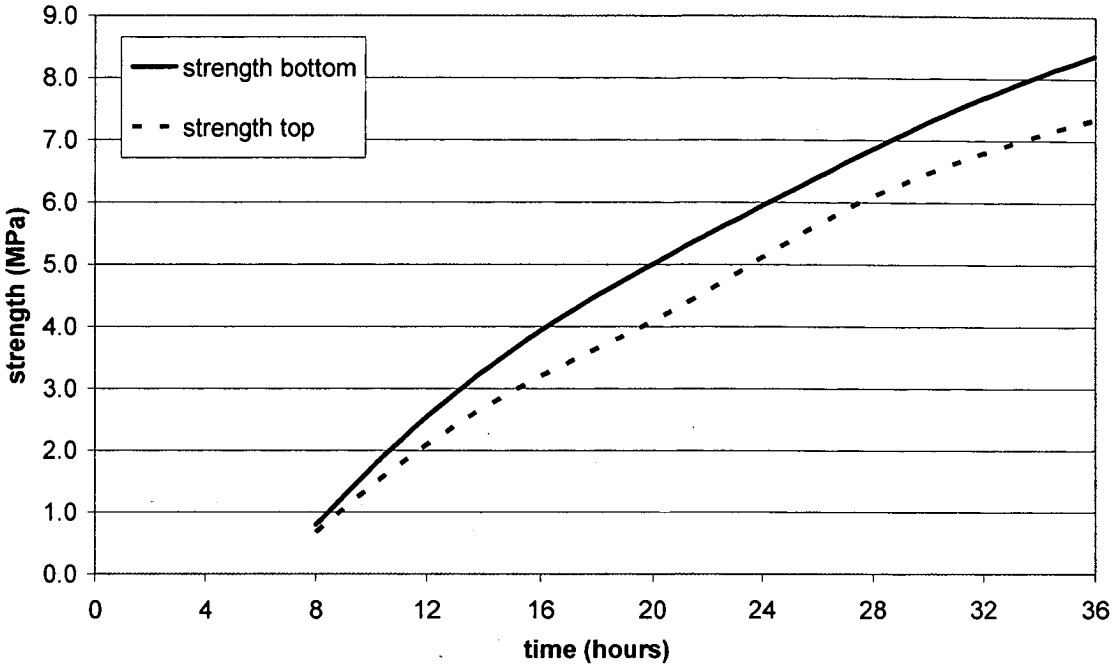

As can be seen, the gap between the strength gain at bottom and top of the concrete slab is not as wide as in 1997. Figure 3.10 shows the different concrete temperatures in the slab up to 36 hours after pouring of concrete.

Figure 3.10 Concrete Temperatures at Different Depths of the Slab at the HP3 Section

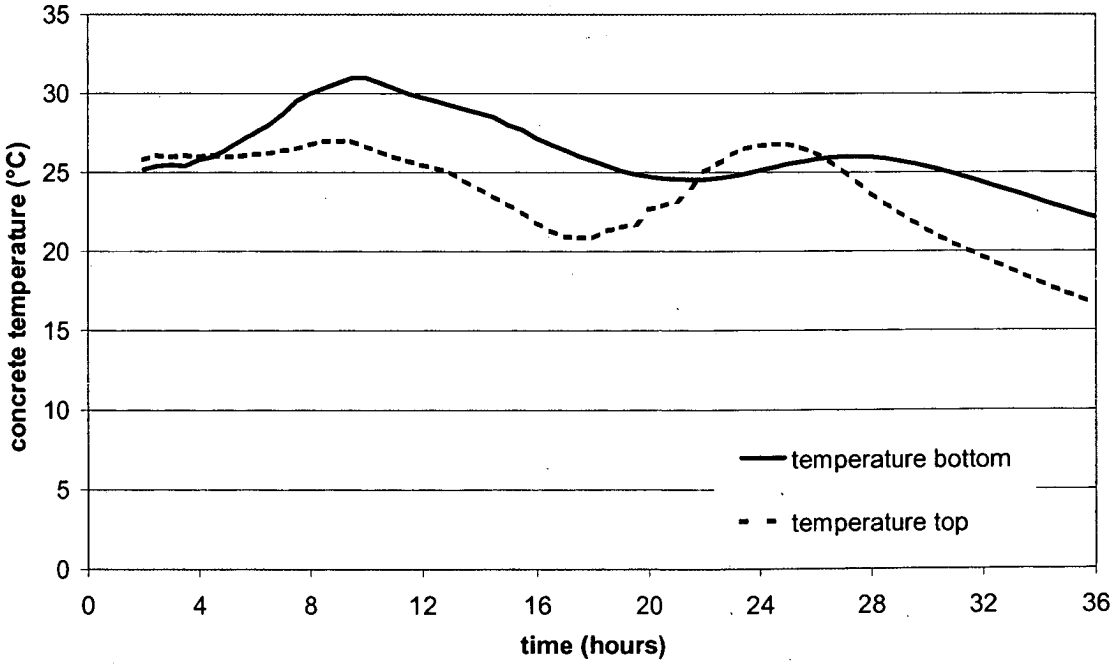

3.6 Estimating Strength of SP Concrete

This section develops a maturity function for a standard concrete mix design in order to compare the maturity-strength development relationship of this function with the field strength data.

In 1998, sections of a standard concrete mix design, in accordance with ODOT Class C Mix Design were placed (see Table 3.3). The instrumentation layout and laboratory specimens were similar to those discussed for the HP concrete sections. The concrete temperature of the slabs during curing was measured by thermocouples that were set 1.5 inches and 8.5 inches below the pavement surface. Six by twelve-inch cylindrical specimens were made from the SP mix used in the field. In addition, beams (6 / 6 / 17 inches) were made and varying strength tests (compressive, split tensile, flexural) were conducted with the specimen after 7, 14, and 28 days.

Table 3.3 SP Concrete Mix Design

Component	Weight per cubic meter (per cubic yard)
Coarse Aggregates	967 kg (1630 lbs)
Fine Aggregates	762 kg (1285 lbs)
Cement Type I	356 kg (600 lbs)
Water	178 kg (300 lbs)

*Note: the w/c ratio for this mix is 0.5

3.6.1 Available Maturity Data for the SP Concrete

Tests in accordance with ASTM Standard Practice C 1074 (1987) for estimating strength by the maturity method were not performed for the SP concrete, and no laboratory maturity data was available. The only reliable data for this mix design is the

compressive strength at 28 days (31.2 MPa = 4520 psi) recorded by ODOT (2001) while curing the specimen in the laboratory under ASTM Standard C 192 (Table 3.4).

Table 3.4 Available Strength Data of the Field SP Concrete

Age (days)	Compressive Strength in MPa (psi)	Split Tensile Strength in MPa (psi)	Flexural Strength in MPa (psi)
7	-	2.4 (347)	3.0 (442)
14	-	3.0 (428)	3.1 (456)
28	30.0 (4356)	3.8 (553)	-

The strength of concrete at an earlier age is deduced from the compressive strength value. The age-strength development of concrete while curing in the lab has been described by Neville, 1997; Nawy, 1997; and Khan et al., 1995. For the development of a maturity function in this investigation, the age-strength development of a mix design was applied with nearly the same w/c-ratio (0.49 vs. 0.5) (Neville, 1997), and a strength gain for a concrete with the same w/c – ratio (Khan et al., 1995).

The crucial point in the development of the maturity function is the determination of the temperature history for the very early stage. In approximately the first two days, hydration takes place and heat raises the temperature of the specimen. After this period, the concrete temperature is assumed to be 23°C in accordance with ASTM Standard C 192. Figure 3.11 shows the temperature history that was assumed for the mix design that cured in the lab. The strength values of Neville (1997) and Khan et al. (1995) were converted into equivalent ages on the basis of this temperature history.

Figure 3.11 Assumed Temperature History of the SP Concrete

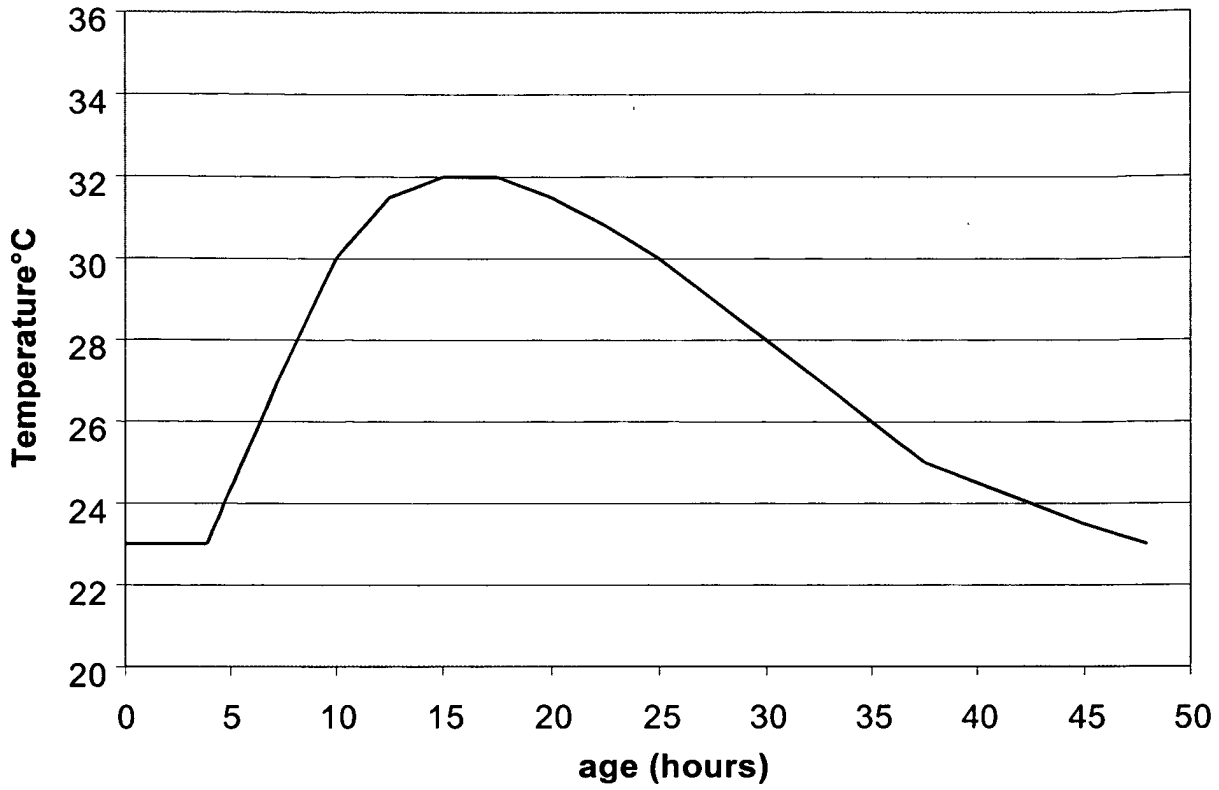

3.6.2 Development of a Maturity Function

Based on the 28-day strength and the strength gain of a concrete with nearly the same w/c-ratio (0.49 vs. 0.5) (Neville, 1997), a maturity function was determined for the SP Concrete used in the U.S. Route 50 project. The maturity of the SP concrete, in this case, is expressed by its equivalent age determined from Equation 3.1 and using the following values:

$$t_e = \Sigma\, e^{\frac{-E}{R}\left(\frac{1}{T}-\frac{1}{Tr}\right)} \Delta t \qquad \text{Eq. 3.1}$$

where,

t_e = equivalent age at the reference temperature (23°C)

E = apparent activation energy, E = 33.5 + 1.47 (20 - T) kJ / mol

when $T < 20°C$, $E = 33.5$ kJ / mol, when $T \geq 20°C$

R = universal gas constant (8.314 J/mol)

T = average absolute temperature of concrete at Δt

T_r = absolute reference temperature (296 °K)

The age at the start of strength development equals the age at the time of final setting, as determined by Neville (1997). The strength up to the age of 28 days was estimated from Equation 3.2, using the following values:

$$\frac{S}{S_{28}} = \beta \frac{k(t - t_0)}{1 + k(t - t_0)} \qquad \text{Eq. 3.2}$$

where

S = strength at equivalent age t

S_{28} = strength at equivalent age of 28 d, $S_{28} = 30.4$ MPa (4,400 psi)

k = rate constant, $k = 0.15$

t_0 = age at start of strength development, $t_0 = 0.125$ days

β = factor describing relative strength gain, $\beta = 1.24$

Figure 3.12 shows the strength data at different equivalent ages deduced from Neville (1997) and Khan et al. (1995) and the maturity function determined with Equation 3.2 for the SP concrete.

Figure 3.12 Strength Data and Maturity Function

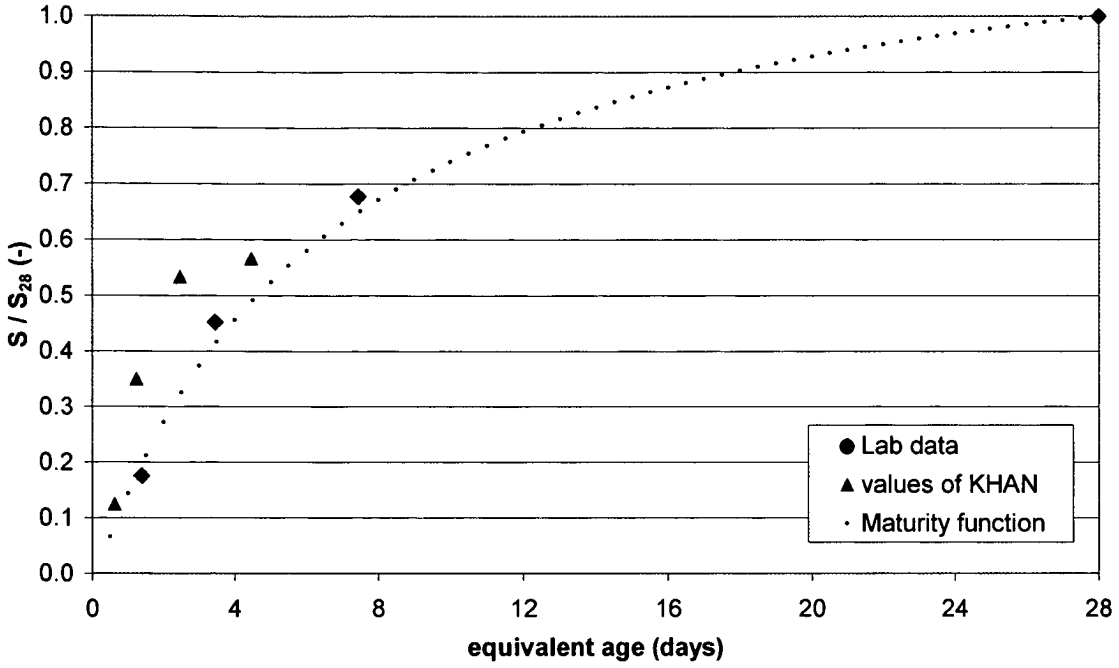

Figure 3.13 shows the strength data at different equivalent ages deduced from the compressive strength values in Table 3.4 and the maturity function determined from the above equation for the SP concrete.

Figure 3.13 Strength vs. Equivalent Age Relationship of the Specimen and of the Maturity Function

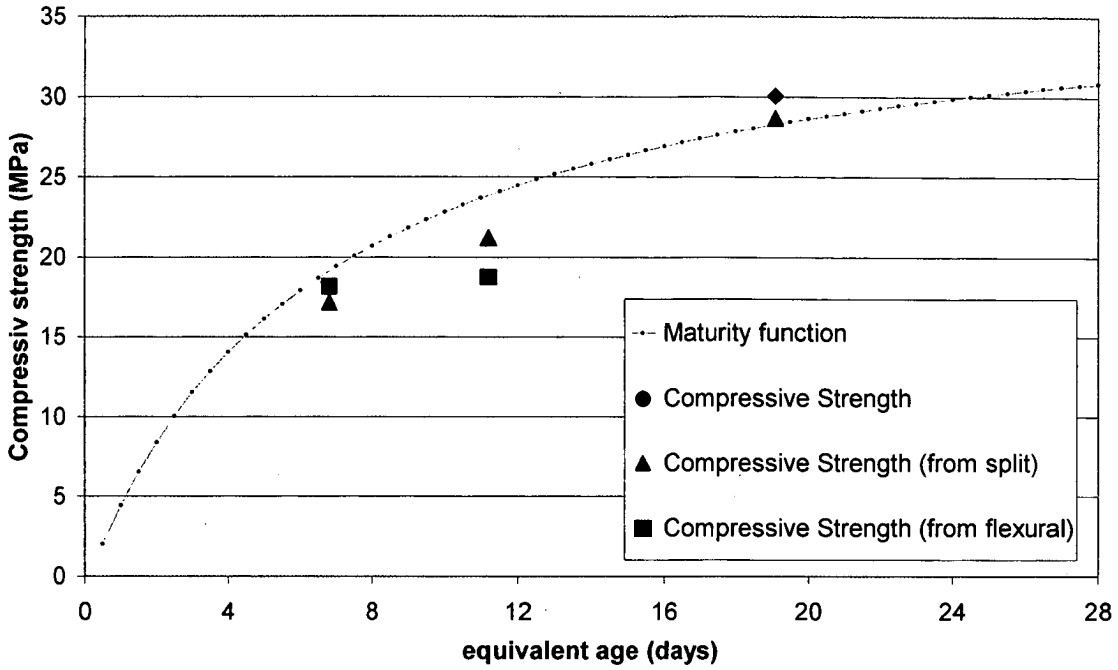

3.7 Application of the Maturity Function to the Field Strength Data

Specimens were made concurrently with the placement of the SP concrete slab. The specimens remained in the field near the slab until the day of testing, which allowed them to cure under similar circumstances as the slab relative to the surrounding air temperature. The temperature history at the bottom layer of the slab was assumed to be the approximate temperature history of the specimen. Therefore, the equivalent age of the specimen was determined by this temperature data.

One specimen was made for each test (compression, split tensile and flexural test) to determine the strength after 7, 14, and 28 days. Table 3.4 shows the strength data that was collected. These values were scattered due to the small number of samples; therefore, the statistical foundation is very poor for graphical analysis.

In order to obtain a slightly better statistical foundation for the field strength data, the split tensile and flexural strength was used to back-calculate the compressive strength according to ACI Model Code 90 (ACI 318-95, 1995) and CEB-FIB Model Code 1990 (Comite Euro-International du Beton, 1993).

The strength versus equivalent age relationship of the specimen is shown in Figure 3.13. The strength is the compressive strength or the calculated compressive strength from the split tensile or flexural strength. The strength versus equivalent age relationship estimated from the maturity function is also shown. The fit between the strength data of the specimen to the estimated strength from Equation 3.5 is good.

3.8 Application of HIPERPAV

The HIgh PERformance PAVing (HIPERPAV) software models the early-age development of concrete strength and stresses that result from moisture and temperature changes within the pavement. From this, the risk of cracking within the first 72 hours can be assessed. HIPERPAV considers the influence of PCC pavement design, concrete mix design, construction methods and environmental conditions on the early-age behavior of Portland cement concrete pavements. The output of the HIPERPAV analysis is a plot of real stress in the slab versus the real strength as shown in Figure 3.14. When the stress and strength lines meet, cracking occurs.

All of the 1997 data for the HP sections concerning pavement design, concrete mix design, construction methods, and environmental conditions were entered into HIPERPAV to assess the risk of early age cracking. However, the current version of HIPERPAV does not have the capability to handle a maturity function as an input.

Figure 3.14 shows the default strength gain of the slab as assumed internally by the software. Line A represents the default strength gain.

The default maturity function of HIPERPAV overestimates the strength gain of the slab. The strength gain was determined with the maturity function (Eq. 3.5), and was used to calculate the tensile strength of the HP concrete. The compressive strength (f_{ck}) and tensile strength (f_{ct}) are related by Equation 3.1 (Comité Euro-International du Béton 1993):

$$f_{ct} = f_{ct0} \cdot \left(\frac{f_{ck}}{f_{ck0}} \right)^{\frac{2}{3}} \qquad \text{Eq. 3.6}$$

where,

$f_{ct0} = 1.85$ N/mm^2

$f_{ck0} = 10$ N/mm^2.

From Equation 3.1 and an assumed average compressive strength at the top of the slab of 2.1 MPa (300 psi) after 20 hours (which is the point of time with the maximum stress), the tensile strength at this point is 0.6 MPa (90 psi). This value is half that is assumed by HIPERPAV. Line B in Figure 3.14 represents the tensile strength gain based on the maturity function (Eq. 3.5). It is apparent that the stress exceeds the strength at the maximum of stress after 20 hours. While the tensile strength is based on the maturity function Eq. 3.5, HIPERPAV indicates cracking and agrees with the observations in the field.

HIPERPAV was run a second time with the 1998 data for the HP 3 section. Figure 3.15 shows the stress and strength development in the slab from this analysis.

Again, the strength gain was calculated externally on the basis of the maturity function (Eq. 3.5). The default strength gain was also calculated.

In accordance with the maturity function, the compressive strength at the maximum stress after 16 hours was assumed to be 3.4 MPa (500 psi). Using Equation 3.6, the tensile strength for 1998 at the stress peak was calculated. Line C in Figure 3.15 represents the tensile strength gain based on the maturity function (Eq. 3.5). The value of the maximum stress after 16 hours was 0.9 MPa (130 psi), and indicates no cracking in 1998, which also agrees with field observations.

Figure 3.14 HIPERPAV Analysis Outputs of the HP Sections in 1997

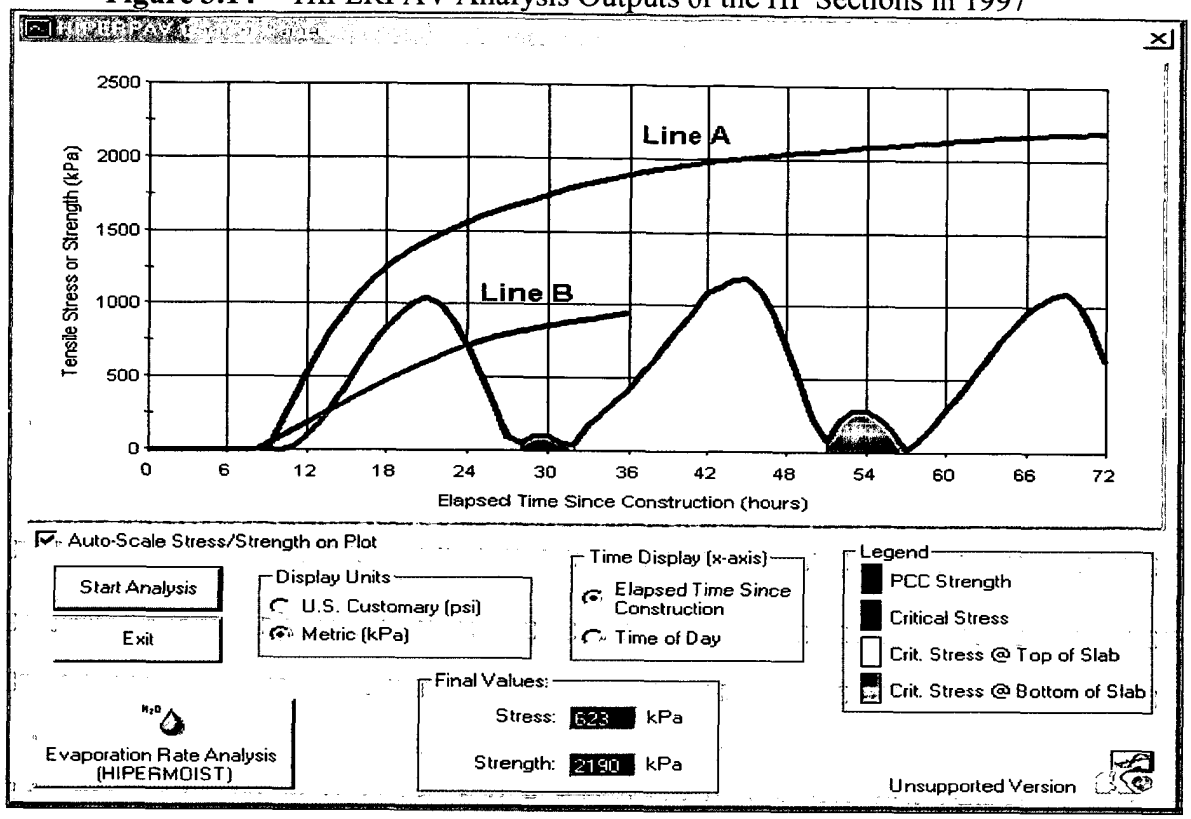

Figure 3.15 HIPERPAV Analysis Output of the HP Section in 1998

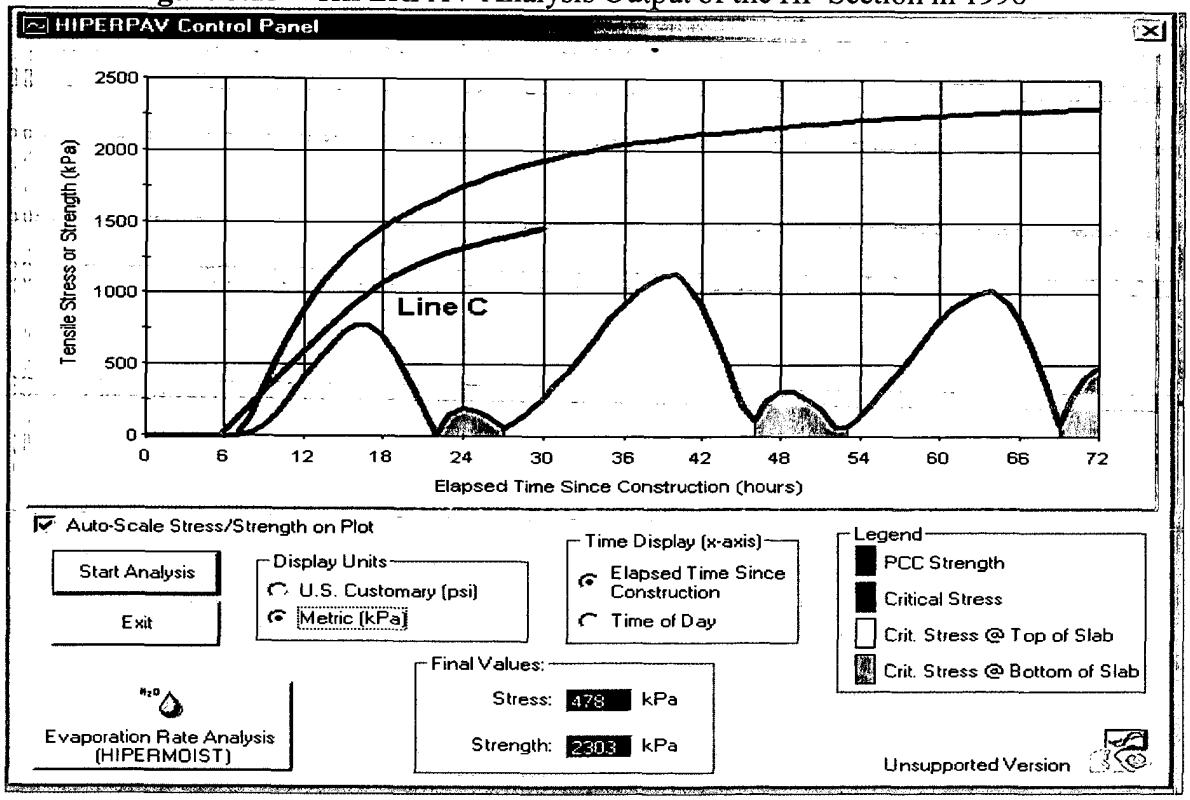

Chapter 4 Analysis of Field Data

4.1 Introduction

This chapter presents the analysis of the data collected in the field to determine differences between the behavior of the HP and SP concrete and characteristics of the sealed and unsealed joints of the HP concrete. The shape and deflection of the HP and SP concrete slabs were examined from the strain data to determine the effects of time and temperature on slab shape. FWD data was used to measure deflection at different locations. Data for the sealed and unsealed joints was analyzed to determine variation in moisture content under the joints, and the deflection and load transfer at the joints.

4.2 Slab Shape

An evaluation of the shape data obtained from the Dipstick 2000® profiler revealed two main tendencies in both the SP and HP sections. First, as to the general shape of the slabs, the corners turn up relative to the center. Second, the slab assumes this shape rapidly after placement. After 3 days, the corners reach half of their maximum value, and in 1 week, the slab is almost the shape it will be after 5 weeks. In the next 4 weeks, up to the end of measurement, no significant changes in the slabs were monitored. After 5 weeks, the corners are higher than the center of the slab. Figures 4.1 to 4.3 show the typical change of the slab shapes in the SP section after 3 days, 1 week, and 4 weeks; Figures 4.4 to 4.6 shows the shape of slab of the HP section for the same time period.

Figure 4.1 Change of the Shape of Slab # 2 in the SP Section after 3 Days

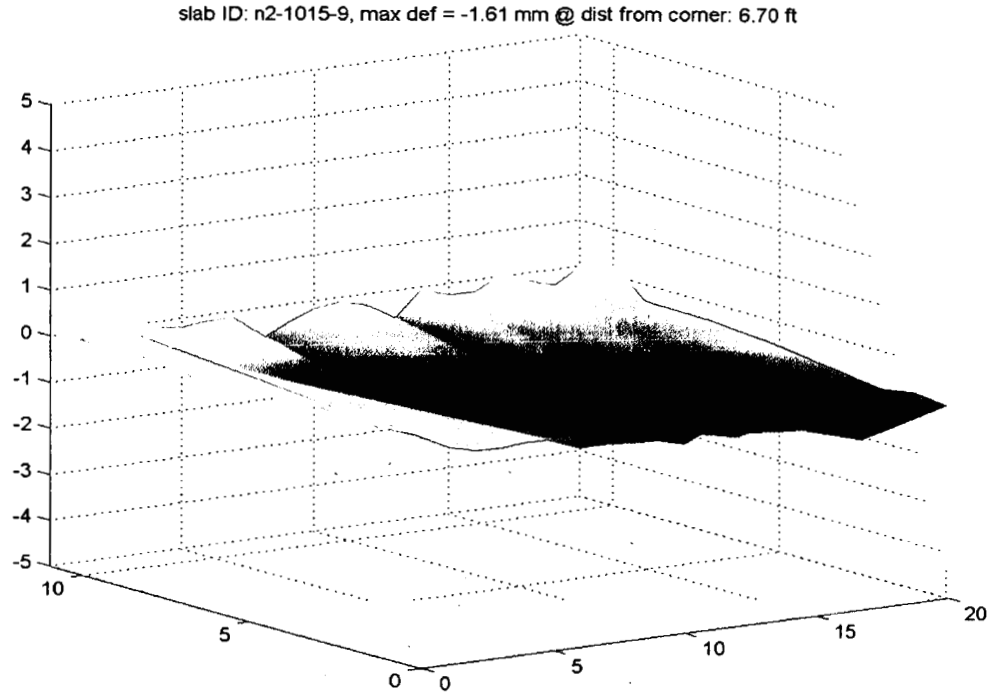

Figure 4.2 Change of the Shape of Slab # 2 in the SP Section after 1 Week

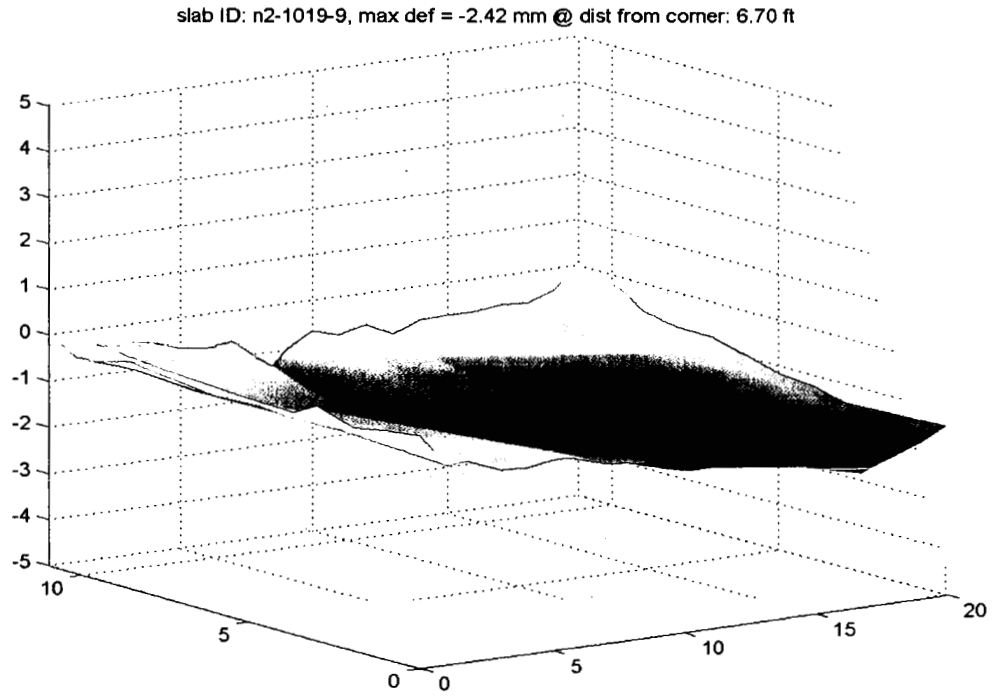

Figure 4.3 Change of the Shape of Slab # 2 in the SP Section after 4 Weeks

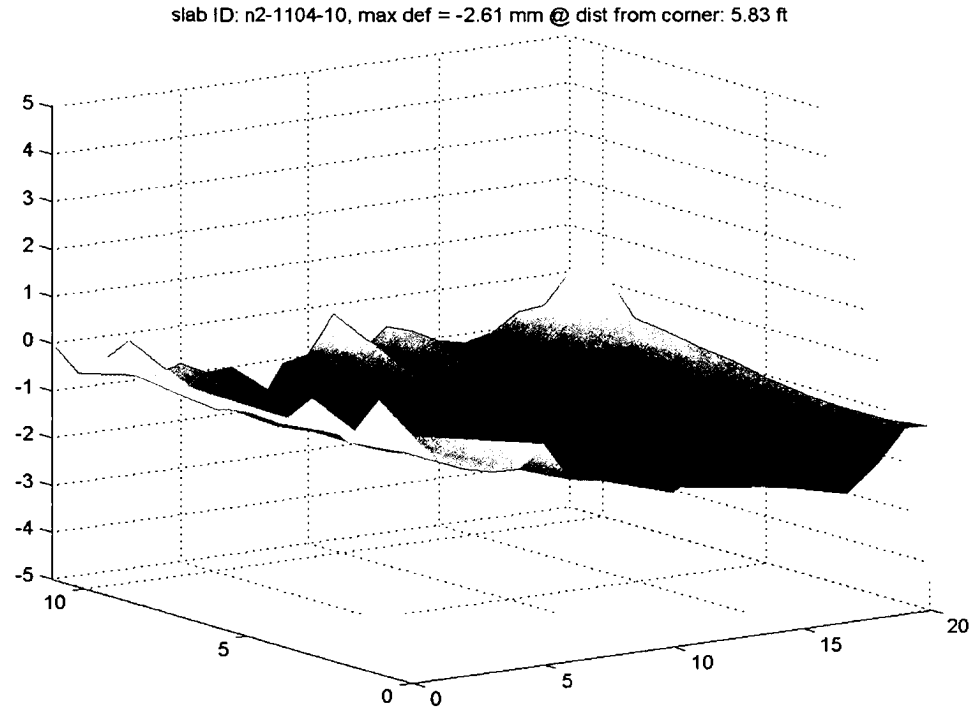

Figure 4.4 Change of the Shape of Slab # 3 in the HP Section after 3 Days

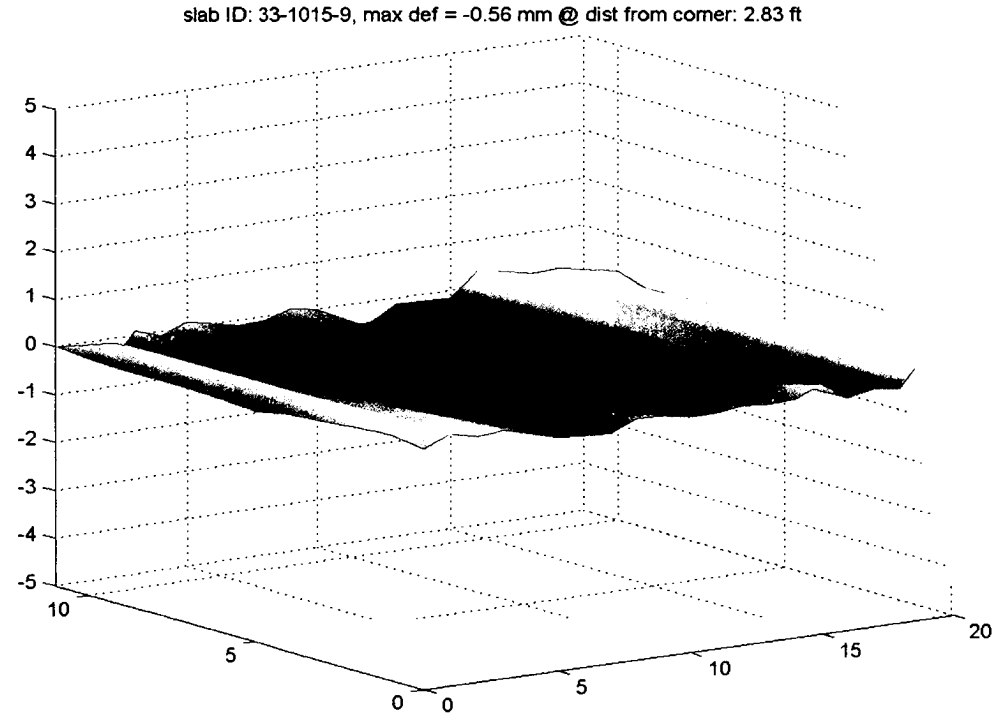

Figure 4.5 Change of the Shape of Slab # 3 in the HP Section after 1 Week

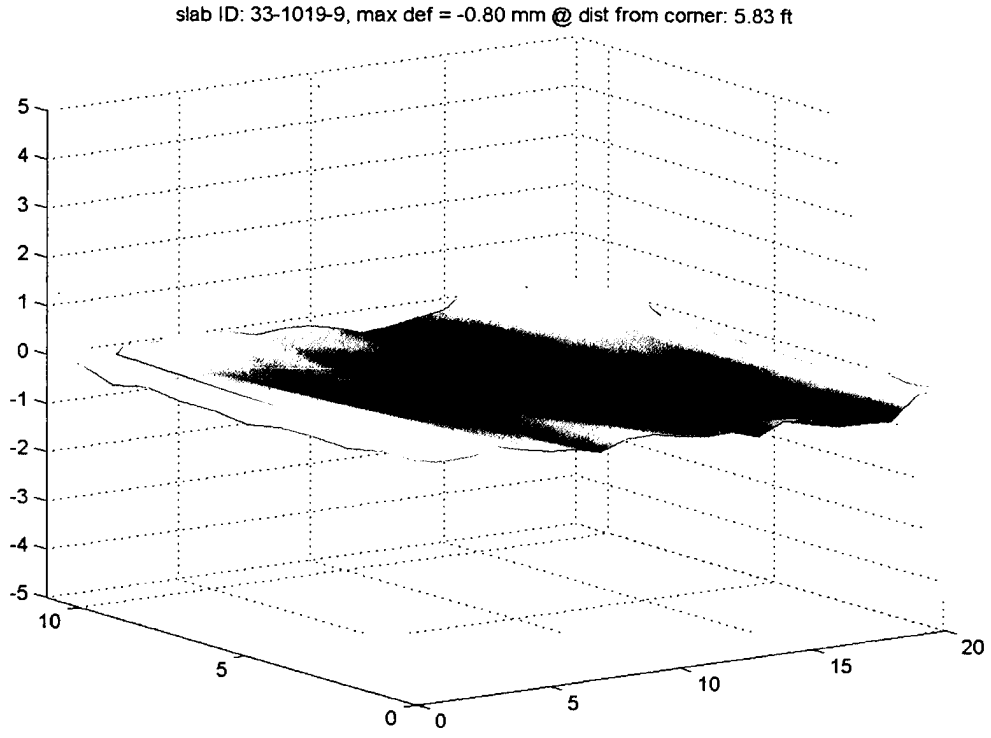

Figure 4.6 Change of the Shape of Slab # 3 in the HP Section after 4 Weeks

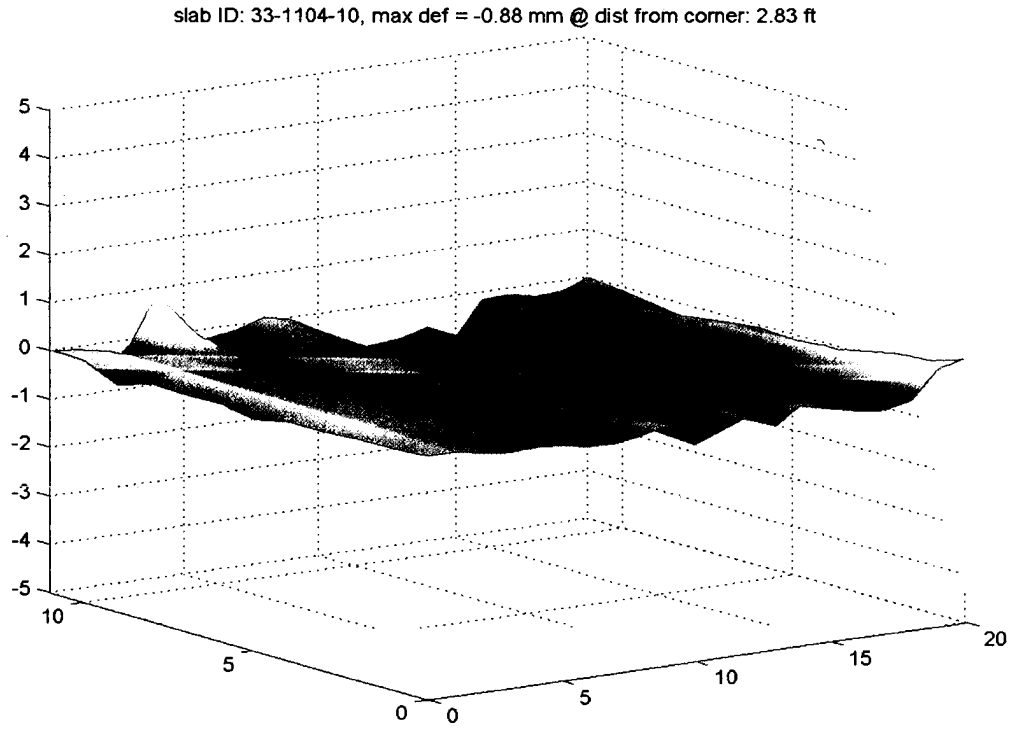

When the SP and HP sections are compared, it is apparent that the edges of the slabs in the SP section turned up more than in HP section. The difference in height between the deepest point measured on the slab relative to the corners was on average 0.097 inches for the SP section, and 0.047 inches for the HP section.

It should be noted that the change in shape was not measured at the edge of the slab. The corner of the box drawn for the Dipstick 2000® was 0.71 feet away from the corner of the slab; thus, the corners will have actually turned up even more. Also, since there were no significant temperature gradients during the test period, no curling of the slabs as a result of temperature differences occurred. The shape of each slab in the morning, when temperatures are lower, was nearly the same as in the afternoon when temperatures are higher and the amount of difference was negligible.

4.2.1 Temperature Effects on the Strain in the Slabs

The change in strain at different points in the slab should explain the change in shape, and the strain data was collected for this analysis. Two prime factors drive the strain in the concrete slabs under load during the period of measurement. The first is the temperature of the concrete and the resulting thermal expansion and contraction. The influence of temperature is apparent from the vibrating wire strain gage data. Figure 4.7 shows a plot of temperature and longitudinal strain data for the SP section (strain gage point 1) the second week after placement.

Figure 4.7 Temperature and Longitudinal Strain Data for the SP Section at the Center of the Slab Two Weeks after Placement

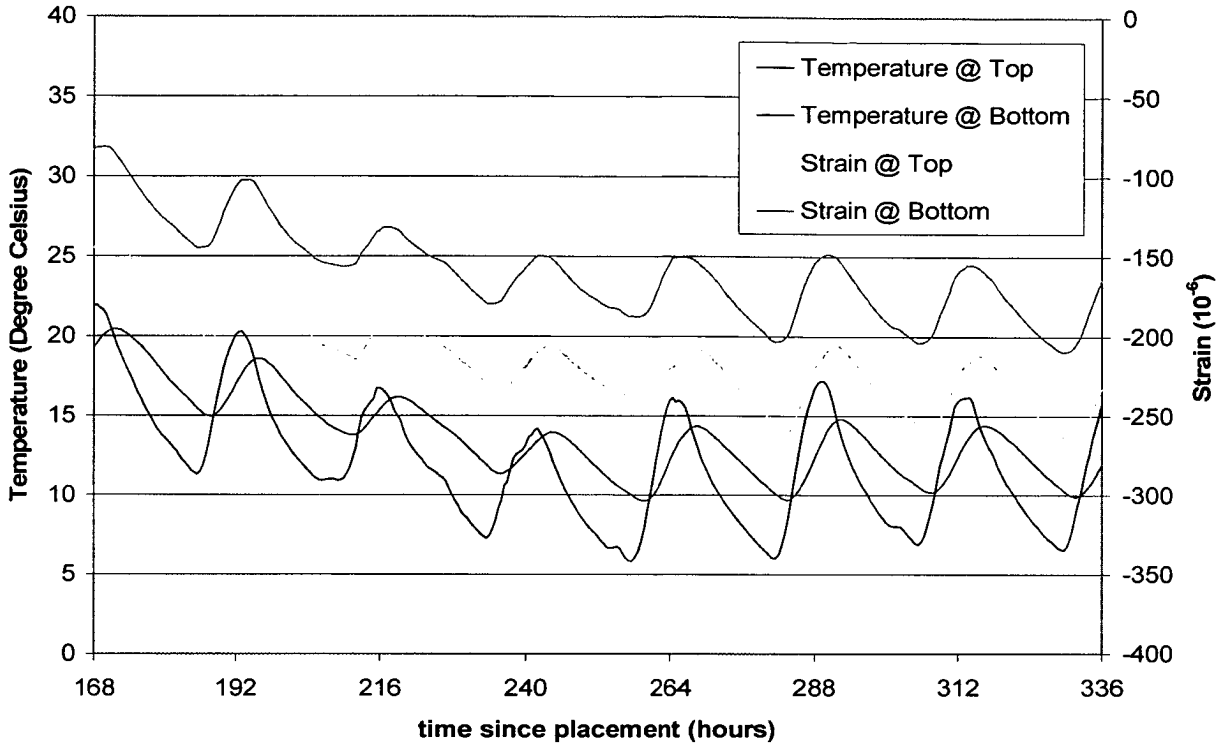

The second factor affecting the strain in the slab is the shrinkage of the concrete. However, this influence is not as evident because of the difficulty in separating shrinkage strain and temperature strain. Temperature is the main influence on the magnitude of induced strain for short periods of time. At an early age, the strain induced by shrinkage is supposedly the main influence on the change of the slab shape. Therefore, for this analysis, the effect of temperature on strain was isolated in order to show the effect of shrinkage on strain within the period of measurement.

The temperature of the concrete influences the strain in the slab in two different ways. On one hand, the strain is dependent upon the absolute value of the temperature; but, it is also influenced by the temperature gradient of the slab. This effect becomes

apparent in the difference between the strain at the top and the bottom of the slab as it relates to the temperature gradient.

Figure 4.8 shows the difference in strain and the accompanying temperature gradient of the slab in the SP section (strain gage point 1) in the second week. The phenomenon of the decreasing difference between the strain at the top and the bottom of the slab with regard to the absolute value at a positive temperature gradient will be discussed later in this section.

Figure 4.8 Differences between the Strain at the Top and the Bottom of the Slab in Comparison to the Temperature Gradient in the SP Section (Strain Gage Point 1) in the Second Week

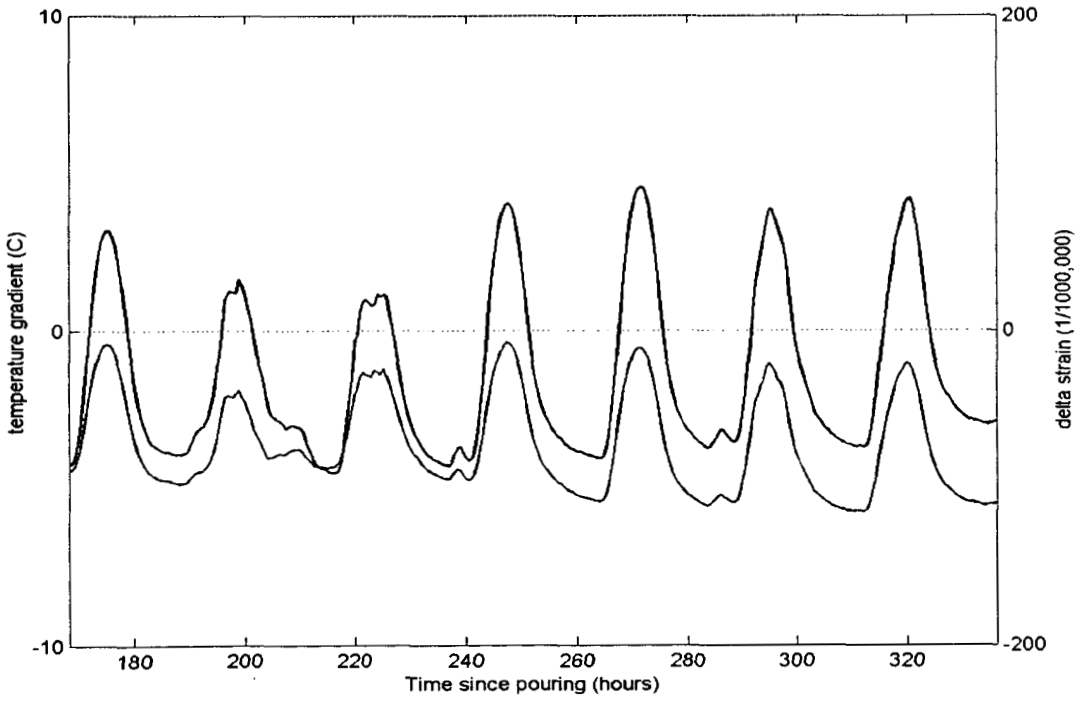

Because of the impact of the temperature gradient on the strain, the first step in isolating the influence of temperature was to use only the strain data points where the gradient was approximately zero. However, the impact of the absolute value of the temperature remained, which is especially important because the absolute value of the

temperature at the zero gradient decreased during the period of measurement. Figures 4.9 and 4.10 illustrate the impact of the absolute value of the temperature on the strain. The data points represent the temperature and the accompanying strain data of the SP section (strain gage point 1) at the zero gradient in the second week.

Figure 4.9 Impact of the Absolute Temperature on Strain, SP (Strain Gage Point 1, Top) in the Second Week

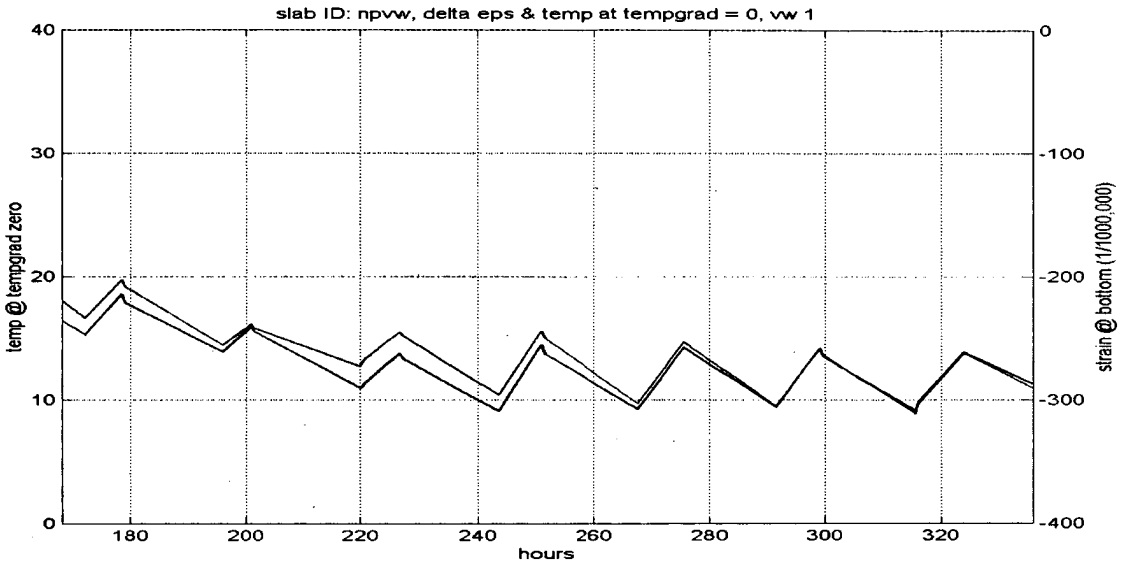

Figure 4.10 Impact of the Absolute Temperature on Strain, SP (Strain Gage Point 1, Bottom) in the Second Week

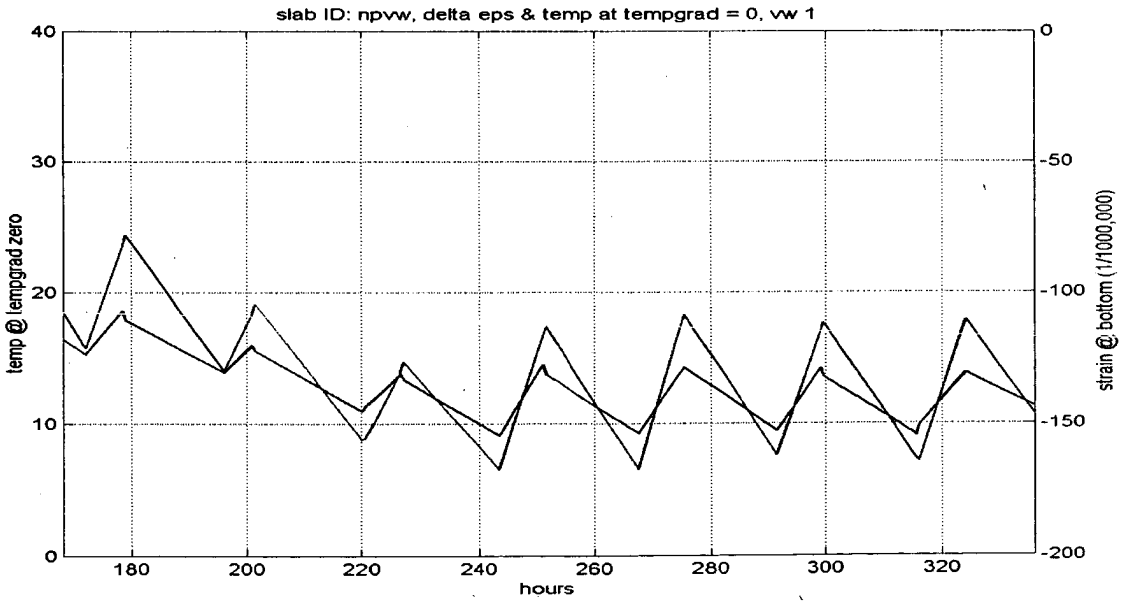

Before isolating the impact of the absolute value of the temperature, this paper will discuss the point at which shrinkage strain measurement occurs. The focus in this section is on the drying shrinkage that takes place after the final setting of concrete. In accordance with Neville (1997), the final setting is assumed to take place at 4.5 hours after the placement of concrete. However, since the slab has an indefinite length at this time, no significant strain in longitudinal direction can occur. Thus, all strain gages were set to zero at the time of sawcutting, which was 10 hours after placement of the SP section and 15 hours after placement of the HP section. It should also be noted that the gages start to read properly only after the concrete in which the instruments are embedded has reached a particular stiffness. At the time of sawcutting, the required concrete stiffness for the internal spring of the strain gage had apparently been reached.

The initial temperature of all of the strain data collected in the first 5 weeks was examined in order to isolate the impact of the absolute value of the temperature. The temperature at the time of sawcutting was chosen as the initial temperature. This choice is not entirely correct because thermal stresses from the heat of hydration exist in the slab at this time, and this condition leads to strain immediately after sawcutting. However, the assumption about the initial temperature is reasonable most of the time since a great deal of stress relaxation takes place in the concrete at this very early age, and the magnitude of stress is unknown (Springenschmid and Fleischer, 1990). The strain at the time after final setting is standardized when referring to the initial temperature by means of the coefficient of thermal expansion. This coefficient is assumed to be 10 x 10-6 per °C (Comite Euro-International du Beton, 1993).

Figure 4.11 shows the top and bottom strain data for the SP section (strain gage point 1) in the first 5 weeks after both standardized and non-standardized placement of the concrete at the zero gradients. The standardized curve is apparently smoother and the magnitude of strain is smaller because the initial temperature was higher than the temperature values at the zero gradient measured later.

Figure 4.11 Top and Bottom Strain Data of the SP Section (Strain Gage Point 1) in the First 5 Weeks after Placement of Concrete at the Zero Gradients

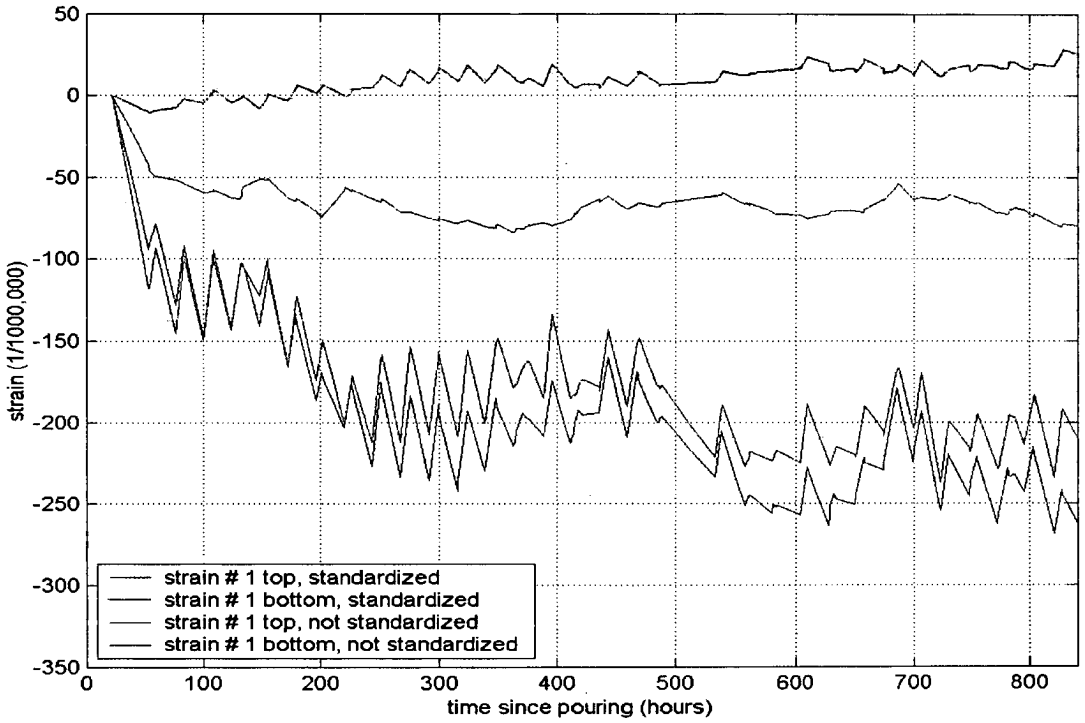

4.2.2 SP Section Strain Data

Upon examination of the longitudinal shrinkage strain data for the SP section, the variation in shrinkage at the top and the bottom becomes apparent. The absolute value of the indicated negative strain at the top of the slab was much higher than at the bottom, where an expansion of the concrete was also observed. The expansion of the bottom portion was caused by the contraction and subsequent warping of the top portion; this

process induces positive strain at the bottom. The shrinkage at the bottom of the slab was smaller than the shrinkage at the top. This different shrinkage behavior complies very well with the monitored change in the shape of the slab. Figure 4.12 shows the shrinkage strain of points 1, 2, and 3 at the top of the slab, and Figure 4.13 shows the bottom strain data.

Figure 4.12 Longitudinal Shrinkage Strains of Points 1, 2, and 3 at the Top of the Slab, SP Section

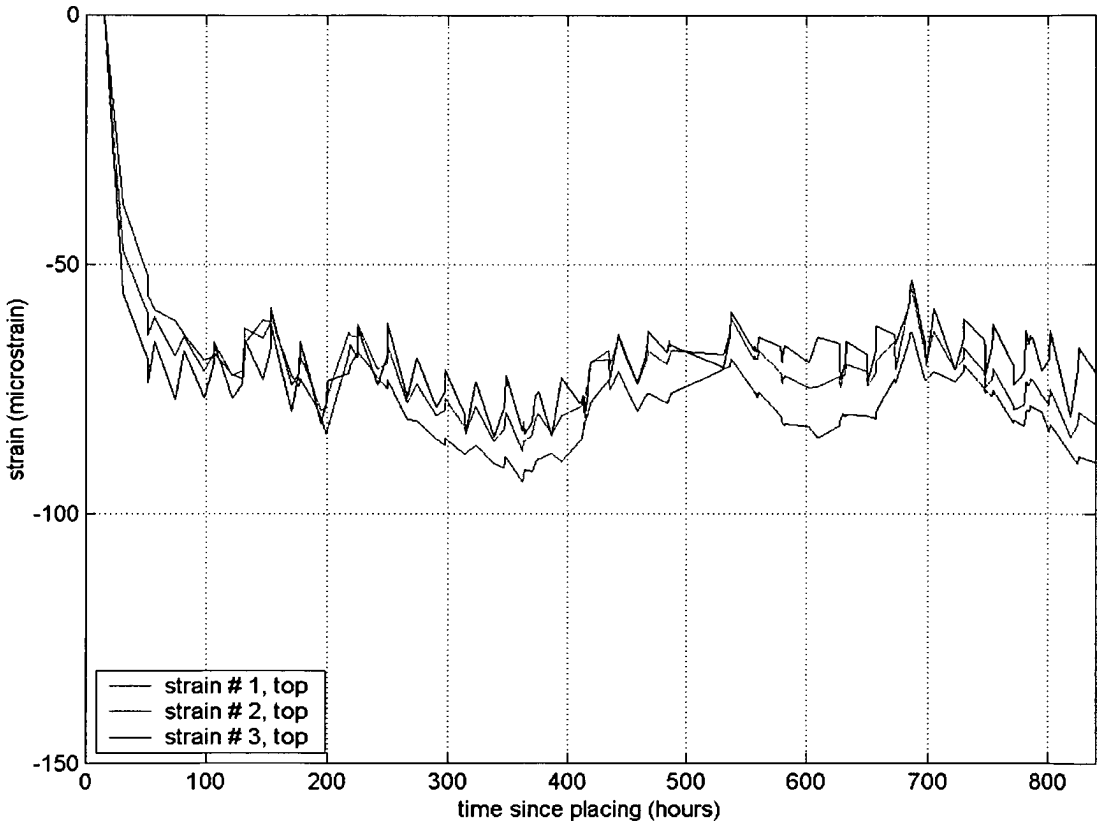

Figure 4.13 Longitudinal Shrinkage Strain of Points 1, 2, and 3 at the Bottom of the Slab, SP Section

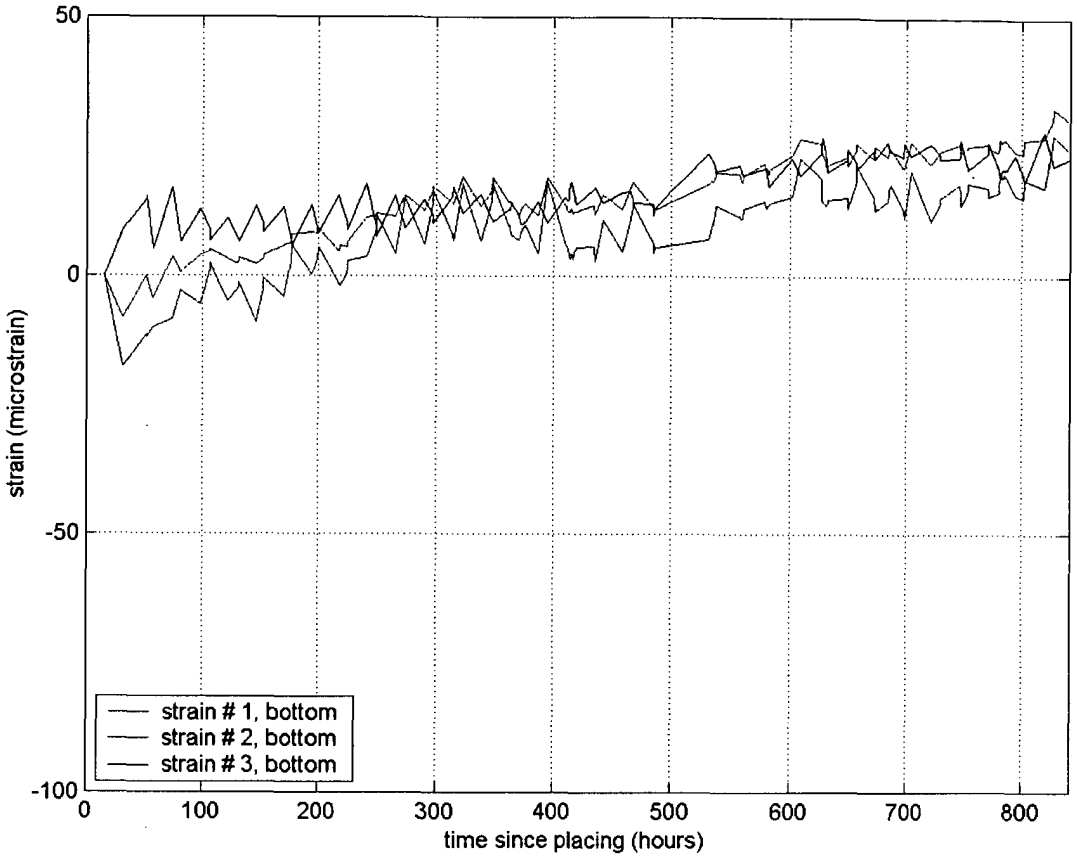

The different shrinkage behavior exhibited at the top and bottom of the slab also explains the decreasing absolute value of the difference between the strain at the top and bottom with an increasing positive temperature gradient as shown in Figure 4.8. The positive temperature gradient causes the top layer to expand and work against the warping caused by shrinkage. Figure 4.14 shows the development of the difference in strain between the top and the bottom layer at points 1, 2, and 3 of the slab. The difference in strain increases with time in accordance with the shape data.

Figure 4.14 Differences in Shrinkage Strain of Points 1, 2, and 3 of the Slab, SP Section

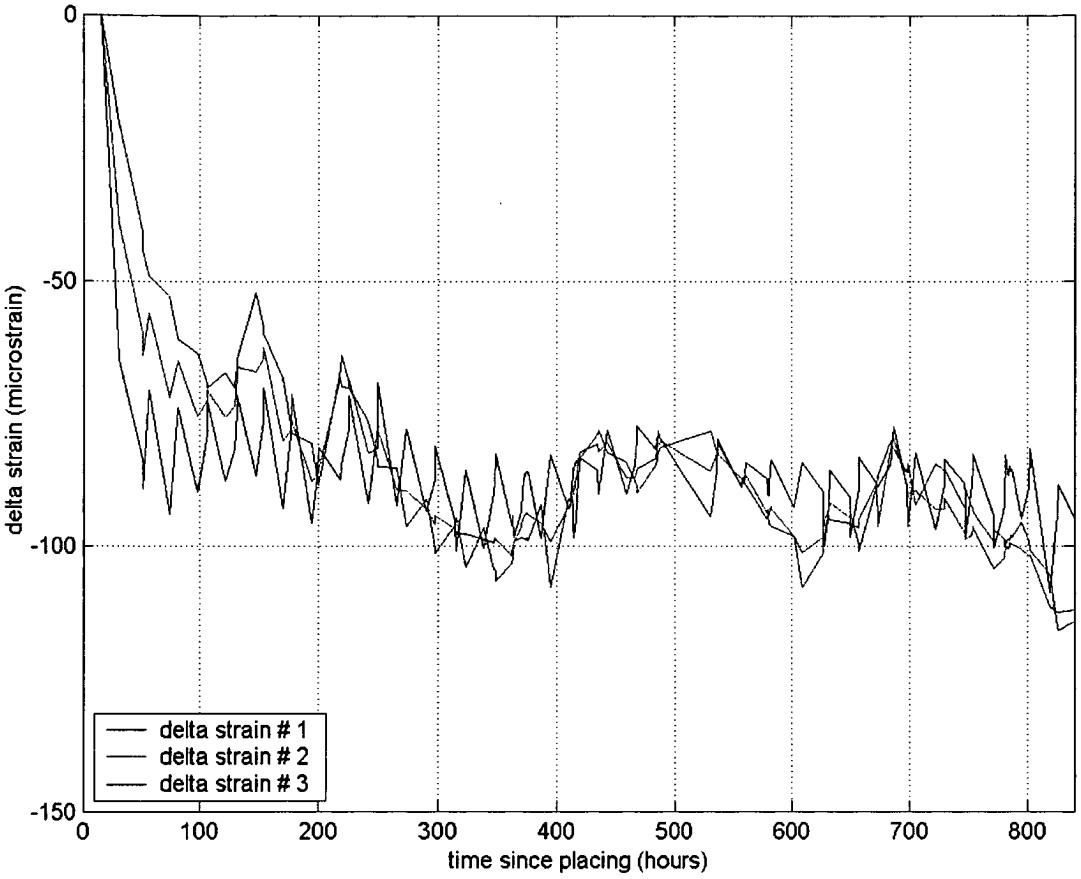

The transverse strain indicates a similar behavior in this direction. Figure 4.15 shows the transverse shrinkage strain of points 12, 13, and 14 at the top of the slab, and Figure 4.16 shows the bottom strain data.

Figure 4.15 Transverse Shrinkage Strain of Points 12, 13, and 14 at the Top of the Slab, SP Section

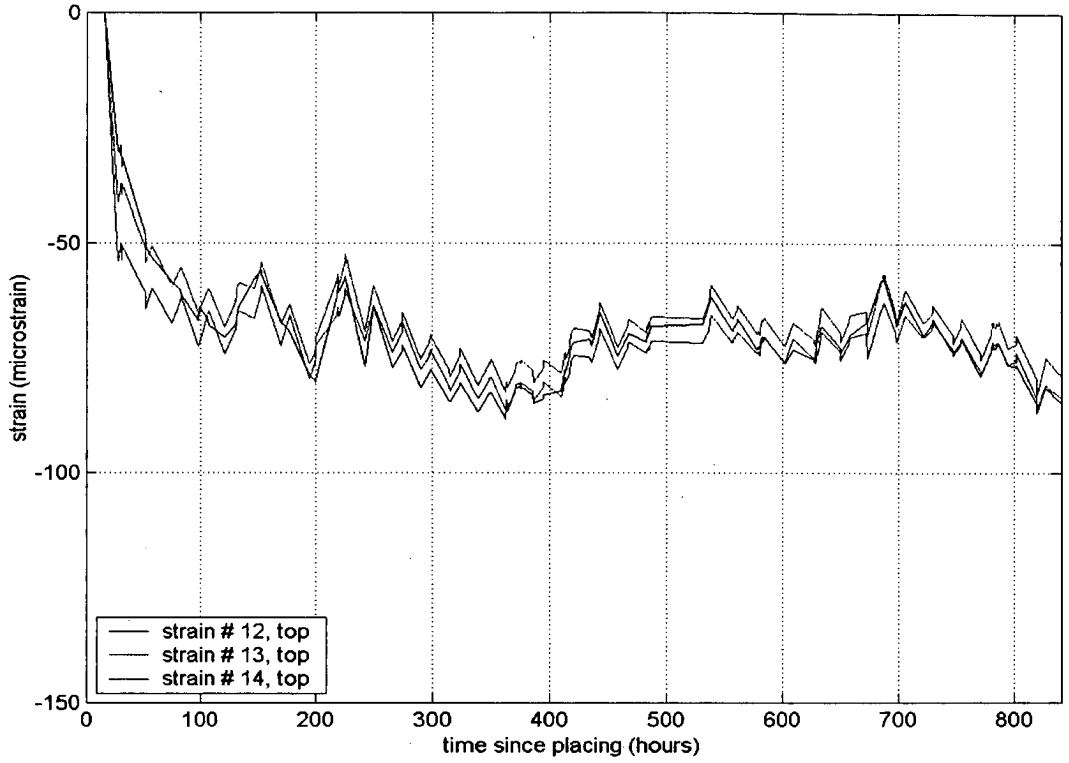

Figure 4.16 Transverse Shrinkage Strain of Points 12, 13, and 14 at the Bottom of the Slab, SP section

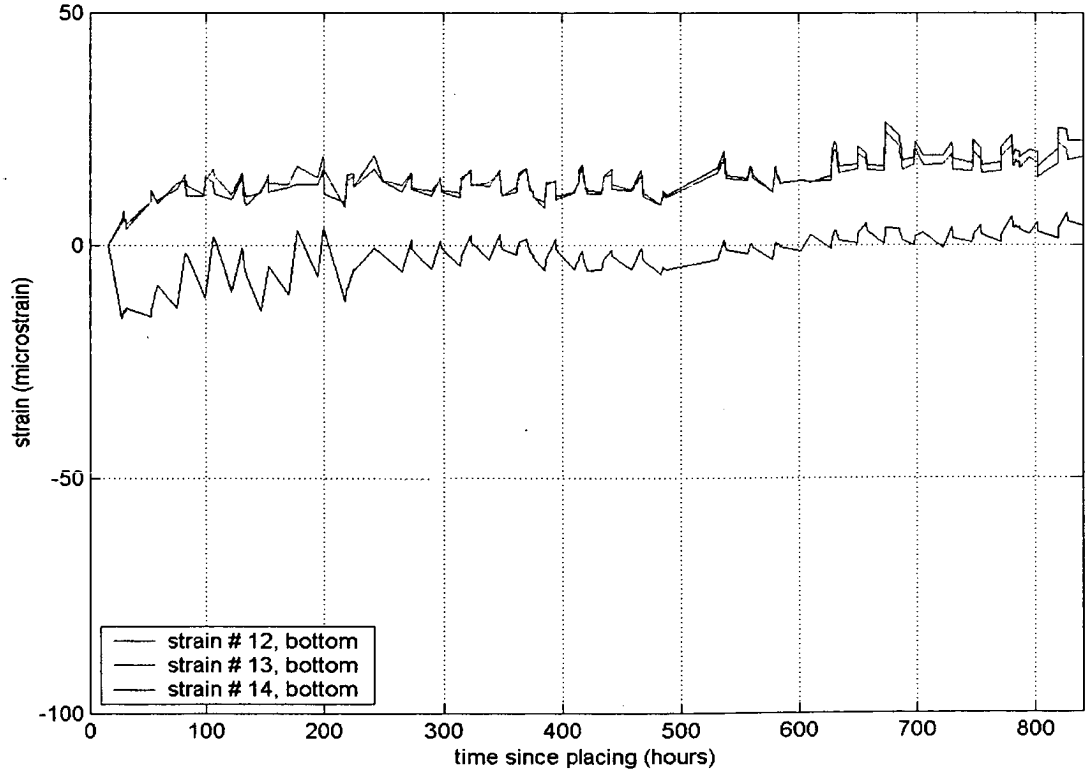

4.2.3 HP Section Strain Data

The strain data for the HP section indicates the different shrinkage behavior of these slabs. In comparison to the SP section, it is first apparent that the HP section does not exhibit the considerably different shrinkage between the top layer and the bottom layer; both layers shrink similarly. Furthermore, the magnitude of the shrinkage strain at the top of the slab is less in the HP section; that is why there is less warping. Figures 4.17 to 4.19 illustrate the strain at the top and bottom portion at points 1, 2, and 3, as well as a comparison of the portions.

Figure 4.17 Longitudinal Shrinkage Strains of Points 1, 2, and 3 at the Top of the Slab, HP Section

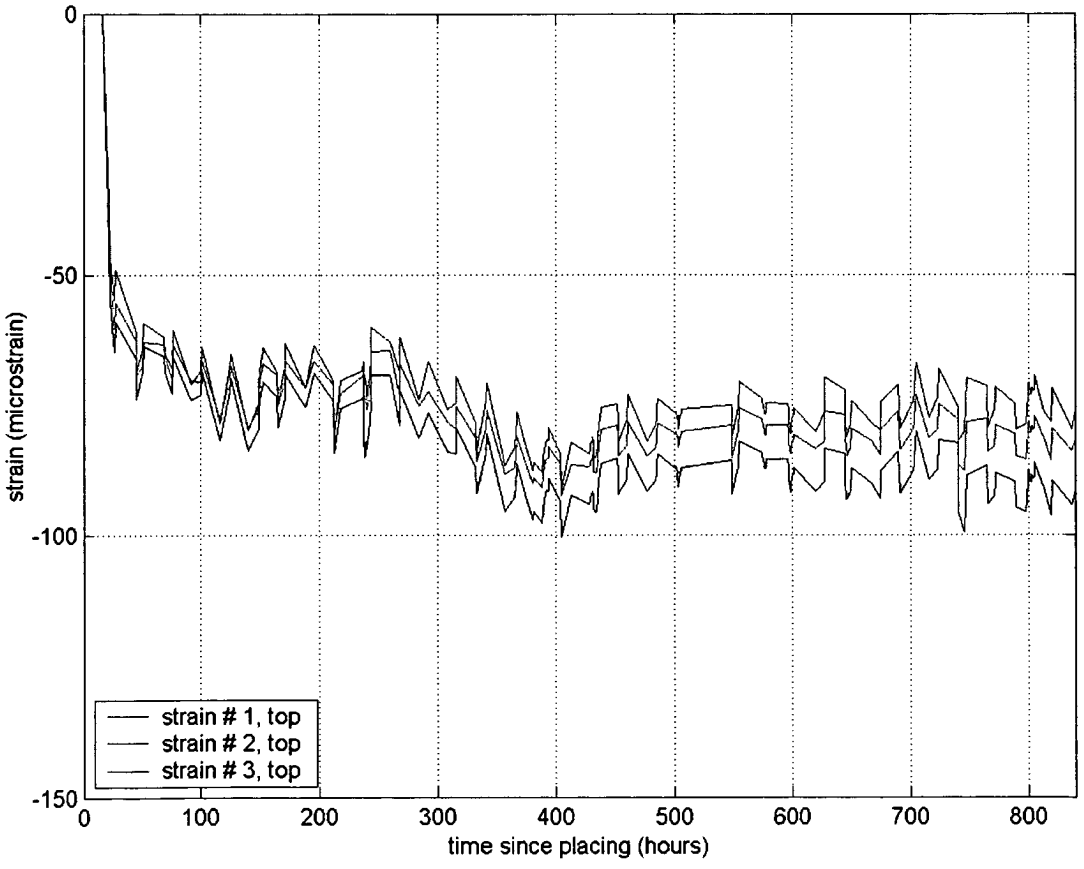

Figure 4.18 Longitudinal Shrinkage Strain of Points 1, 2, and 3 at the Bottom of the Slab, HP Section

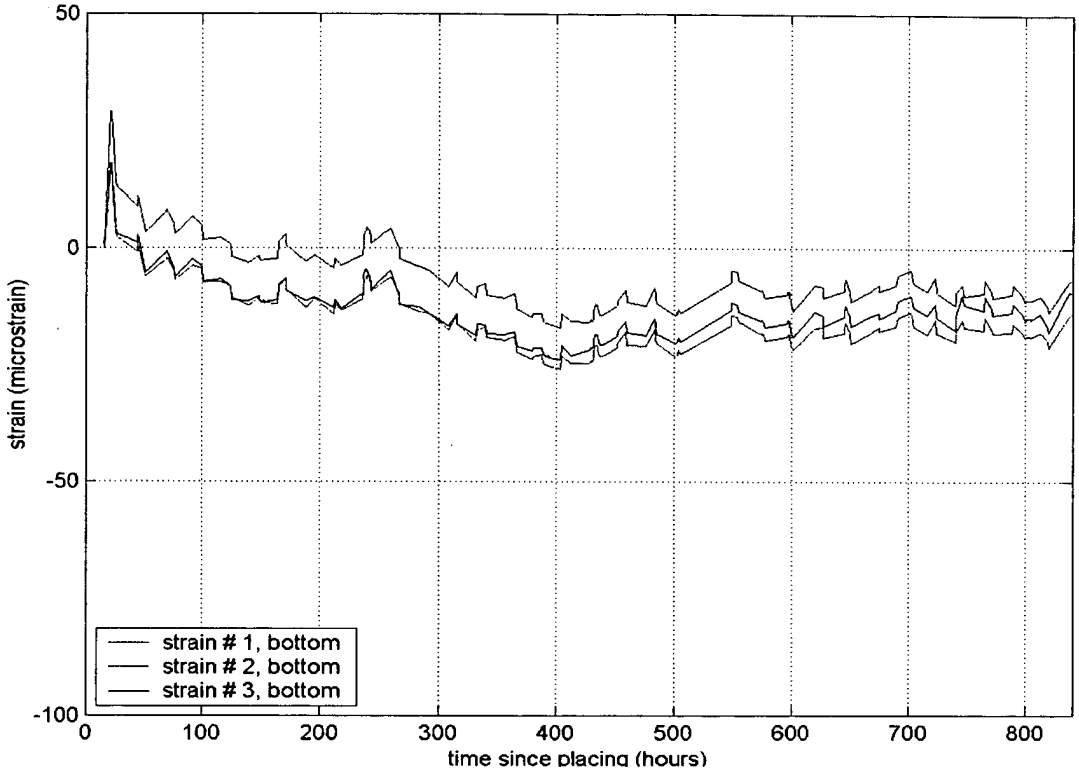

Figure 4.19 Difference in Shrinkage Strain of Points 1, 2, and 3 of the Slab, HP Section

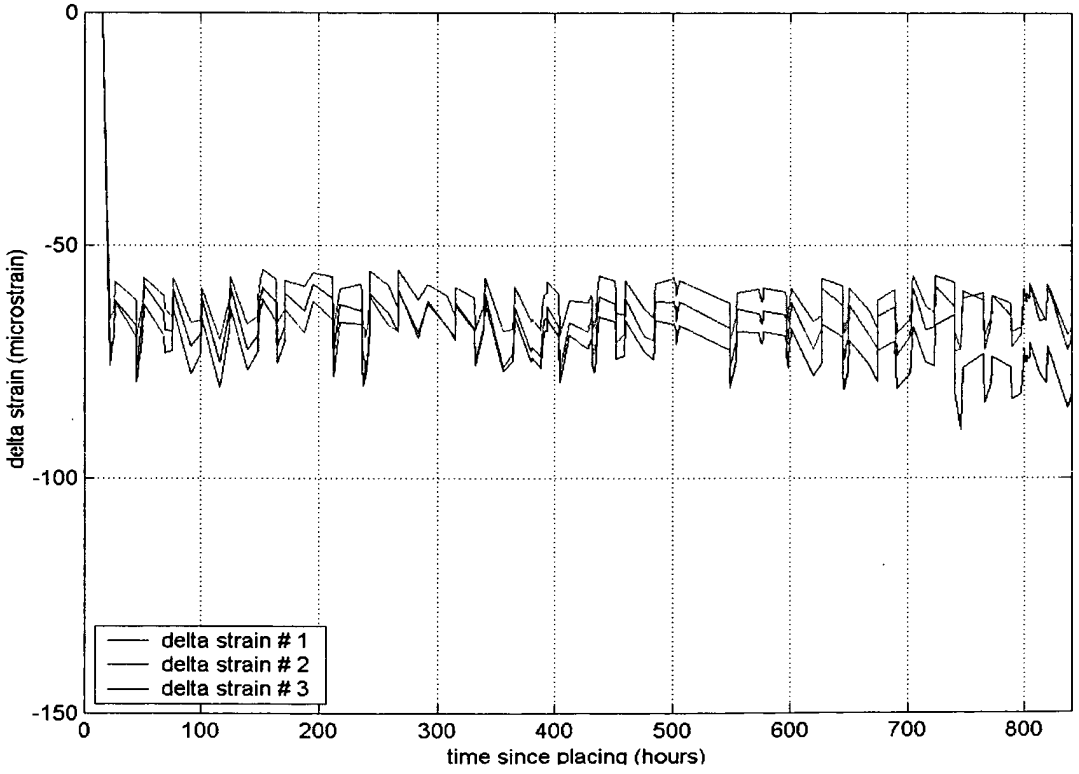

The transverse shrinkage strain in the HP section is basically the same as the longitudinal strain. The transverse strain on the bottom is somewhat less. Figure 4.20 shows the transverse shrinkage strain of the points 10, 11, and 13 at the top of the slab, and Figure 4.21 shows the bottom strain data.

Figure 4.20 Transverse Shrinkage Strain of Points 12, 13, and 14 at the Top of the Slab, HP Section

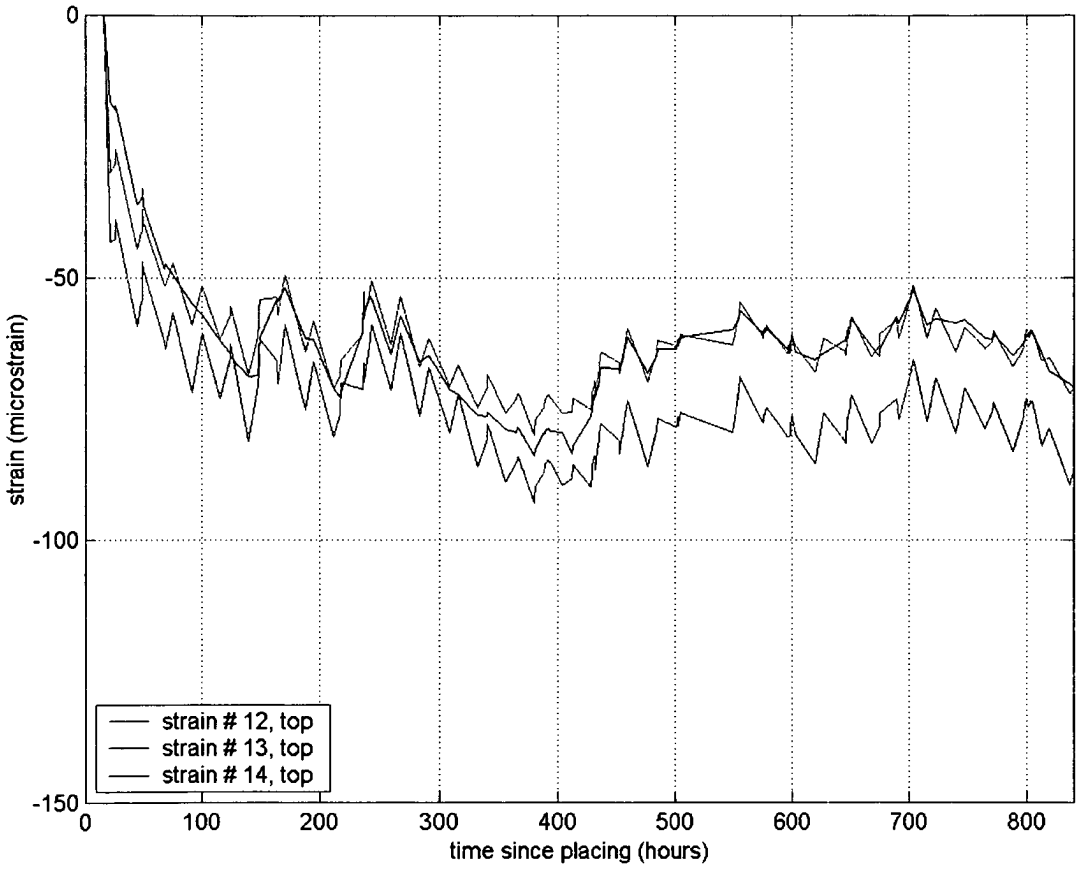

Figure 4.21 Transverse Shrinkage Strain of Points 12, 13, and 14 at the Bottom of the Slab, HP Section

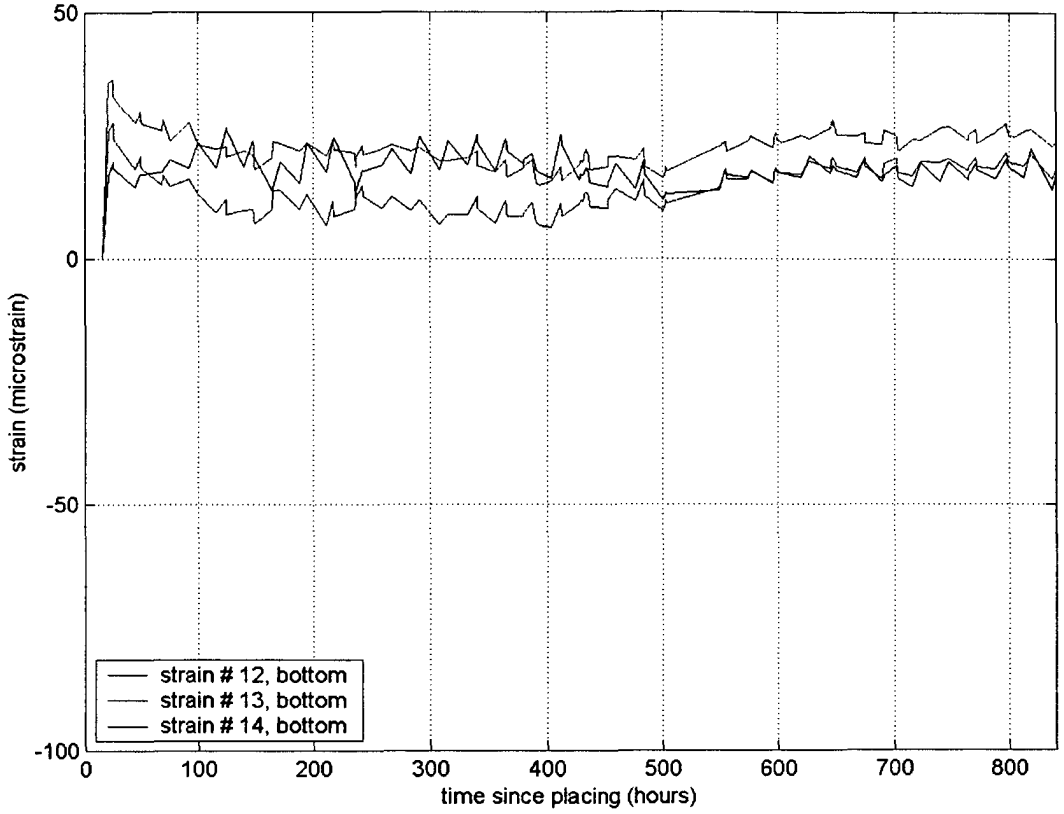

Overall, the impact of temperature on the deflection of the slabs seems to be less in the HP section than in the SP section. The change in the difference between the strain in the top and bottom layer due to the temperature gradient is also less prominent. This is shown in figure 4.22. The amplitude in this case is only $\Delta\varepsilon$ = 20 10-6, which is approximately one-third of the amplitude in the SP section.

Figure 4.22 Differences Between the Strain at the Top and the Bottom of the Slab in Comparison to the Temperature Gradient at the HP Section (Strain Gage Point 1) in the Second Week

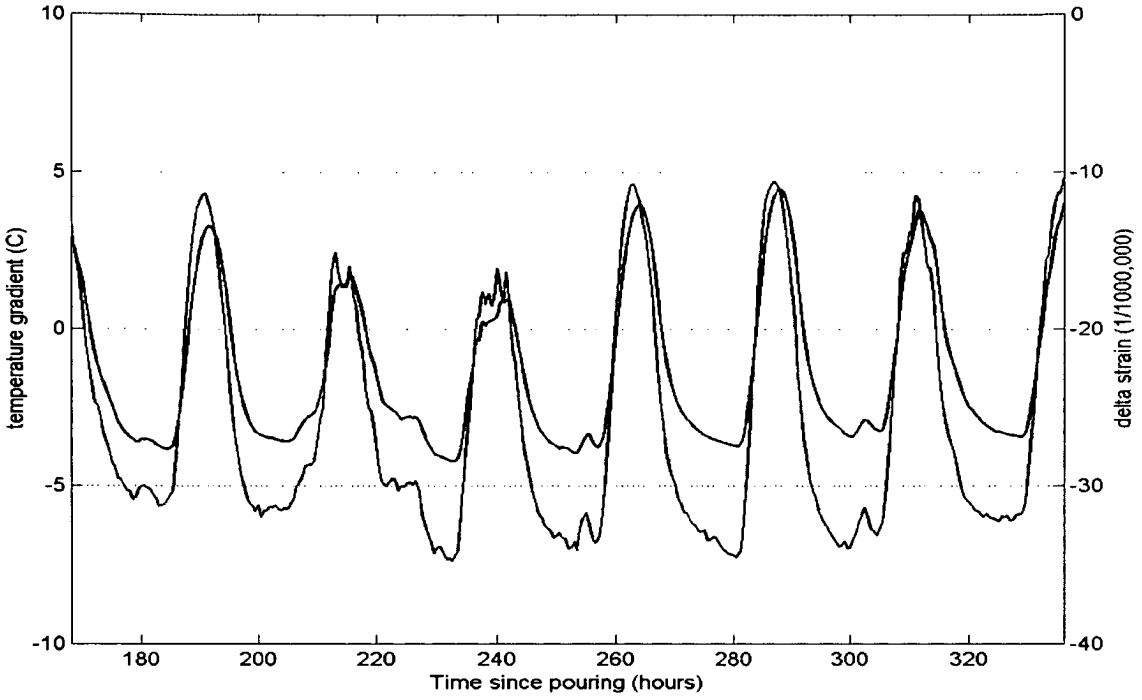

4.3 Comparison of Behavior at a Very Early Age

There are two reasons for the different deformations observed in the HP and SP slabs at a very early age. First, there are the varying mix designs between the HP and SP concrete and their apparent impact on behavior. Second, the two concrete sections were placed under different environmental conditions. The SP concrete was placed in the morning, while the HP concrete was placed in the afternoon. This lead to a different temperature gradient in the slab during the very early hardening, i.e. in the time from final set to sawcutting. Figure 4.23 shows the temperature gradients of the slab during this period in the SP section and Figure 4.24 shows temperature gradients in the HP section.

Figure 4.23 Temperature Gradients of the SP Section

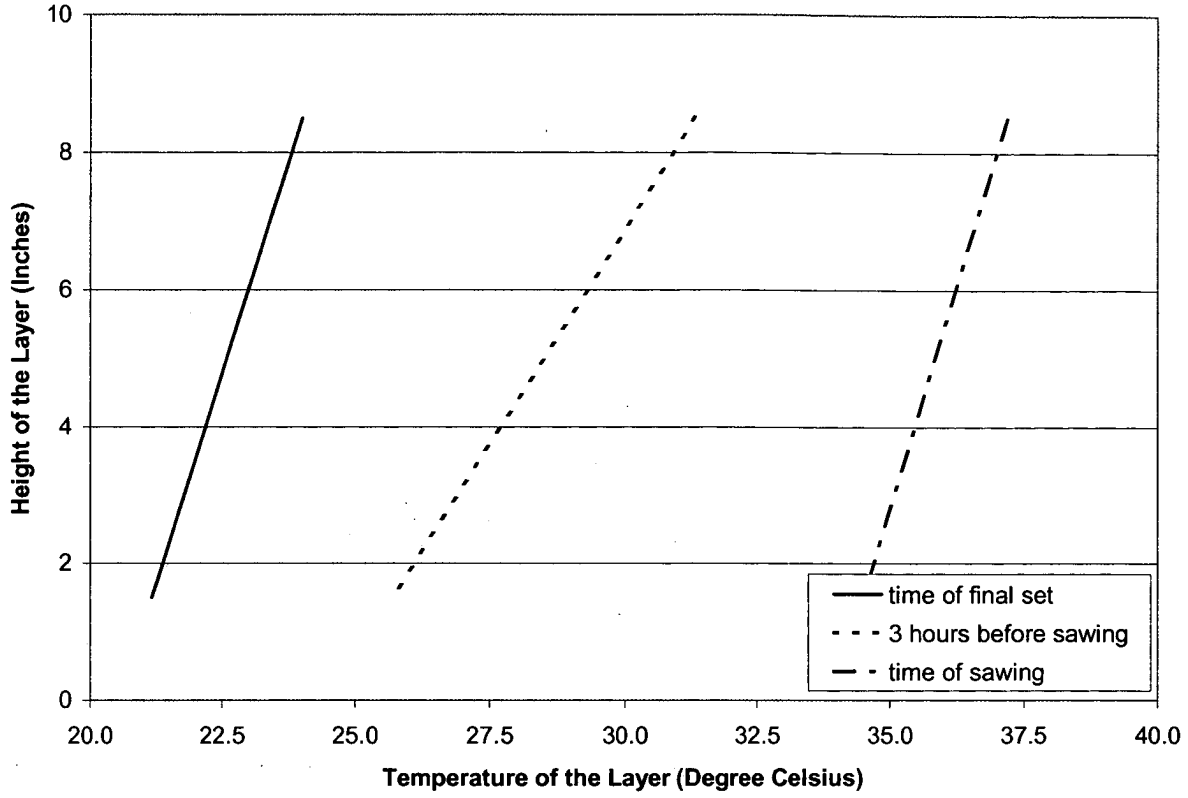

Figure 4.24 Temperature Gradients of the HP Section

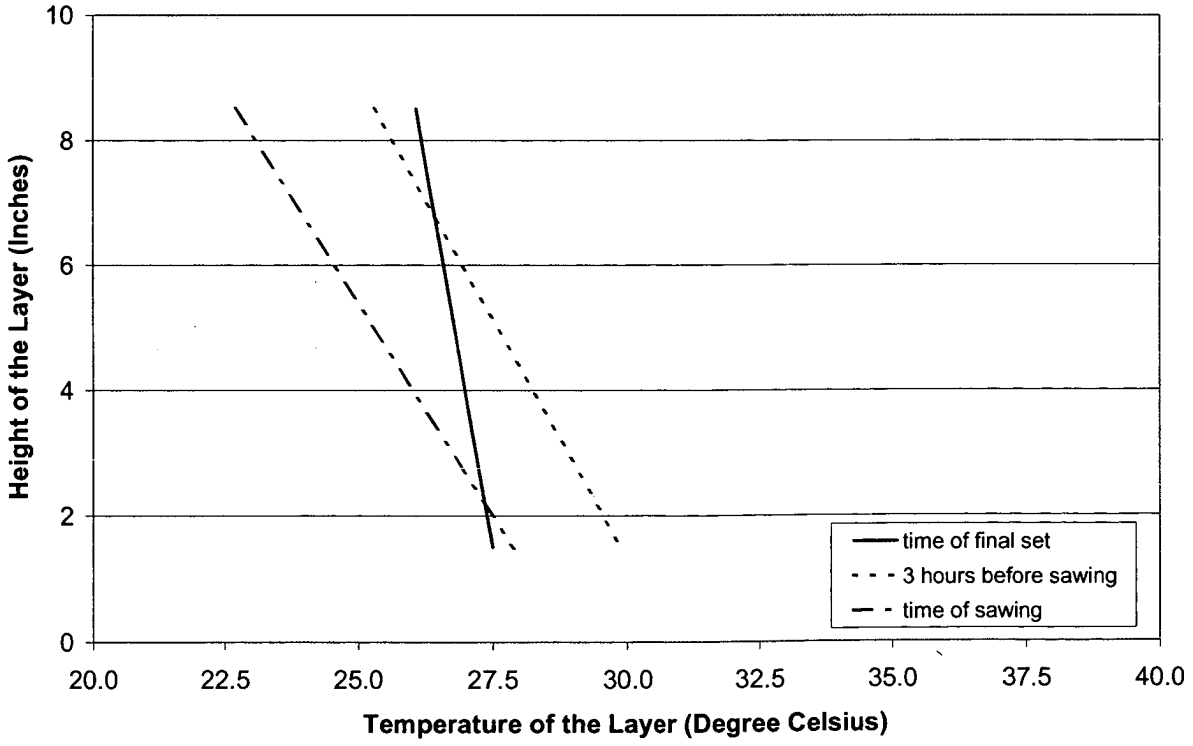

If the slab had not been constrained longitudinally after its final setting, the concrete would have expanded due to the heat of hydration. However, the slab itself restrained this deformation at this time, and compressive stresses arose in the longitudinal direction. Stress-relaxation in the young concrete caused only a small amount of stress to remain. After cooling, the slab experienced a momentary non-stress state. The crucial point is the curvature of the temperature distribution through the slab while hardening. Subsequently, all the stresses in the slab due to temperature gradients have to be related to this zero-stress temperature gradient (Springenschmid and Fleischer, 1991; Zachlehner, 1990).

In this case, temperature distributions in the slab can be described as a positive gradient in the SP section where the surface is warmer than the bottom and a negative gradient in the HP section where the bottom is warmer than the surface. Thus, for the SP section, the temperature gradients typical after saw cutting caused upward curling of the slab, while downward curling was experienced in the HP slab.

4.4 Analysis of Deflection Using FWD Data

In November 1999, the deflection of the pavement was measured using the Dynatest Falling Weight Deflectometer (FWD) at different locations on the slab. In this investigation, the data for the HP2, HP3, and SP section were used, and the deflections at four locations of one slab in each section were compared.

Three different FWD loads, approximately 600, 800, and 1000 kPa, were applied at each location. The deflection was measured by geophones directly under the load and at a radius of 305, 457, 610, 914, and 1524 mm. For comparison of the sections, only the

data relative to the highest loading was used. The FWD test points were located at the micro measurement (MM) points 4, 5, 6 and 7 (see Figure 2.5).

4.4.1 Comparison of the Deflections Bowls

The deflection bowls of the slabs for the specified locations in each section are shown in Figures 4.26 through 4.29. The deflection bowls show a different behavior of each section. The first two figures describe the deflection while loading near the edge. The edge of the slab in the HP2 and SP sections behaves like a cantilever, which is characteristic of a low load transfer in the transverse joint. The deflection in the SP section is less than in the HP2 section, thus the SP section is stiffer. The behavior of the HP 3 section points to a considerably higher load transfer in the transverse joint.

The deflection bowls at point MM 5 support the low load transfer in the transverse joints. The deflection bowls in the center of the slab in the HP2 and SP section support the indication that the SP section has a higher stiffness. The deflection bowl of the HP3 section can only be explained by a lower stiffness of the system. This is not contradictory relative to the shape of the deflection bowls in this section at the other locations.

These results indicate that further investigations are necessary with regard to the load transfer and the stiffness of these pavement systems.

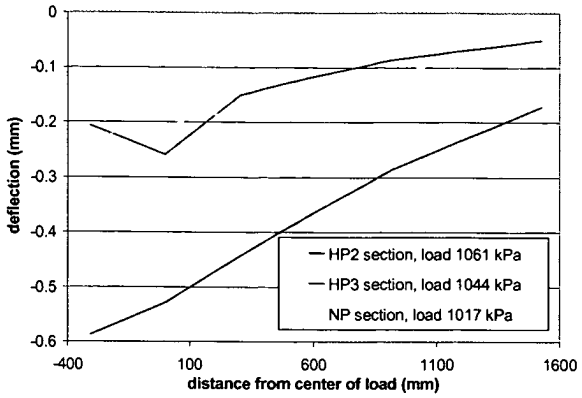

Figure 4.25 Deflection Bowls at Point MM 7

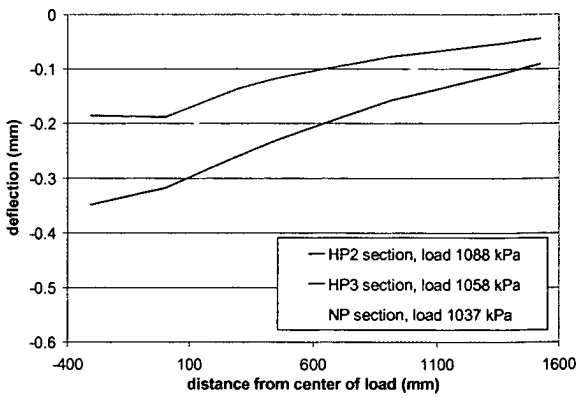

Figure 4.26 Deflection Bowls at Point MM 4

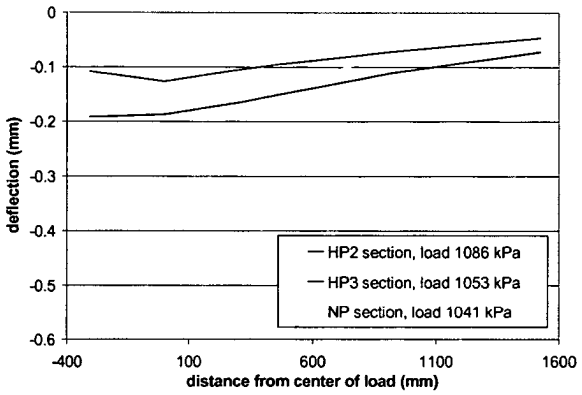

Figure 4.27 Deflection Bowls at Point MM 5

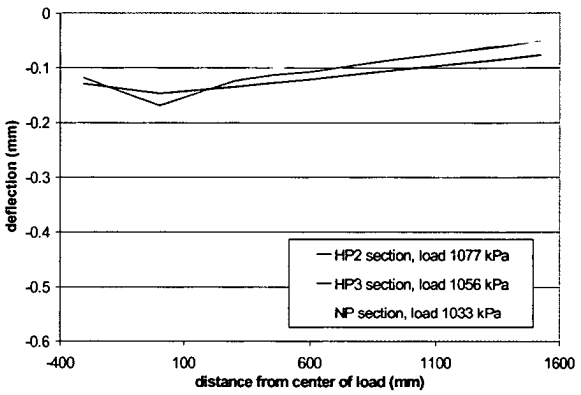

Figure 4.28 Deflection Bowls at Point MM 6

4.5 Variation of Moisture Under Joints

It is well known that joints are sealed to reduce the intrusion of foreign objects and water into the joints. One objective of this investigation was to monitor moisture under sealed and unsealed joints, and under the center of the slab.

Figures 4.29 through 4.33 illustrates that moisture does not fluctuate drastically over time. No significant difference between moisture under sealed and unsealed conditions was recorded; however, the trend was that moisture under sealed joints was slightly greater than under unsealed joints. Moisture under the center of the slab was

similar to moisture under sealed joints. In summary, it appeared that the sealed joint did not have much influence on moisture content of the subgrade.

Figure 4.29 TDR 5 Data Middle of Unsealed Joint

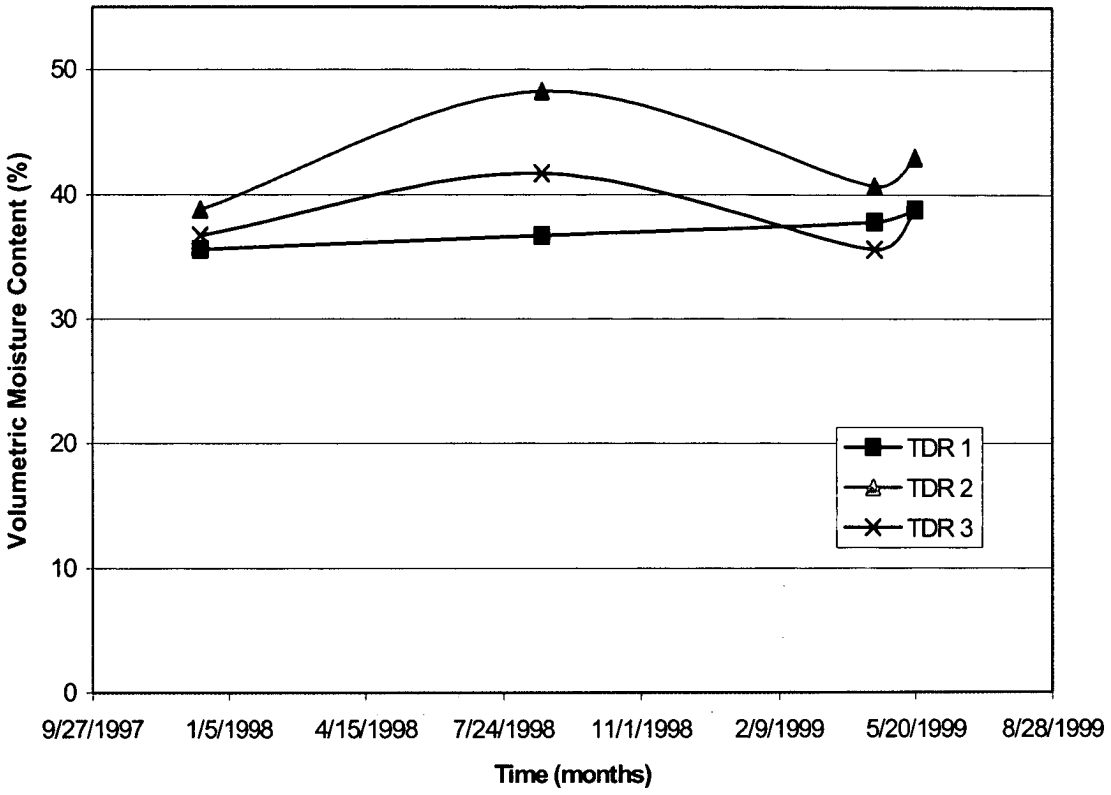

Figure 4.30 TDR 4 Data Middle of Sealed Joint

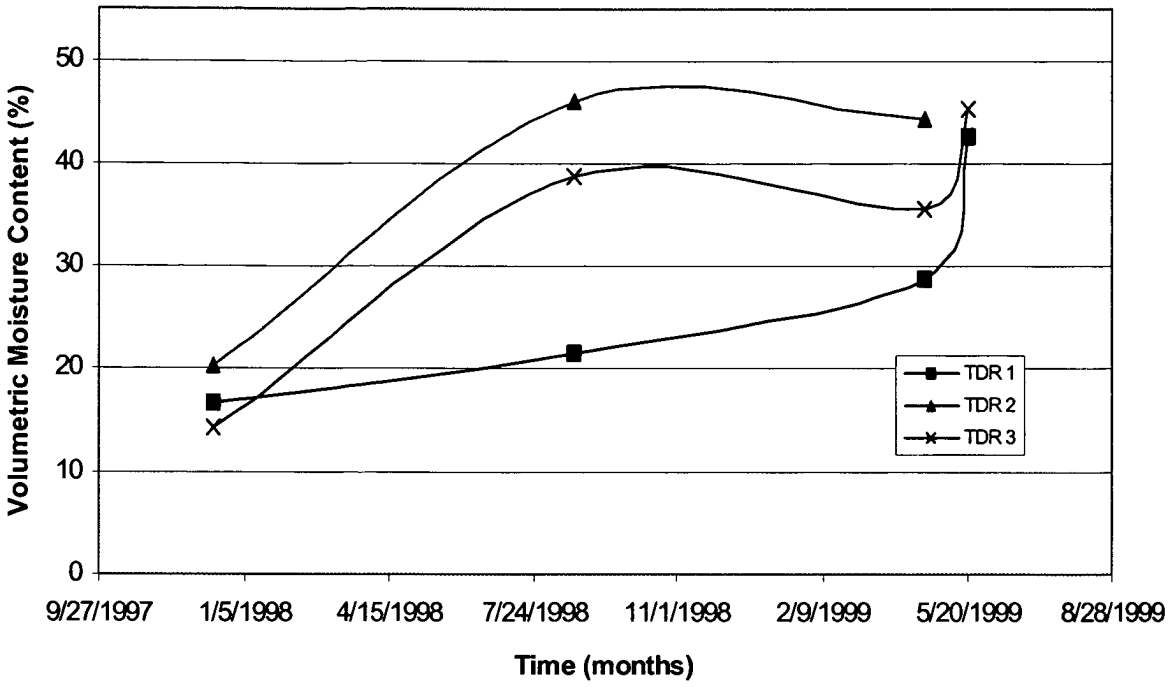

Figure 4.31 TDR 3 Data Edge of Sealed Joint

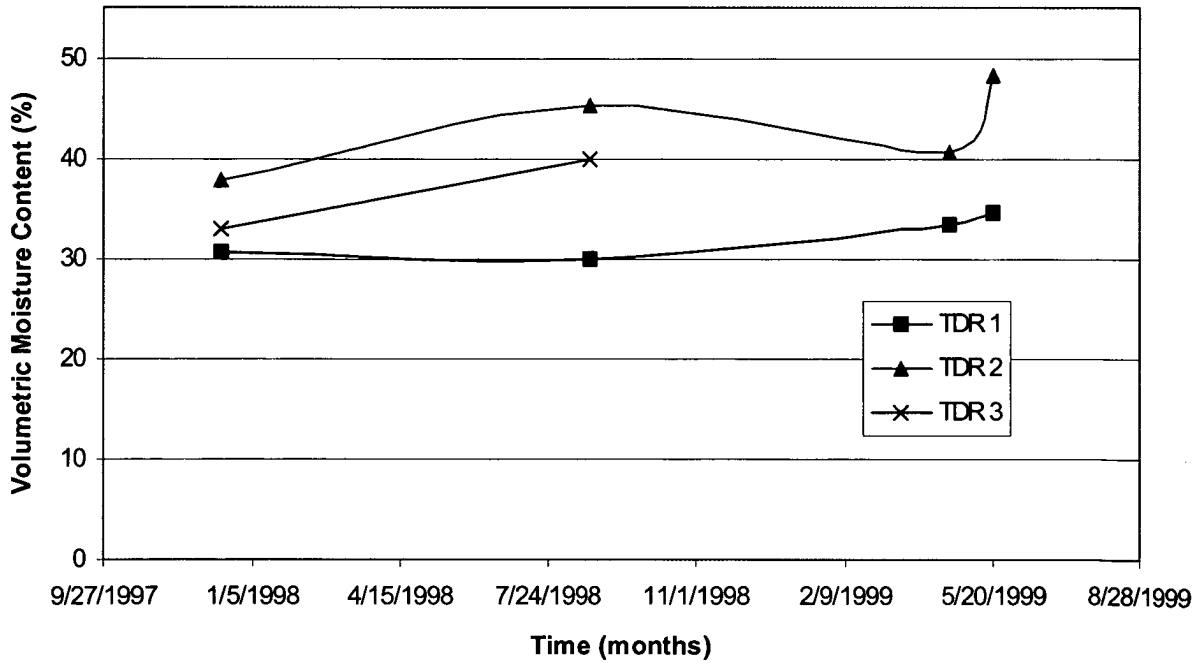

Figure 4.32 TDR 1 Data Middle of HP2 Slab

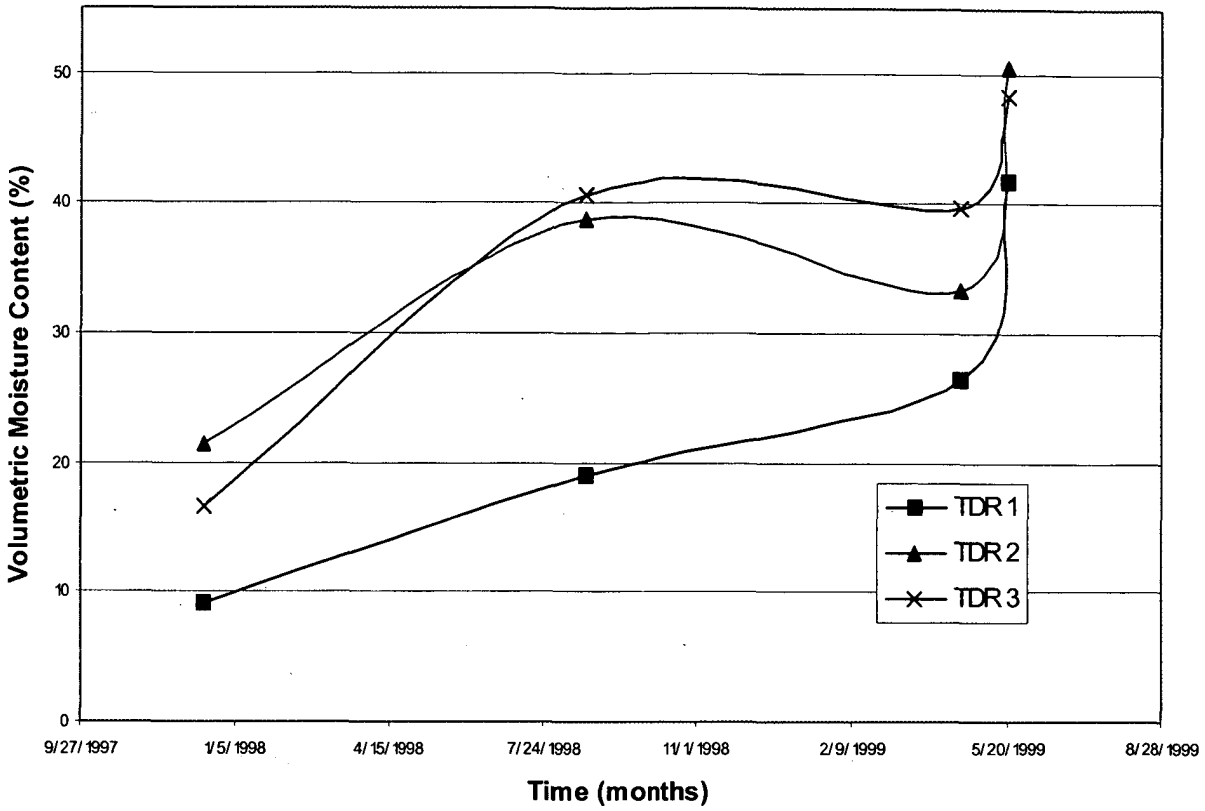

Figure 4.33 TDR 2 Data Shoulder Edge of HP2 Slab

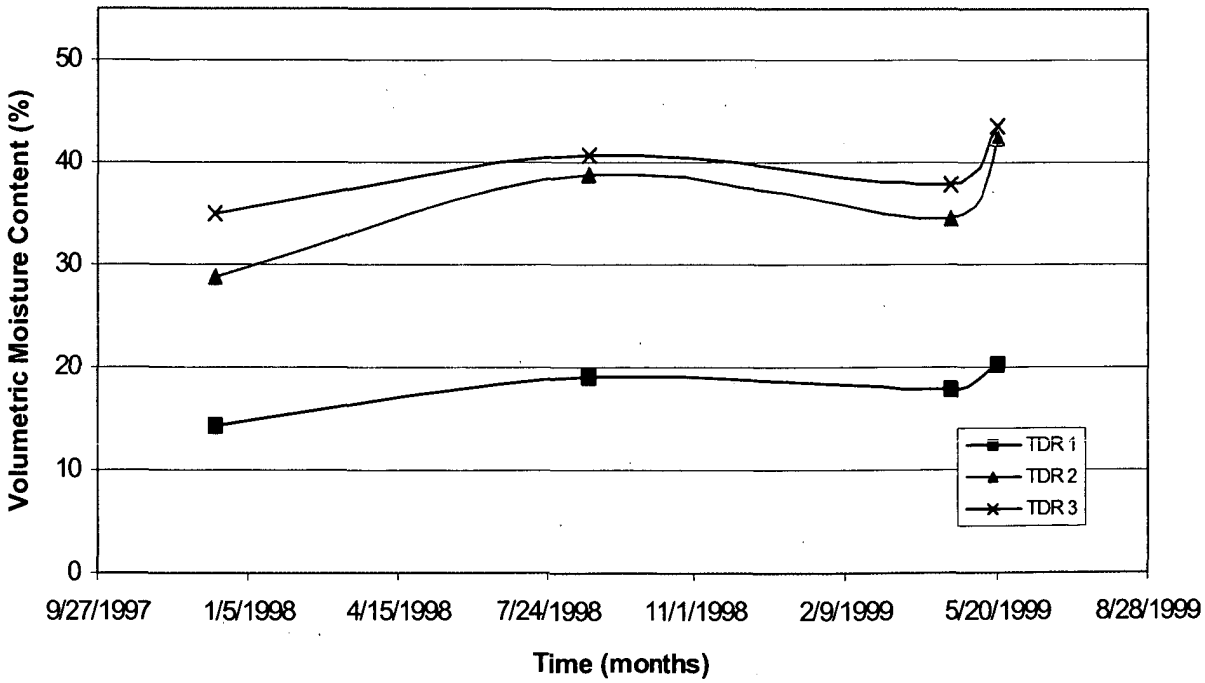

4.6 Joint Deflection and Load Transfer

Based on the above findings, a series of FWD tests were conducted at sealed and unsealed joints in the westbound and eastbound lanes. The data was used to examine the deflection at the joints and compute the load transfer. Load transfer was calculated as a percentage by dividing the deflection measured at –12 inches by the deflection measured at the center of the load plate and multiplying by 100. When joints were tight, both slab ends should theoretically deflect downward about the same amount, giving a load transfer of about 100%. If the slabs are totally independent, the sensor across the joint from the load plate will experience very little deflection when load is applied, giving a load transfer of about 0%.

Tables 4.1 to 4.4 present deflections and load transfer for sealed and unsealed joints. Slightly higher deflections at the sealed joints suggest there was more moisture at these locations. This phenomenon confirmed that joint sealing does not necessarily prevent excessive moisture in the subgrade, because it appears that moisture can be drawn upward to the top of the subgrade by soil suction. Sealing may, in fact, retard the evaporation of moisture from the subgrade. After one year of service, deflections increased and there was a slight drop in the load transfer percentage, thereby suggesting some reduction in transfer efficiency and loss of support at the joints. Figure 4.34 provides an example of distress near a joint.

Table 4.1 FWD Data Unsealed Joints West Bound Lanes

Joint Approach				Joint Leave		
Joint No.	Normal Df1A (mils)	LT (%) Df3/Df1		Normal Df1L (mils)	LT (%) Df2/Df1	Joint Support Ratio (Df1L/Df1A)
1	0.61	89.30		0.54	97.70	0.89
2	0.56	89.90		0.50	95.70	0.89
3	0.55	87.40		0.48	97.50	0.87
4	0.48	89.10		0.44	91.90	0.92
5	0.53	90.40		0.48	93.90	0.91
6	0.54	91.50		0.49	94.90	0.91
7	0.51	89.40		0.46	95.40	0.90
8	0.49	87.40		0.43	93.30	0.88
9	0.40	90.00		0.44	97.50	0.90
10	0.60	88.80		0.54	93.70	0.90
11	0.55	87.00		0.47	96.50	0.85
12	0.54	86.90		0.44	102.40	0.81
Average	0.53	88.93		0.48	95.87	0.89

Table 4.2 FWD Data Sealed Joints West Bound Lanes

Joint Approach				Joint Leave		
Joint No.	Normal Df1A (mils)	LT (%) Df3/Df1		Normal Df1L (mils)	LT (%) Df2/Df1	Joint Support Ratio (Df1L/Df1A)
1	0.98	85.30		0.66	84.10	0.97
2	0.52	71.30		0.45	80.80	0.87
3	0.67	86.30		0.64	89.00	0.96
4	0.54	82.50		0.46	91.80	0.85
5	0.51	79.10		0.61	63.90	1.20
6	0.50	76.40		0.43	85.10	0.86
7	0.47	85.80		0.39	106.70	0.83
8	0.61	72.50		0.50	82.80	0.82
9	0.77	80.80		0.81	70.80	1.05
10	0.83	81.30		0.67	93.70	0.81
11	0.75	83.80		0.64	90.40	0.85
12	0.62	71.80		0.56	75.10	0.90
Average	0.65	79.74		0.57	84.52	0.91

Table 4.3 FWD Data Unsealed Joints East Bound Lanes

Joint Approach				Joint Leave		
Joint No.	Normal Df1A (mils)	LT (%) Df3/Df1		Normal Df1L (mils)	LT (%) Df2/Df1	Joint Support Ratio (Df1L/Df1A)
1	0.62	88.30		0.57	91.30	0.92
2	0.58	96.90		0.58	93.70	1.00
3	0.61	85.10		0.56	89.10	0.92
4	0.66	88.20		0.61	91.60	0.92
5	0.64	90.00		0.59	93.90	0.92
*6	*1.32*	*63.20*		*1.26*	*37.30*	*0.95*
7	0.50	92.90		0.46	98.80	0.92
8	0.52	92.60		0.478	96.80	0.92
9	0.58	93.50		0.57	92.00	0.98
10	0.61	90.00		0.64	84.00	1.05
11	0.51	96.00		0.52	89.20	0.12
12	0.51	91.70		0.49	91.00	0.96
Average	0.64	86.78		0.61	87.39	0.96

** Data was not used to calculate average*

Table 4.4 FWD Data Sealed Joints East Bound Lanes

Joint Approach				Joint Leave		
Joint No.	Normal Df1A (mils)	LT (%) Df3/Df1		Normal Df1L (mils)	LT (%) Df2/Df1	Joint Support Ratio (Df1L/Df1A)
1	0.79	99.60		0.72	104.60	0.91
2	0.85	99.70		1.00	83.50	1.18
3	0.68	90.80		0.66	90.00	0.97
*4	*1.69*	*19.40*		*1.34*	*27.10*	*0.79*
5	0.71	88.90		0.67	91.30	0.94
6	0.74	83.50		0.68	89.50	0.92
7	1.06	70.20		0.81	89.60	0.76
8	0.72	103.90		0.79	89.60	1.10
9	0.71	94.20		0.72	88.70	1.01
10	0.72	95.00		0.69	94.20	0.96
11	0.79	88.50		0.73	92.20	0.92
12	0.73	84.20		0.65	91.00	0.89
Average	0.85	84.83		0.79	85.94	0.95

** Data was not used to calculate average*

Figure 4.34 Pavement Distress Near a Joint

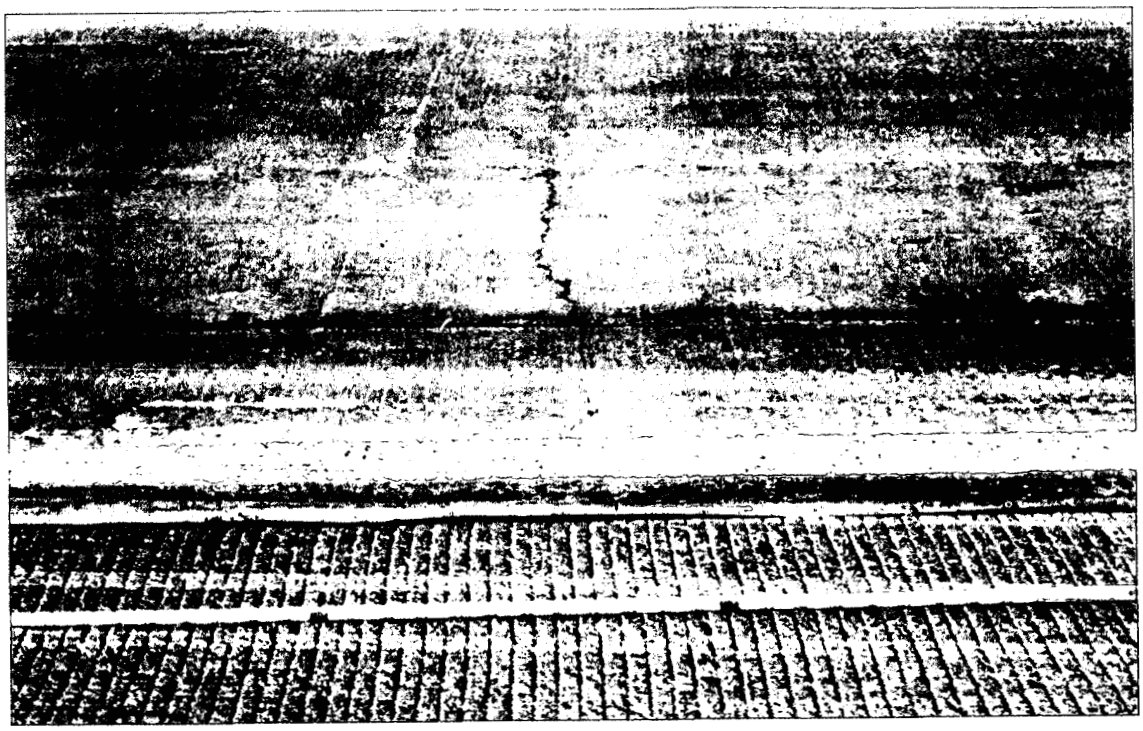

Chapter 5 Summary, Conclusions and Implementation

5.1 Summary

The main objectives of this study were to evaluate the construction, environmental response, and load response of high performance concrete pavement constructed on US 50, and to compare the results with standard Portland cement concrete (PCC) pavement constructed on the same project with the same materials and design parameters. Ground granulated blast furnace slag was used as a cementitious partial replacement of Portland cement in the high performance concrete (HPC). A series of laboratory tests were conducted to determine the mechanical properties and maturity constants for both mixes.

Sensors were installed to monitor environmental conditions, environmental response and dynamic load response on two HPC sections (HP 1 and HP 2) built at the same time in October 1997, and also one HPC section (HP3) and one standard ODOT Class C PCC section (SP) built in October 1998. The latter two sections were constructed one year later but the weather was warmer. Each of these sections was instrumented identically to monitor strain and temperature at various locations in the pavement structure. Surface profiles of individual slabs were measured in all sections with a Dipstick during the early stages of curing. Subsurface moisture was monitored under the slabs and at joints with Time Domain Reflectometry (TDR) probes. A Dynatest Falling Weight Deflectometer (FWD) was used to measure load transfer across the joints.

5.2 Conclusions

Based upon laboratory tests and field data obtained during this study, the following conclusions were derived for this HPC pavement:

- Temperature gradients generated between the surface and bottom of concrete slabs during the curing process can have a significant impact on the formation of early cracks. Gradients of 10°C were observed in sections placed in 1997 compared to gradients of 5°C for sections placed in 1998. Sections placed in 1997 experienced cracking within eighteen hours of placement. These larger gradients were due to the arrival of a cold front shortly after placement.
- Large values of strain recorded with the vibrating wire gauges and output from the maturity meter all indicated that Sections HP 1 and 2 would likely experience early cracking, as was observed in the field. HP 3 was constructed one year later with the same mix as HP 1and HP 2, but the air temperature was warmer at the time of concrete placement. Strain and maturity meter data obtained in the field indicated that Section HP 3 had a lower probability of exhibiting early cracking. No cracks were observed in Section HP 3.
- Results from HIPERPAV also suggested that Sections HP 1 and 2 would crack and Section HP 3 would not crack, confirming results obtained from the vibrating wire gauges, the maturity meter and field observations.
- Section HP 3 had less initial warping than did section SP constructed with standard ODOT Class C concrete. Early cracking in Sections HP 1 and 2 precluded any comparison of curvature in these sections with curvature in the other two uncracked sections.

- FWD data indicated that, under similar loading conditions, Section HP 3 experienced slightly less deflection at the joints than did the section containing standard concrete, suggesting more curvature and more loss of support under slabs constructed with standard concrete than under slabs constructed with HPC. Higher deflections obtained from sections HP 1 and 2 could be attributed to the early cracking observed in these sections.
- After one year of service, FWD joint deflections were higher in Sections HP 1 and 2 than before the pavement was opened to traffic. This could be due to the occurrence of early cracking during the first year of service, different temperature conditions, and/or densification of the New Jersey base.
- With limited data available, it was suggested that moisture in the base at sealed and unsealed joints was similar. In some cases, however, moisture under sealed conditions was observed to be slightly higher, indicating that joint seals may trap moisture under the pavement.
- During FWD tests the deflection at sealed joints was generally higher than at the unsealed.
- A parametric study should be conducted utilizing HIPERPAV and available field data to develop improved specifications for controlling the placement of PCC pavement with environmental-based criteria rather than seasonal–based criteria.

5.3 Implementation

- ODOT should consider adopting/accepting HIPERPAV in conjunction with the maturity technique to reduce the occurrence of early cracking and to improve the performance of PCC pavement.

- Based upon observations from this project and findings reported from other projects in Ohio, New Jersey base should not be used under PCC pavement.
- The upper range of the Iowa base is similar to New Jersey base and should not be utilized under PCC pavements
- ODOT should collect additional field data to determine the effectiveness of sealing the joints.

BIBLIOGRAPHY

American Concrete Institute, 1987. ACI Committee 226, "Ground Granulated Blast-Furnace Slag as a Cementitious Constituent in Concrete," ACI Materials Journal, Vol. 84 Issue 4, American Concrete Institute, Farmington Hills, MI.

American Concrete Institute, 1995. ACI Committee 318: Standard Building Code, "Building Code Requirements for Structural Concrete (ACI 318-95) and Commentary (ACI 318 R95), American Concrete Institute, Farmington Hills, MI

American Society for Testing and Materials (ASTM) Standards, 1987. Annual Book of ASTM Standards, Vol. 04.02. C 403 "Time of Setting of Concrete Mixtures by Penetration Resistance", The ASTM, Philadelphia, PA

American Society for Testing and Materials (ASTM) Standards, 1987 Annual Book of ASTM Standards, Vol. 04.02. C 1074 "Estimating Concrete Strength by the Maturity Method", The ASTM, Philadelphia, PA.

American Society for Testing and Materials (ASTM) Standards, 1987. Annual Book of ASTM Standards, Vol 04.02. C 192 "Standard Practice for Making and Curing Concrete Test Specimens in the Laboratory", The ASTM, Philadelphia, PA

Boltz, E. 1998. Early Performance of Concrete Pavement Containing GGBF Slag. Master's Thesis, Ohio University, Athens, Ohio 182 pp.

Carino, N.J. 1997. "Nondestructive Test Methods." in: Concrete Construction Engineering Handbook. Nawy, E.G. editor, CRC Press, FL.

Carino, N.J. and Tank, R.C. 1992. Maturity Functions for Concrete Made with Various Cements and Admixtures. ACI Materials Journal 89 (2), American Concrete Institute, Farmington Hills, MI pp. 186-188

Comité Euro-International du Béton 1993. CEB-FIB Model Code 1990 Design Code.

Freiesleben, H.P. and J. Pedersen. 1977. "Maturity Computer for Controlled Curing and Hardening of Concrete." Nordisk Betong Vol. 21, Stockholm. Sweden, pp. 19-34

Gauthier, E. and M. Regourd. 1982. The Hardening of Cement in Function of Temperature. Proceedings, RILEM, France. pp. 145-150

Guo, C. 1989. "Maturity of Concrete: Method for Predicting Early-Stage Strength." ACI Materials Journal, Vol. 86 Issue 4, American Concrete Institute, Farmington Hills, MI. pp. 341-553

Geokon Inc., Technical Notes, Lebanon, Hew Hampshire, 1994Cambell Scientific, Inc., "CR7 Measurement and Control Module Operator's Manual." Logan, Utah, 1994

Khan, A.A., W. D. Cook, and D. Mitchell. 1995. "Early Age Compressive Stress-Strain Properties of Low, Medium, and High-Strength Concretes." ACI Materials Journal 92 (6). American Concrete Institute, Farmington Hills, MI pp. 617-624

Malhotra, V.M. and N. J. Carino. 1991. CRC Handbook on Nondestructive Testing of Concrete. CRC Press, FL.

Miura, Takashi and Iwaki, Ichiro, 2000. "Strength Development of Concrete Incorporating High Levels of Ground Granulated Blast-Furnace Slag at Low Temperatures." ACI Materials Journal Vol. 97 No. 1, American Concrete Institute, Farmington Hills, MI p. 66 – 70

Nawy, E.G. 1997. "Long Term Effects and Serviceability." in: Concrete Construction Engineering Handbook. E. G. Nawy, editor, CRC Press, FL.

Neville, A.M. 1997. Properties of Concrete. John Wiley & Sons, NY.

Ohio Department of Transportation, "Construction and Materials Specifications," Columbus, Ohio.

Omega Engineering, Inc., "Practical Guidelines for Temperature Measurements."

Saul, A.G.A. 1951. "Principles Underlying the Steam Curing of Concrete at Atmospheric Pressure." Mag. Concr. Res. 2 (6).

Springenschmid, R., and W. Fleischer. 1990. "Effects of Temperature and Moisture on Concrete Pavements." Sixth International Symposium on Concrete Roads, Madrid, Spain.

Tokyo Sokki Kenyojo Co., Ltd., Technical Notes, Tokyo Japan, 1995 ASTM Designation: C1074-87, "Standard Practice for Estimating Concrete Strength by the Maturity Method"

Zachlehner, A. 1990. "Restraint Stresses in Young Concrete Roads." Sixth International Symposium on Concrete Roads, Madrid, Spain.

Zhang, M. H., A. Bilodeau, and V.M. Malhotra, 1999. "Concrete Incorporating Supplementary Cementing Materials: Effect on Compressive Strength and Resistance to Chloride-Ion Penetration," ACI Materials Journal, Vol. 96 No. 2, American Concrete Institute, Farmington Hills, MI p.181-189.